

Structures and Properties of the Chiral Smectic C Liquid Crystal Phases

Ferro- and Antiferroelectricity in Soft Matter

JAN P. F. LAGERWALL

Department of Microelectronics and Nanoscience
CHALMERS UNIVERSITY OF TECHNOLOGY
GÖTEBORG UNIVERSITY
Göteborg, Sweden 2002



THESIS FOR THE DEGREE OF DOCTOR OF PHILOSOPHY

STRUCTURES AND PROPERTIES OF THE CHIRAL SMECTIC C LIQUID CRYSTAL PHASES

Ferro- and Antiferroelectricity in Soft Matter

Jan P. F. Lagerwall



Department of Microelectronics and Nanoscience
Chalmers University of Technology
Göteborg University
Göteborg, Sweden, May 2002

Structures and Properties of the Chiral Smectic C Liquid Crystal Phases
Ferro- and Antiferroelectricity in Soft Matter
Jan Lagerwall

ISBN 91-7291-155-7

© JAN P. F. LAGERWALL, 2002

Doktorsavhandlingar vid Chalmers tekniska högskola
Ny serie nr 1837
ISSN 0346-718x
(Göteborg, 2002)

Department of Microelectronics and Nanoscience
Chalmers University of Technology
SE-412 96 Göteborg,
Sweden
Telephone: +46 (0) 31 - 772 10 00
E-mail: jan_lagerwall@mac.com

Front cover

Ferro- and antiferroelectric domains coexisting next to one another in a 4 μm thick planar-aligned sample with the chiral-dopant mixture (R/S)-10F1M7 + (S)-IGS97 at room temperature (observed through crossed polarizers). The ferroelectric and antiferroelectric regions are clearly distinguishable from each other as dark and bright UP and DOWN domains of varying shape on one hand (mainly left part of the image), and the long and thin dark-blue stripes (right part) on the other hand.

Back cover

Schematic illustrations of the molecular organizations within the layers of the SmA and SmC phases, and the corresponding symmetries.

Printing: Chalmers reproservice
Göteborg, Sweden 2002

Structures and Properties of the Chiral Smectic C Liquid Crystal Phases

Ferro- and Antiferroelectricity in Soft Matter

JAN P. F. LAGERWALL

Department of Microelectronics and Nanoscience

Chalmers University of Technology

ABSTRACT

Liquid crystals constitute a form of soft matter possessing lower symmetry than isotropic liquids but higher symmetry than solid crystals. In smectic A and C liquid crystals, the rodlike molecules are arranged in layers and the medium has crystal order in one dimension and liquid order in the other two. Liquid crystals with a spontaneous electric polarization were discovered in 1975 and five years later it was realized how to turn them into truly ferroelectric samples. The phase where spontaneous polarization appears is the chiral smectic C phase, *i.e.* a phase which lacks mirror symmetry and where the long molecule axes are inclined with respect to the layer normal. Materials exhibiting this phase are therefore often referred to as *ferroelectric liquid crystals* (FLCs). It was realized at an early stage that FLCs can be extremely useful in high-speed, high-resolution electrooptic devices, such as flat panel displays and the research in the field of chiral smectics greatly expanded. In 1989 this led to the discovery of *antiferroelectric liquid crystals* (AFLCs). Also these belong to the class of chiral smectic C, but it was now realized that this class had to be subdivided into several different phases.

Although a number of FLC devices have now reached the market and several prototype AFLC displays have been shown, many fundamental problems still have to be solved before the inherent rich potential of the FLC and AFLC technology could be fully developed. Most of these problems have to do with our lack of understanding of the nature of the major physical phenomena involved. In the present thesis special emphasis is given to issues and concepts like symmetry, order, chirality and polarity. Numerous materials problems are also being addressed, like phase-sequence, confinement, surface-controlled phase-behavior, non-shrinking smectic layer materials, and chemical as well as optical purity – all with the general aim to comprehend the subtle balance between synclinic and anticlinic, between polar and antipolar, order in liquid crystals.

Keywords: *ferroelectric liquid crystals, antiferroelectric liquid crystals, confinement, subphase suppression, orientational order, smectic layer shrinkage*

Publications included in the thesis

- PAPER 1. OPTICAL AND X-RAY EVIDENCE OF THE 'DE VRIES' SM-A* - SM-C* TRANSITION IN A NON-LAYER SHRINKAGE FERROELECTRIC LIQUID CRYSTAL WITH VERY WEAK INTERLAYER TILT CORRELATION
Jan P. F. Lagerwall, Frank Gießelmann, Marc D. Radcliffe
Submitted for publication in Physical Review E (2002)
- PAPER 2. ANTIFERROELECTRIC LIQUID CRYSTAL MIXTURE WITHOUT SMECTIC LAYER SHRINKAGE AT THE DIRECT SM-A* - SM-C_A* TRANSITION
Frank Gießelmann, Jan P. F. Lagerwall, Gunnar Andersson, Marc D. Radcliffe
Submitted for publication in Physical Review Letters (2002)
- PAPER 3. PHASES, PHASE TRANSITIONS AND CONFINEMENT EFFECTS IN A SERIES OF ANTIFERROELECTRIC LIQUID CRYSTALS
J. P. F. Lagerwall, D. D. Parghi, D. Krüerke, P. Jägemalm, F. Gouda
Liquid Crystals, **29**, 2, pp. 163-178 (2002)
- PAPER 4. ON THE PHASE SEQUENCE OF ANTIFERROELECTRIC LIQUID CRYSTALS AND ITS SENSITIVITY TO CHEMICAL PURITY
Jan P. F. Lagerwall, Per Rudquist, Sven T. Lagerwall, Frank Gießelmann
Submitted to Liquid Crystals (2002)
- PAPER 5. ANTIFERROELECTRIC LIQUID CRYSTALS WITH 45° TILT – A NEW CLASS OF PROMISING ELECTRO-OPTIC MATERIALS
K. D'havé, A. Dahlgren, P. Rudquist, J.P.F. Lagerwall, G. Andersson, M. Matuszczyk, S.T. Lagerwall, R. Dabrowski, W. Drzewinski
Poster presentation at FLC'99 (Darmstadt, Germany), Aug. 29 - Sep. 3, 1999. Published in Ferroelectrics, volume 244, pages 115-128 (2000).
- PAPER 6. SURFACE- AND FIELD-INDUCED AFLC STRUCTURES DETECTED BY DIELECTRIC SPECTROSCOPY
J. P. F. Lagerwall, P. Rudquist, S. T. Lagerwall, B. Stebler
Oral presentation at FLC 2001. Submitted for publication in Ferroelectrics (2001)
- PAPER 7. THE TILT PLANE ORIENTATION IN ANTIFERROELECTRIC LIQUID CRYSTAL CELLS AND THE ORIGIN OF THE PRETRANSITIONAL EFFECT
P. Rudquist, J. P. F. Lagerwall, J. G. Meier, K. D'havé, S. T. Lagerwall
Submitted to Physical Review E (2002)

Other publications by the author, not included in this thesis

THE CASE OF THRESHOLDLESS ANTIFERROELECTRICITY: POLARIZATION-STABILIZED TWISTED SMC* LIQUID CRYSTALS GIVE V-SHAPED ELECTRO-OPTIC RESPONSE.

P. Rudquist, J. P. F. Lagerwall, M. Buivydas, F. Gouda, S. T. Lagerwall, N. A. Clark, J. E. MacLennan, R. F. Shao, D. Coleman, S. Bardon, T. Bellini, D. R. Link, G. Natale, M. A. Glaser, D. M. Walba, M. D. Wand, X. H. Chen
Journal of Materials Science, volume 9, pages 1257-1261 (1999)

UNRAVELING THE MYSTERY OF "THRESHOLDLESS ANTIFERROELECTRICITY": HIGH-CONTRAST ANALOG ELECTROOPTICS IN CHIRAL SMECTIC LIQUID CRYSTALS

P. Rudquist, J. P. F. Lagerwall, M. Buivydas, F. Gouda, S. T. Lagerwall, R. F. Shao, D. Coleman, S. Bardon, D. R. Link, T. Bellini, J. E. MacLennan, D. M. Walba, N. A. Clark, X. H. Chen
SID 99 digest, pages 409 - 411 (1999)

ON THE COEXISTENCE OF SMC* AND SMC_A* PHASES IN BINARY CHIRAL-DOPANT ANTIFERROELECTRIC MIXTURES

J. P. F. Lagerwall, D. D. Parghi, G. Heppke
Poster presentation at FLC'99 (Darmstadt, Germany), Aug. 29 - Sep. 3, 1999. Published in Ferroelectrics, volume 244, pages 211-221 (2000)

OPTIC, ELECTROOPTIC AND DIELECTRIC PROPERTIES OF NOVEL ANTIFERROELECTRIC LIQUID CRYSTAL COMPOUNDS

P. Jägemalm, J. P. F. Lagerwall, A. Dahlgren, L. Komitov, A. S. Matharu, C. Grover, F. M. Gouda, A. A. Kutub
Poster presentation at FLC'99 (Darmstadt, Germany), Aug. 29 - Sep. 3, 1999. Published in Ferroelectrics, volume 244, pages 147-157 (2000)

ELECTROOPTIC AND DIELECTRIC PROPERTIES OF NEW ANTIFERROELECTRIC LIQUID CRYSTAL MIXTURES

G. Andersson, R. Dabrowski, W. Drzewinski, J. P. F. Lagerwall, M. Matuszczyk, T. Matuszczyk, P. Perkowski, Z. Raszewski
Poster presentation at FLC'99 (Darmstadt, Germany), Aug. 29 - Sep. 3, 1999. Published in Ferroelectrics, volume 244, pages 137-146 (2000)

THE DEPENDENCE ON THE HELICAL PITCH OF THE ANTIFERROELECTRIC DIELECTRIC MODES

J. P. F. Lagerwall, T. Fütterer, D. Moro, G. Heppke
Poster presentation at FLC'99 (Darmstadt, Germany), Aug. 29 - Sep. 3, 1999. Published in Ferroelectrics, volume 244, pages 223-231 (2000).

ELECTROOPTIC AND DIELECTRIC SPECTROSCOPY MEASUREMENTS OF BINARY CHIRAL-DOPANT ANTIFERROELECTRIC MIXTURES

D. D. Parghi, J. P. F. Lagerwall, G. Heppke
Poster presentation at ECLC'99 (Crete, Greece), April 25-30, 1999. Published in Molecular Crystals & Liquid Crystals, volume 351, pages 361-370 (2000).

PHASE CHARACTERIZATION OF POLAR LIQUID CRYSTALS USING DIELECTRIC SPECTROSCOPY

Jan Lagerwall
Thesis for the degree of Licentiate of Technology, Chalmers University of Technology, Göteborg, Sweden (2000)

OPTICAL IMPLEMENTATION OF NEURAL NETWORKS FOR PATTERN RECOGNITION

Jan Lagerwall
Masters thesis, Chalmers University of Technology, Göteborg, Sweden (1997)

Table of contents

1. Liquid Crystals and the Description of Imperfect Order 1

- 1.1. *The liquid crystalline state 1*
- 1.2. *Nematic order and the director concept 3*
- 1.3. *The smectic phases 5*
 - 1.3.1. The smectic A phase 5
 - 1.3.2. Tilted smectics 9
 - 1.3.2.1. Syn- and anticlinicity 11
 - 1.3.3. Ordering the liquid 12
- 1.4. *The director concept in biaxial liquid crystals 13*

2. Chirality and Polarity in Liquid Crystals 15

- 2.1. *Ferroelectric liquid crystals 15*
 - 2.1.1. The helical bulk SmC* structure 17
 - 2.1.2. Small-signal response of the SmA* and helical SmC* phases in planar-aligned samples 18
 - 2.1.2.1. Tilt-angle fluctuations 18
 - 2.1.2.2. Phase-angle fluctuations 19
 - 2.1.3. A comparison with solid ferroelectrics 20
- 2.2. *Antiferroelectric liquid crystals 20*
 - 2.2.1. The bulk structure of the SmC_a* phase 20
- 2.3. *A terminology for describing anticlinic smectics 21*
- 2.4. *The consequences of the anticlinic structure for the optical properties 23*
- 2.5. *The dielectric properties of the SmC_a* phase 25*
 - 2.5.1. The small-signal dielectric signature 25
 - 2.5.2. The types of fluctuations behind the SmC_a* dielectric absorptions 28
- 2.6. *Surface-stabilization of polar phases 29*

3. The SmA-C Transition and the Issues of Tilt and Layer Thickness in Smectics 31

- 3.1. *The mysteries of the 'orthogonal' smectic A phase 31*
 - 3.1.1. Adriaan de Vries, Alan Leadbetter and the idea of a SmA phase with tilted molecules 32
 - 3.1.2. The non-correlation model 32
 - 3.1.3. The diffuse cone model 33
 - 3.1.4. The zig-zag model 36
 - 3.1.5. The effect of molecular interdigitation on the smectic layer structure 37
- 3.2. *The molecular origin of the optical SmC^(*) tilt 38*
 - 3.2.1. The diffuse cone model descriptions of the onset of tilt 38
 - 3.2.1.1. The asymmetric diffuse cone model SmA-C transition 38
 - 3.2.1.2. The tilted diffuse cone model SmA-C transition and the skewed cybotactic nematic phases 39
 - 3.2.1.3. Shortcomings of the diffuse cone model SmC descriptions 42

3.2.2.	Other ways of explaining a non-layer shrinkage SmA-C transition	43
3.3.	<i>The electroclinic effect and the de Vries SmA* models</i>	44
3.4.	<i>Two examples of tilting transitions without layer shrinkage</i>	45
3.4.1.	Determination of the phase sequence	45
3.4.2.	Measuring the orientational distribution	47
3.4.3.	The correlation between orientational distribution and smectic layer spacing	50
3.4.4.	The optical evidence for the validity of the diffuse cone model in the SmA*, SmC* and SmC _a * phases	51
3.4.4.1.	The peculiar natural textures	51
3.4.4.2.	The effects of an electric field on the optical properties	54
3.5.	<i>First- and second-order transitions to the SmC^(*) phase</i>	56
3.5.1.	Observations and predictions regarding the order of the non-layer shrinkage tilting transition	56
3.5.2.	The thermodynamics of the transitions in the 3M materials	57
4.	Electrooptic Mechanisms of Polar Liquid Crystals	59
4.1.	<i>Quadratic and linear field effects</i>	59
4.2.	<i>Electric helix unwinding in the SmC* and SmC_a* phases</i>	60
4.2.1.	Unwinding a SmC* helix	60
4.2.2.	The helix unwinding process in the SmC _a * phase	63
4.3.	<i>The dielectric signatures of switching non-helical, surface-stabilized, samples</i>	65
4.3.1.	Switching an SSFLC sample	65
4.3.2.	The SSAFLC Frederiks transition	66
5.	The Subphases of Antiferroelectric Liquid Crystals	69
5.1.	<i>A brief history of antiferroelectric liquid crystals</i>	69
5.2.	<i>Ferro-, ferri- and antiferroelectricity</i>	70
5.3.	<i>What is the repeating unit in the subphases?</i>	71
5.3.1.	The subphase terminology problem	73
5.4.	<i>Experimentally verified properties of the subphases</i>	74
5.4.1.	The SmC _α * phase	75
5.4.1.1.	The SmC _α * dielectric signature	75
5.4.1.2.	The birefringence of a planar SmC _α * sample	76
5.4.2.	The SmC _β * and SmC _γ * phases	77
5.5.	<i>The SmC* phase in AFLCs</i>	78
5.5.1.	The issue of smectic and nematic order in AFLCs	79
5.6.	<i>Can we find a convergent picture of the AFLC phase sequence?</i>	80
6.	The Effect of Confinement on Polar Liquid Crystals	81
6.1.	<i>How do surfaces affect the liquid crystal?</i>	81
6.1.1.	The encounter of polar surfaces and (anti-) polar smectics	82
6.2.	<i>Phase-angle fluctuations in thin cells</i>	82
6.3.	<i>The cell-gap dependence of the AFLC phase sequence</i>	85
6.3.1.	Surface-enhanced supercooling and phase coexistence	86

6.3.2. Subphase quenching 89

6.3.3. Metastable surface-induced structures 90

6.4. *Chevron and parabolic focal conic defects in antiferroelectric liquid crystals* 92

6.4.1. The formation of horizontal chevron defects at the onset of tilt 92

6.4.2. Horizontal chevrons in antclinic structures 94

7. Conclusions and Outlook 97

Appendix I.1. Hard core, chains and other essential ingredients 99

Appendix II.2. The molecules of polar liquid crystals 102

Appendix III.3. Molecular packing and freedom of movement in liquid crystal phases 103

1 LIQUID CRYSTALS AND THE DESCRIPTION OF IMPERFECT ORDER

'I shall begin at the beginning,' said the DHC, and the more zealous students recorded his intention in their notebooks: Begin at the beginning.

Aldous Huxley, Brave new world

OVERVIEW

In this chapter, the conceptual toolbox needed for the study of liquid crystals is developed. The different types of liquid crystalline order will be described, concentrating on thermotropic smectic and nematic phases. In connection to this, the fundamental concepts, such as director, order parameter and director tilt, are defined and their meaning in various liquid crystalline phases discussed. We end the chapter by discussing the general problems imposed by biaxiality in describing liquid crystalline order.

1.1 The liquid crystalline state

– a delicate balance in order

Liquid crystals are ordered fluids. They are liquids in the sense that the molecules have no, or limited, translational (or positional) order. In contrast to a solid crystal, where the molecules or atoms are located on the points of a three-dimensional lattice, the molecules in a liquid crystal phase are distributed more or less at random along all three, or at least two, directions of space. Unlike isotropic liquids, which possess only short-range order, liquid crystal phases are characterized by long-range *orientational order*. The molecules – which have an anisotropic shape – are (on the average) locally oriented in a common well-defined way, giving these materials anisotropic macroscopic properties. The intermediate role between fully ordered and completely disordered systems has given the liquid crystalline state the name *mesomorphic* state, and liquid crystal phases are sometimes referred to as *mesophases*. Likewise, a molecular structure generally compatible with the formation of liquid crystalline phases is called *mesogenic* and liquid crystal molecules *mesogens*. In the following, we will use these different terms alternately. (A good and compact overview of the present terminology situation is given in the introductory chapter by J. Goodby and G. Gray of the Handbook of Liquid Crystals [1].)

There are two fundamentally different types of liquid crystal: *thermotropics* and *lyotropics*. The difference is the origin of the mesomorphic order and the corresponding parameters regulating which phase is thermodynamically stable at a certain set of conditions. In the case of lyotropics, the mesogens (which are generally amphiphilic,

i.e. the two ends of the molecules have contrasting character) are dissolved in a suitable solvent, and the characteristic regulating parameter is the concentration of the solution. Thermotropics, on the other hand, exhibit liquid crystalline properties in their pure state and the basic parameter determining the phase is the temperature. Of course, also the pressure can be used as regulating parameter, but as liquid crystals are almost always used as well as studied under atmospheric pressure, the role of the pressure is often forgotten. The optical and dielectric anisotropies of thermotropic liquid crystals, together with the liquid-like ease of reorienting the molecules, make them ideal materials for many electrooptic devices such as flat panel displays, sensors, optical switches, etc. While the last few years have shown a tremendous development of such devices, in particular flat, thin computer displays, the commercial importance of thermotropics is still far behind that of lyotropics. The simple reason is that all detergents are actually lyotropic liquid crystals. However, the study of thermotropics can in many respects, in particular for a physicist, be considered as more interesting and fascinating. While lyotropic liquid crystals from a physical standpoint are still mainly understood in a geometric and crystallographic description, and are much closer to the realm of physical chemistry than to chemical physics, the analytic physical description of thermotropic liquid crystals is far more advanced (*cf.* the classical treatises by de Gennes - Prost and Chandrasekhar [2, 3]).

The shape of the anisotropic mesogenic molecules can vary substantially between different thermotropic compounds. Most compounds belong to the class of rod-like, or *calamitic*, liquid crystals. Other shapes which one may encounter in the study of liquid crystals are disc-like (such compounds are either called *discotics* or *columnars*, the latter name given due to the organization of the discs into columns) and bowl-like. In this thesis, lyotropic liquid crystals will not be treated at all, and among thermotropics we will restrict ourselves to the calamitics. The term ‘liquid crystal’ should in the following therefore be interpreted as ‘calamitic thermotropic liquid crystal’. The direction of the ‘rod’, *i.e.* the long molecular axis, will be denoted by the symbol **m**.

A thermotropic liquid crystal has, like other materials, a solid phase (normally crystalline, containing both orientational and 3D translational order) and a liquid (isotropic) phase. However, at temperatures between these two states the material has one or more intermediate mesomorphic phases, all characterized by the presence of orientational order. They may differ in the degree of this orientational order, but also in whether or not any translational order is present. Depending on the latter, liquid crystal phases are categorized into two basic classes: the *nematic*¹ phase, which is positionally completely disordered, and the *smectic*² phases, which in addition to the orientational order possess translational order in one dimension as seen through a layered structure. Within the layers the molecules are, however, distributed without long-range translational order, and the smectic molecular organization can thus be said to be equivalent to a two-dimensional liquid.

1. The name *nematic* comes from the Greek adjective νηματικός (*woven*), in turn derived from the Greek word for *thread*, νήμα. It refers to the threadlike defects which are typical of the phase when observed through a polarizing microscope.

2. Smectic phases were first observed in ammonium and alkali soaps, and hence the phases are named after the ancient Greek word for soap, σμῆγμα. The names *nematic* and *smectic* were introduced in 1922 by George Friedel.

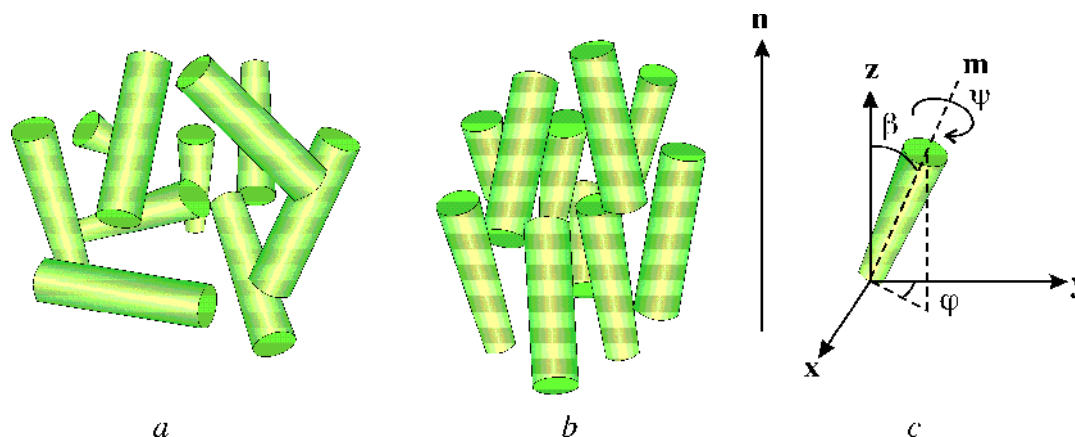


Figure 1.1 Schematic illustrations of the isotropic (a) and nematic (b) phases. Neither phase possesses translational order, but at the transition to the nematic phase, the molecules tend to align along a preferred direction, given by the director \mathbf{n} . The nematic phase has cylindrical, $D_{\infty h}$, symmetry, with order in the angle β , but not in φ and ψ (c).

1.2 Nematic order and the director concept

The nematic phase (abbreviated N) is the simplest type of mesomorphic organization we can imagine, and for compounds exhibiting a nematic phase it is therefore the first liquid crystal phase which we encounter when we cool it from the isotropic liquid³, *c.f.* figure 1.1 a and b. At the phase transition, the symmetry of the system is reduced from spherical to cylindrical (crystallographic point group $D_{\infty h}$ [4]) reflecting the appearance of long-range orientational order. The symmetry axis (the ‘cylinder axis’) is a local direction along which the molecular long-axes \mathbf{m} prefer to align. It is traditionally described by a unit vector called the *director*, generally denoted by the symbols \mathbf{n} or \hat{n} (in this thesis I will use the former notation). The director has no sign ($\mathbf{n} = -\mathbf{n}$) *i.e.* up and down are equivalent. The orientational order is far from perfect in liquid crystals so in practice \mathbf{m} will not be parallel to \mathbf{n} , but fluctuate around this direction. Macroscopic anisotropic properties reflect the orientation of the director, *e.g.* the optic axis in a uniformly aligned (non-chiral) nematic liquid crystal sample will be along \mathbf{n} .

The director sign invariance applies to all liquid crystal phases⁴, including the chiral ones, which will soon catch most of our attention. A chiral molecule is a molecule which may exist in two enantiomeric forms, meaning that the two forms are mirror images of each other. The word *enantiomeric* is derived from the Greek, meaning ‘opposite’ and the two forms are distinguished in the *R/S* nomenclature, denoting right- and left-handedness, respectively. Under certain circumstances, the two forms may coexist in equal quantities, in which case the material is said to be *racemic*. When speaking of chiral molecules in the following we will not include this case. If the rod-

3. Certain chiral nematics also exhibit phases referred to as blue phases in a small temperature range between the nematic and the isotropic phase.

4. The observation of a special SmA-type phase, characterized by a uniform ordering within the layers of the longitudinal molecular dipoles, has been claimed, but its existence is a controversial question. If it exists, this phase might constitute an exception.

like molecule building up the nematic phase is chiral (or if the nematic has been doped with solvable chiral molecules) the phase is called *chiral nematic* and denoted N^* . For historical reasons the N^* phase is also referred to as the *cholesteric* phase. It has the reduced symmetry D_∞ – the chirality removes the mirror plane – but the director still obeys the $\mathbf{n} = -\mathbf{n}$ condition.

The cylindrical symmetry of the nematic phase allows order only in the angle β , describing the inclination between the long axis \mathbf{m} of a rod-like molecule and the director (see figure 1.1 c). The orientational fluctuations in the nematic phase are centered around $\beta = 0$, describing the tendency of the molecules to align with \mathbf{m} parallel to \mathbf{n} . Any preference on a global scale in the azimuthal angle φ or the angle ψ , expressing rotations about \mathbf{m} , would violate the cylindrical symmetry and hence such order is absent in the nematic phase (locally, the situation may be slightly different, *cf.* appendix A.3). For describing the degree of orientational order in a nematic, a single scalar order parameter is thus sufficient, and the first thought might be to use the average molecular inclination with respect to the director, $\langle \beta \rangle$. However, since an order parameter should preferably be zero at total disorder and one at perfect order, this would not be a very convenient choice. Instead we base the order parameter on the average long-axis projection on the director, $\langle \cos \beta \rangle$, which is maximum when \mathbf{m} is parallel to \mathbf{n} . Next, due to the head-tail symmetry imposed by the $\mathbf{n} = -\mathbf{n}$ condition, we take the square of this quantity, $\langle \cos^2 \beta \rangle$. This will indeed be one for perfect order, *i.e.* if all ‘rods’ are aligned with the director, but at complete disorder, when all values of θ are equally probable, $\langle \cos^2 \beta \rangle = 1/3$. In order to normalize the order parameter, we therefore choose the expression:

$$S = \frac{1}{2}(3\langle \cos^2 \beta \rangle - 1) = \langle P_2 \rangle \quad (1.1)$$

This form of the orientational order parameter was first introduced by P. H. Hermans in 1939 and adopted for liquid crystals three years later by Tsvetkov. The right-hand side of equation (1.1) indicates that we recognize this expression as the average of the second Legendre polynomial of $\cos \beta$, denoted $P_2(\cos \beta)$, and sometimes we therefore see the nematic order parameter denoted by the symbol $\langle P_2 \rangle$ instead of the more common choice S . The order parameter can be experimentally determined by means of for instance birefringence measurements or X-ray diffraction experiments. It turns out that S in the nematic phase typically increases from 0.4 close to the clearing temperature up to 0.6 or 0.7 on cooling. The fact that one always sees a jump from $S = 0$ to $S \sim 0.4$ at the isotropic to nematic phase transition reflects the first-order nature of this transition. The upper limit of S shows that the nematic phase is always substantially disordered – more ordered phases, smectic or crystalline, become stable long before the nematic phase would approach an order parameter of $S = 1$.

The orientational order parameter in equation (1.1) is often referred to simply as the nematic order parameter. However, its application is not restricted to the nematic phase but one often speaks of the nematic order, meaning simply the degree of orientational order, also in the case of smectic phases. For uniaxial smectics, one can still use S which thus is a very useful parameter with large importance for the discussion in this thesis. It is illustrative to expand equation (1.1) up to second-order terms in β :

$$S \approx 1 - \frac{3}{2} \langle \beta^2 \rangle + \dots \quad (1.2)$$

Even though equation (1.2) is valid strictly only in the limit $S \rightarrow 1$, we can use it to get a rough estimate of the root mean square inclination of the long molecular axis \mathbf{m} with respect to the director \mathbf{n} , even at a certain degree of disorder. If we insert the highest typical nematic order, $S = 0.7$, in equation (1.2), we obtain an average molecular inclination of $\sqrt{\langle \beta^2 \rangle} \approx 26^\circ$, *i.e.* quite a substantial inclination. (Note that in equation (1.2) the angle is given in radians.) In the smectic phases, the nematic order does not increase very much – typically S reaches values in the order of 0.8 – which means that also in smectics we must expect a fairly high average long-axis inclination with respect to the director.

1.3 The smectic phases

– *stacks of two-dimensional liquids*

1.3.1 The smectic A phase

The nematic phase will not be discussed much in this work, but instead we will concentrate on the more ordered smectics. A number of different smectic phases exist, varying in degree of orientational order (‘orthogonal’ and ‘tilted’ phases), in-layer translational order (liquid-like layers or layers with short-range translational order), or both. Following the chronological order of their discovery, the smectic phases are named smectic A, smectic B, smectic C, etc., but most often the corresponding abbreviations SmA, SmB, SmC, ... are used. The most important smectic phase is SmC, the chiral versions of which will play the lead role of this thesis. There is, however, good reason to discuss also a few other smectic phases, and I will begin with the simplest one, the smectic A.

The difference between the nematic and the smectic A phase is the appearance of translational order along the director. The point group symmetry is the same, $D_{\infty h}$, but the translational symmetry is spontaneously broken at a phase transition from the nematic to the SmA phase (the phase following SmA at higher temperature is generally either the nematic phase or the isotropic phase⁵). The layers in the SmA phase are formed such that the director is oriented along the layer normal (in this thesis denoted \mathbf{k}), and the phase is therefore called an ‘orthogonal’ smectic phase, referring to the orthogonality between the layers and the director. However, it is not uncommon to find this attribute interpreted as if the molecules were oriented with their long axes essentially perpendicular to the layers, a picture which is actually much further away from the truth than one might first realize. The reason is that the orientational order is only little higher in SmA than in the nematic phase, and as shown above, there is thus a substantial average angle between the director and the long molecular axes. This important fact, and its far-reaching consequences for the smectic layer structure, will be discussed extensively in chapter 3.

5. In chiral smectic compounds, there may also be special smectic phases referred to as Twist Grain Boundary (TGB) phases above the SmA* phase.

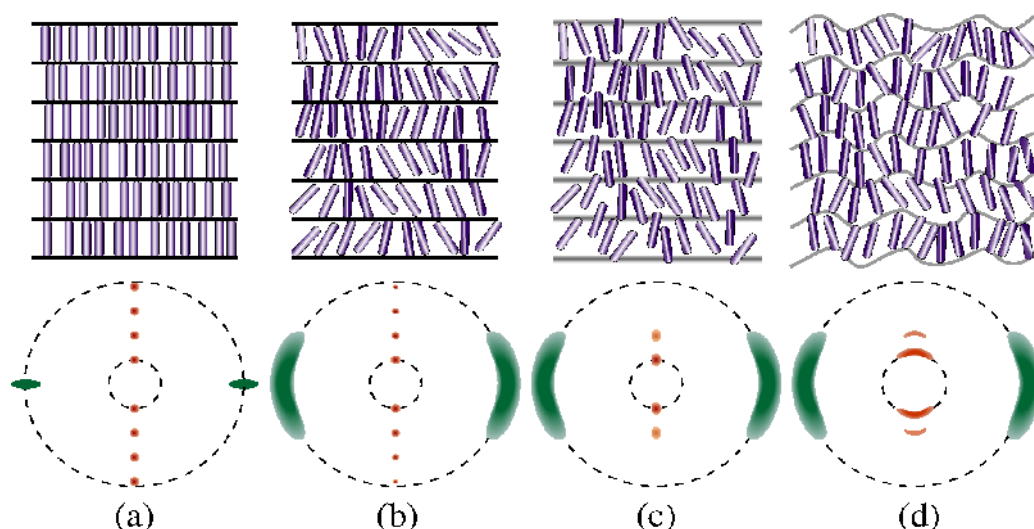


Figure 1.2 Various simplified sketches of the molecular arrangement (with molecules simplified to rigid rods) in a smectic A phase (upper row), and the diffraction pattern which would arise from each one in an X-ray scattering experiment on an aligned bulk sample (lower row). The aligning magnetic field is thought to be directed vertically. The scattering peaks due to the layer periodicity then fall on a vertical line, the peaks due to the intra-layer lateral molecular spacing on a horizontal. The different cases are (a) perfect orientational and one-dimensional translational order along the layer normal \mathbf{k} , (b) perfect translational order along \mathbf{k} but imperfect orientational order, (c) imperfect orientational and translational order (interdigitation) with straight layer interfaces, and (d) imperfect orientational and translational order with undulating layer interfaces.

One of the most important experimental techniques to study the molecular organization in liquid crystals is X-ray scattering. It is instructive to consider which types of X-ray diffraction patterns could be expected from different imaginable types of smectic organization and to compare the results with the actual diffractograms obtained from real samples. In figure 1.2, the SmA-type of organization of rod-like molecules is drawn (for simplicity, strictly two-dimensionally and without considering the effect of the disorder on the layer spacing) with varying degree of simplification. In the lower row, the two-dimensional X-ray diffraction patterns which could be expected from an aligned sample of each type are drawn, very schematically. The aligning magnetic field, defining the *meridional* direction, is thought to be vertical, and the X-ray beam is supposed to be directed out of the paper.

In the left-most example, figure 1.2 a, the SmA-type order is exaggerated to the degree of one-dimensional crystallinity, *i.e.* perfect orientational and translational order along the layer normal \mathbf{k} prevails. In the diffraction pattern this situation is reflected in two sets of well-focused spots. The closely spaced spots on the meridian correspond to the order along \mathbf{k} , *i.e.* the spacing reflects the typical layer thickness of $\sim 30\text{\AA}$. The sharpness of the spots shows that the layers are straight, the layer spacing is constant and the correlation length is very large. As the orientational and translational order along \mathbf{k} is perfect, the density variation along the layer normal will qualitatively be equal to a translational replication of the density variation along a single molecule. This means that we are as close to a rectangular density wave as we can possibly be, resulting in higher orders of diffraction maxima clearly visible within the limits of the diffractogram. The wide-angle diffraction peaks, located on the equator (the direction perpendicular to the magnetic field), reflect the in-layer order. The much smaller average molecule spacing in this direction, typically $4\text{-}5\text{\AA}$, is reflected in the larger diffraction angle, hence a larger radial distance between the center of the diffrac-

togram and the maxima. The absence of perfect translational order along the layers means that we have a distribution of inter-molecular distances, which is reflected in the wide-angle maxima being smeared out radially.

In the next case, *b*, we add orientational disorder. This will smear out the wide-angle maxima azimuthally, reflecting that periodic structures can now be found also along directions close to, but not necessarily exactly parallel to the layers. The orientational disorder should also lead to slightly softer density variation along \mathbf{k} , as the centers of mass are no longer necessarily located exactly in the middle of the layers. As we still restrict ourselves to sharp layer boundaries, repeated regularly over infinite distances, the effect on the small-angle scattering is small, but we would expect higher order peaks to become increasingly weak. In the next case, *c*, we have also allowed for a large degree of molecular interdigitation through the layer boundaries. The rectangular density variation along \mathbf{k} is thus replaced by a more or less sinusoidal one, resulting in the disappearance of higher orders of diffraction maxima along the meridian. The range of constant phase of this density wave (that is, the range over which the layer boundaries fall on the points of a one-dimensional lattice, *i.e.* the correlation length) is now finite, leading to more diffuse peaks. In the final sketch, *d*, we have in addition let go of the condition that the layers should be straight. This results in an azimuthal smearing out of the small-angle scattering peaks and we end up with a diffractogram which has no well-focused spots, but only diffuse arcs of varying size.

Let us now compare the above sketches with a real smectic A diffraction pattern. In figure 1.3, upper row, right column, the wide-angle X-ray scattering pattern from the SmA phase of the achiral liquid crystal compound 8OCB is shown. Comparing with the models in figure 1.2, it is clear that the most realistic description is somewhere between cases *c* and *d*, *i.e.* a high degree of orientational and in-layer translational disorder coupled with some molecular interdigitation through slightly undulating layer boundaries. In general, the radial smearing out of the layer spacing diffraction peak is very small, smaller than the practical resolution of most experimental equipment, indicating that the layer spacing is indeed very well defined and that the periodicity along \mathbf{k} can be described as quasi-long range [5].

One can take the above reasoning one step further and really ‘simulate’ X-ray diffraction patterns from a proposed liquid crystalline system. Chistyakov has described experiments where photographic masks with patterns similar to that in figure 1.2 *d*, upper row, were manufactured. The features were reduced to a size suitable for optical diffraction, and then the laser diffraction pattern was recorded [6]. The result was very similar to the typical X-ray diffractograms recorded with real SmA samples, as in figure 1.3.

To describe the order of a stratified mesophase the orientational order parameter S is no longer sufficient – we also need some way of describing the translational order along \mathbf{k} . Such an order parameter is generally referred to as a smectic order parameter and often denoted by σ or τ . Unfortunately, the task of describing the smectic order is much more complex than that of describing the orientational order, simply because of the many aspects of the order along \mathbf{k} . We can think of at least four aspects which one might want to take into account:

- the *amplitude* of the density wave along \mathbf{k} , *i.e.* the difference in molecule density between the layer centers and the layer boundaries
- the *type* of density modulation, ranging from sinusoidal at the low-order extreme to a perfect translational replication of the single-molecule density

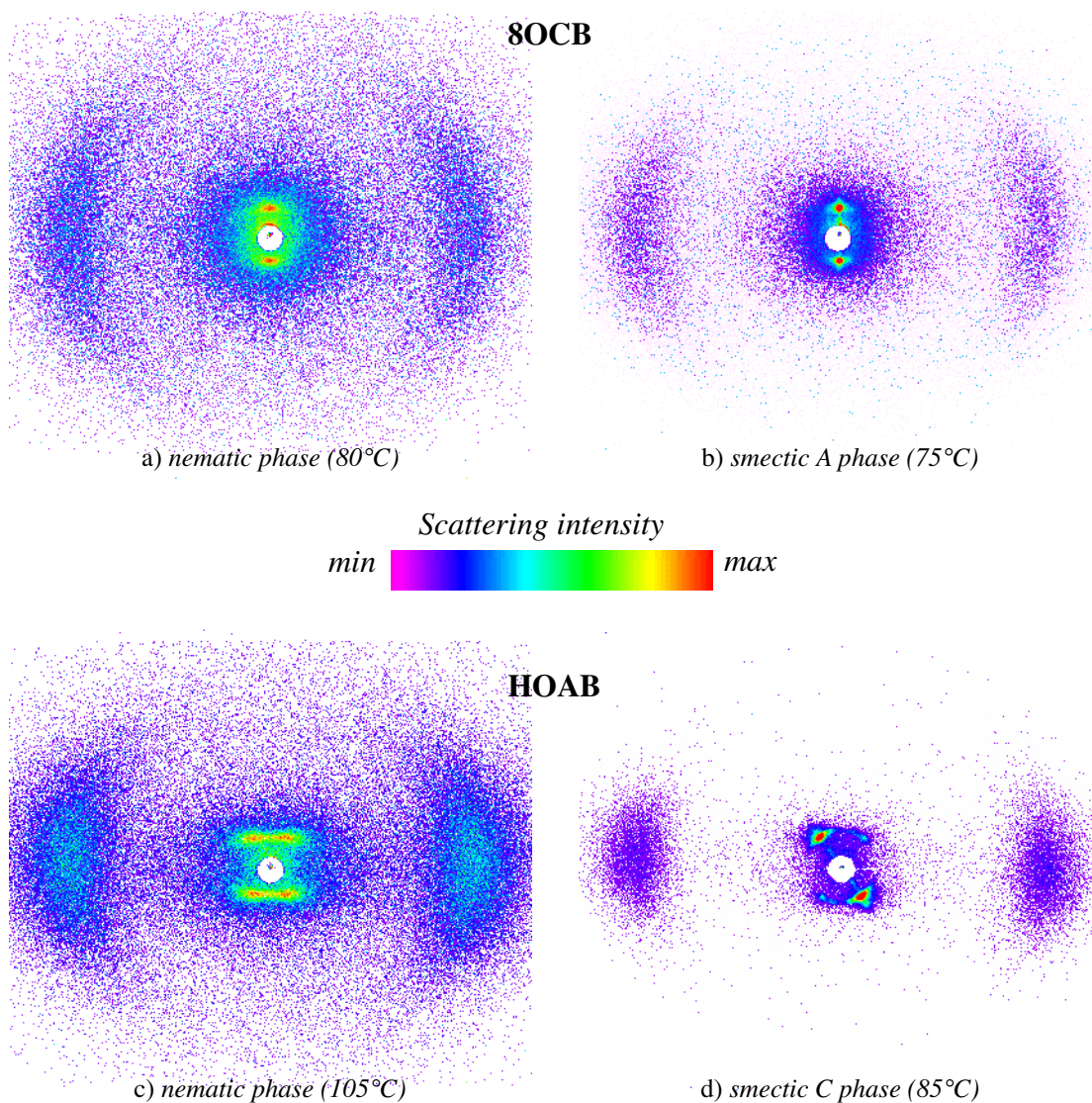


Figure 1.3 Transitions from the orientationally ordered nematic phase (left column) to an orientationally and translationally ordered smectic phase (right column), as seen through X-ray scattering from aligned samples of two achiral liquid crystals. Upper row: 8OCB; lower row: HOAB. The arc-like wide-angle diffraction maxima lying on the equator (horizontal), reflecting the liquid-like in-layer order, are fairly similar in the left and right pictures of each row. The orientational order is thus not so much affected by the nematic-smectic transition. In the nematic phase, smectic-like fluctuations (cybotactic clusters) give rise to easily visible small-angle features: the translational order of the lower-lying smectic phase is announced by quite strong but diffuse peaks at radii corresponding to the smectic layer spacing. In 8OCB, where the low-temperature phase is the orthogonal SmA phase, there are two such peaks located on the meridional line (vertical, along the aligning magnetic field). In the case of HOAB, exhibiting a direct N-SmC transition, the tilted geometry is present already in the cybotactic clusters (which are therefore referred to as ‘skewed’) and the small-angle regime exhibits four maxima. The angle between the maxima and the meridional line is equal to the angle between the layer normal and the director. The latter is fixed by the magnetic field, resulting in an inclined layering. In the right picture, two of the four peaks have almost disappeared, indicating that one of the two possible layer directions was rejected when cybotactic clusters merged into a long-range stratified structure at the transition to SmC. For each compound, the exposure time and contrast are the same in both pictures. The 8OCB pictures are courtesy of F. Gießelmann.

variation in the crystalline case

- the *correlation length* of the translational order
- the *shape* of the layer boundaries (straight or undulating).

Restricting ourselves to the first two aspects (the other two are much more difficult to describe analytically), a generic smectic order parameter would be an infinite sum of harmonic functions, corresponding to the Fourier components of the density wave. For practical reasons, it is customary to limit oneself to the first term, thus restricting the description to sinusoidal density waves. The basic smectic order parameter is then [7]:

$$\sigma = \left\langle \cos \frac{2\pi z}{d} \right\rangle \quad (1.3)$$

where z denotes the position along \mathbf{k} of each molecule included in the averaging, and where we have introduced the symbol d to denote the smectic layer spacing. In the following we will often use this shorthand. This solution obviously has the drawback of completely neglecting the second aspect of smectic order listed above, instead assuming a sinusoidal modulation. As discussed in paper 4, this aspect actually seems very important in the case of antiferroelectric liquid crystals, and the usefulness of the most common smectic order parameters is therefore limited. Hence, when we speak of high or low smectic order, it is not just a question of a high or low value of a certain choice of order parameter, but rather of all aspects of smectic order listed above, with emphasis on the first two. In order to get an estimate of the type of the density variation one can measure the intensities of the first-, second- and possibly third-order layer diffraction peaks in an X-ray scattering pattern [8, 9]. If the intensity falls off rapidly with increasing peak-order, the density wave is more sinusoidal, whereas strong second- and third-order peaks indicates a high smectic order.

1.3.2 *Tilted smectics*

The point group symmetry of the SmA phase is $D_{\infty h}$ and the director is thus confined to the direction of the layer normal \mathbf{k} . If we remove the condition of cylindrical symmetry, this restriction disappears, *i.e.* there can be a non-zero angle θ between the director \mathbf{n} and \mathbf{k} . (Note that this also means that the very simple, inherently cylindrically symmetric, definition of the director which we used above is no longer strictly valid, *cf.* section 1.4.) This geometry is what we find in the biaxial⁶ smectic C phase, for which the tilt angle θ is normally taken as the primary order parameter. However, to fully describe the SmC geometry it is not enough to express the magnitude of tilt, but we must also give its direction. This is usually accomplished by introducing the *azimuthal*, or *phase*, angle φ . Thus, the complete order parameter of the SmA-C tilting transition must have two components. It can conveniently be written in complex form, $\psi = \theta e^{i\varphi}$.

6. Optical biaxiality and uniaxiality can be understood in terms of the optical indicatrix. If this is cylindrically symmetric, there is only one circular cross section, the normal of which is the symmetry axis. Light propagating along this direction experiences no birefringence, hence this must be the optic axis of the system which, consequently, is called uniaxial. If the three principal axes of the indicatrix instead are different from one another, there will be two circular cross sections of the indicatrix. Their normals then define the two optic axes of the system, which is biaxial.

An alternative way of expressing the tilt direction is to define a unit vector along the projection of \mathbf{n} onto the layer plane. This construct was introduced by de Gennes [2] who called it the *C-director*, abbreviated \mathbf{c} . The name reflects the similarity with the director \mathbf{n} of the nematic phase: a *quasi-homeotropic* (layers, and hence C-director, parallel to the substrates) SmC sample will in the polarizing microscope look very much like a planar-aligned nematic (director \mathbf{n} parallel to the substrates), with the same type of characteristic disclinations (with the important difference that disclinations of strength $\pm 1/2$ are not possible in the SmC phase [2]). Furthermore, the range of the order in \mathbf{c} is similar to that of \mathbf{n} in the nematic and the types of fluctuation are also similar. However, an important difference between \mathbf{n} and \mathbf{c} is that the latter has a sign, $\mathbf{c} \neq -\mathbf{c}$.

The choice of ψ as order parameter for the smectic C phase is not an unproblematic one. It may first of all seem that ψ actually describes neither the orientational nor the translational order at all. The magnitude θ and direction φ of tilt only describe the geometry of the phase – they say nothing about the magnitude of the fluctuations around the director, nor about the nature of the layer interfaces. In the nematic and SmA phases, the orientational order is described by the scalar order parameter S , but this is unfortunately not a solution for the SmC phase. S is by definition a cylindrically symmetric order parameter and therefore cannot describe the orientational order in the smectic C phase, where this symmetry is absent. This is only one aspect of the increased degree of complexity in the liquid crystalline order, imposed by the appearance of director tilt. We will return to this issue towards the end of this chapter.

Without a parameter describing the fluctuations in orientational order, it is not obvious why a tilted smectic should be regarded as more ordered than an orthogonal one – we might have exactly the same degree of orientational disorder, only with the energy-minimizing orientation changed. However, the tilt at least leads to a lower symmetry than in SmA, and a lowering of the symmetry usually means that the order increases. We will furthermore see in chapter 3 that one can actually model the onset of tilt in a way such that θ is a direct manifestation of increased orientational order. For now, we will just accept the idea that the SmA-C transition constitutes an increase in order. This correlates well with the fact that the SmC phase always appears at lower temperatures than SmA for mesogenic compounds exhibiting both phases.

The SmC phase is not necessarily preceded by an SmA phase at higher temperatures. In figure 1.3, lower row, some very illustrative X-ray diffraction patterns from the compound HOAB, exhibiting a nematic - SmC phase sequence on cooling, are reproduced. Such a phase sequence means that the translational order appears simultaneously with the director tilt, and this leads to some rather peculiar characteristics of the transition. When a SmA phase forms on cooling from the nematic, the first signs of translational order observed in an X-ray experiment will be the appearance of small-angle peaks centered on the meridional line, as seen in the upper row of figure 1.3, where the diffractograms of the N-SmA transition of 8OCB is shown. When the smectic phase forming is instead SmC, the direction of the layers will no longer be perpendicular to the director, hence to the magnetic field, and the small-angle peaks will show up at a certain angle away from the meridian. Above the phase transition, the pre-translational fluctuations will lead to small volumes of stratified positional order rapidly appearing and disappearing. As the only direction which is fixed is that of the director, set by the magnetic field, there will be just as many ‘pseudo-strata’ inclined with a positive angle to \mathbf{n} as those with a negative angle, and thus we will see four symmetrically positioned small-angle peaks in the nematic phase. These peaks were in the early

1970s studied by Adrian de Vries and co-workers [10] who gave the pseudo-strata the name *skewed* (in the case of the N-SmC transition) *cybotactic clusters*. Below the phase transition, two of the cybotactic peaks have disappeared, indicating that one of the two possible layer inclinations dominated over the other as the translational order increased from fluctuating short-range to stable long-range.

The formation of tilted layers directly from the nematic phase, and the more or less temperature-independent tilt angle connected to such a transition, can be easily understood by considering what drives the transition from the nematic to the smectic phase. Of course, there is no global layer structure latently present in the nematic phase which tells the molecules how to order below the transition to the smectic phase. Instead, it is the lateral interactions between adjacent molecules which render a certain positional correlation between neighbor molecules energetically favorable to others. The interactions may for instance be between lateral molecular dipoles. Below the transition to the smectic phase, the molecules will (in principal) adopt the optimum positional correlation on a global scale, which means that the smectic layers are formed. If the optimum positional correlation is with molecule ends next to neighboring molecule ends, a smectic A phase is formed, *i.e.* the director will be parallel to the layer normal. But if the optimum choice for a molecule is to keep its center part close to the external parts of the neighbor molecules, the smectic phase will instead be a tilted smectic C. The tilt angle will depend mainly on how the molecules best pack relative to one another, which means that the tilt angle in this case is set mainly by the molecular constitution, for instance with respect to the positions of lateral dipoles. Hence, the tilt can be expected to be quite temperature-independent.

1.3.2.1 Syn- and anticlinicity

Towards the end of the 1980's, it became clear that there are actually several different variants of the smectic C phase. As we will see in the following chapter, the chiral version of the ordinary SmC phase (denoted SmC*) can, under certain constraints, develop *ferroelectric* properties. The SmC* phase has a local non-zero spontaneous polarization. In some special chiral tilted smectics with very high value of this polarization, the first examples of *antiferroelectric* phases were observed, as well as a few so-called subphases with unclear properties and small temperature range of stability. In the beginning of the analysis of these new phases, it was contemplated that the tilt magnitude, as well as the tilt direction, could change throughout the sample, but it was soon concluded that the former is a global variable, *i.e.* there are no spatial variations in the equilibrium magnitude of the director tilt. Instead it became clear that a constant tilt direction is not always the case, and that the antiferroelectric phase was a phase where the tilt direction alternates from layer to layer. Such a structure is referred to as *anticlinic*, as opposed to the *synclitic* normal SmC phase, where the director tilts in the same direction in adjacent layers. In order to distinguish it from the ordinary SmC phase, the anticlinic variant is usually denoted SmC_a or SmC_A, where the index is best interpreted as either “anticlinic” or “alternating tilt”⁷.

7. Not seldom, the *a* is interpreted as “antiferroelectric”. This is however misleading, since the anticlinic SmC_a structure occurs also for achiral or racemic liquid crystals, which are not polar, and thus should not be called antiferroelectric. (One may call an antiferroelectric phase anti-polar, but this is quite different from non-polar.) In this thesis, I have chosen to use lower-case *a* as the index for the anticlinic phase, SmC_a, since capital letters in the case of smectics are already used for the main phase designation.

If a tilted smectic structure forms directly from a nematic phase, it must obviously have the director leaning in the same direction away from the layer normal in consecutive layers, *i.e.* it must be the synclinic SmC phase. Lately, a large interest has arisen in high-tilt antiferroelectric liquid crystals due to their peculiar optical properties, *cf.* paper 5. The usual way of finding a high-tilt smectic C is, as discussed above, to look for a material with a direct transition from the nematic to the tilted smectic phase. As this solution is not available in the case of the SmC_a* phase one instead focuses on materials with a first-order transition from the SmA* phase to the tilted phase. The anticlinic SmC_a structure is actually observed only in compounds which exhibit no nematic phase at all. The lack of nematic phases in antiferroelectric liquid crystals can tell us something about the processes giving rise to anti- or synclinic structures.

1.3.3 Ordering the liquid

– the higher-order smectics and the soft crystals

While the different variants of smectic C, as well as the smectic A phase, have no in-layer translational order at all, such order to some extent exists in the other smectic liquid crystal phases, SmB, SmF, SmI, and their different modifications, often collectively referred to as ‘higher-order smectics’. These phases will not be given any principal attention in this thesis, but, as the chiral SmI* and its anticlinic variant SmI_a* are quite common in antiferroelectric liquid crystals we should spend a few words on giving a very brief description of the order also in these phases.

The high-ordered smectic phases all exhibit so-called *hexatic* in-layer translational order, which means that the molecules locally are hexagonally close-packed. There is however no long-range translational order within the layers, a property which distinguishes the high-ordered smectics from the many phases which have earlier been called smectic but are today recognized as ‘smectic-like’ soft crystal phases [11]. These are today called Crystal B, E, G, H, J, K and abbreviated only with the capital letter, without the prefix “Sm” [1]. The hexatic order is such that two groups of molecules separated by more than some 70 nm will not be located on the same hexagonal lattice in the SmB, SmF or SmI phase. The SmB phase (not to be mixed up with the Crystal B phase) is orthogonal while SmI and SmF are tilted. The difference between the latter two phases is that the tilt in SmI is along the hexagonal grid lines, towards the nearest neighbor, while the molecules in SmF tilt towards the next-nearest neighbor, ‘into’ the triangle building up the hexagon (see the illustrations in [11]). Chiral smectic I exists in a synclinic as well as in an anticlinic version, SmI_a*. On the other hand, an

Table 1.1 The most important chiral smectic phases and their types of order

Phase	Director tilt relative to layer normal	In-layer (short-range) translational order
SmA*	No tilt	No order
SmC*	Synclinic	No order
SmC _a *	Anticlinic	No order
SmI*	Synclinic	Hexagonal order
SmI _a *	Anticlinic	Hexagonal order

achiral SmI_a phase, or anticlinic versions of smectic F (chiral or achiral), have to the best of my knowledge so far not been observed. The varying order in the most important chiral smectic phases is summarized in table 1.1.

1.4 The director concept in biaxial liquid crystals

The lack of a symmetry axis coinciding with the director \mathbf{n} in the tilted smectic phases makes the definition of \mathbf{n} slightly problematic. It must be perpendicular to the axis of rotational symmetry, the C_2 -axis, (*cf.* section 2.1) but otherwise there are no fundamental restrictions on the direction of \mathbf{n} . It is desirable from a practical point of view to relate it to the orientation of macroscopic observables, such as the long axis of the optical indicatrix, the *slow axis*. In uniaxial, cylindrically symmetric phases, such as the nematic and SmA phases, where the slow axis coincides with the optic axis, this works fine. But the slow axis of the chiral SmC^* and SmC_a^* phases in bulk will be along the layer normal \mathbf{k} if the pitch of the helicoidal structure is short enough (in the order of $1 \mu\text{m}$). In a non-chiral SmC, the indicatrix is biaxial with its long axis in the tilt plane. In case of a non-helical anticlinic phase the slow axis is along \mathbf{k} , but the indicatrix is biaxial, with the optic axes generally located in the plane spanned by \mathbf{k} and the C_2 axis [12]. No one would here say that \mathbf{n} coincides with \mathbf{k} , but rather that \mathbf{n} either precesses around \mathbf{k} , as in helicoidal SmC^* , or alternates in tilt direction, as in the anticlinic phases.

In general, the view of the director as the time average (or local space average) direction of the molecular long axis (or rather, the axis of inertia of the most probable molecular conformation) \mathbf{m} prevails, and unless otherwise stated, this is how we interpret the director concept in this thesis. The problem is that there is no experimental way of exactly determining \mathbf{n} defined in this way. In practice, we are left with three approximative approaches. The biaxiality of SmC and SmC_a is generally so small that it for most practical purposes can be neglected, and the director is therefore often approximated with the experimentally determined slow axis direction. This will then give us the *optical tilt angle*. However, it actually turns out that the optical indicatrix orientation of SmC (and all other tilted smectics) has a quite substantial wavelength dependence [13], rendering the optical tilt angle unambiguous only if the wavelength at which it is defined is specified. Furthermore, the only way of measuring the optical tilt angle in the case of SmC_a^* is to switch it to the synclinic state. The characterization of the optical indicatrix of the SmC_a^* phase in its *anticlinic* state is a non-trivial issue (conceptually and practically) which becomes particularly interesting in the case of high-tilt ($\theta \sim 45^\circ$) antiferroelectric liquid crystals, also referred to as *orthoconic AFLCs*, *cf.* paper 5.

Another common alternative is to measure the smectic layer spacing d_C at the temperature where we want to determine the tilt, and compare this with the corresponding value d_{AC} at the SmA-C transition temperature. Through the assumption that the layers shrink according to the tilting of the director (an assumption which is not at all uncontroversial, as will be shown in chapter 3), we can then calculate the *small-angle X-ray tilt angle* θ_{SAXS} (also called *structural tilt angle*) from the relation

$$d_C = d_A \cdot \cos\theta_{SAXS} \quad (1.4)$$

where all variables refer to spatial and temporal *average* quantities, since this averaging is inherent to the X-ray experiment.

The experimentally determined tilt angle which probably comes closest to the true director tilt angle θ , is also extracted from X-ray measurements, but as it is impossible to obtain for many compounds, and requires a slightly more complicated experiment in the case that it can be obtained, one does not encounter this as often as the optical tilt or the small-angle X-ray tilt. If one performs an X-ray scattering experiment on an *aligned* sample (we require a uniform direction of the layer normal as well as of the director across the sample area which is exposed by the X-ray beam) and records the two-dimensional scattering pattern where both the wide- and small-angle scattering peaks are visible (*e.g.* figure 1.3 *b* and *d*), one can extract the *wide-angle X-ray tilt angle* θ_{WAXS} . The wide-angle scattering peaks appear perpendicular to the average direction of an axis which depends on the electron density across the molecule, where the average includes orientational as well as rotational fluctuations. To a good approximation this axis coincides with the axis of inertia of the molecule, and its average direction is thus close to the director as defined above. The layer normal direction is easily found from the locations of the small-angle scattering maxima, and the tilt angle θ_{WAXS} is thus easily found as $90^\circ - \alpha$, where α is the angle between the SAXS and WAXS maxima.

As pointed out by Giebelmann *et al.* [13], the problems in defining the director are not only of geometrical nature, but the choice of the tilt angle θ , defined as the angle between \mathbf{k} and \mathbf{n} , as the order parameter for the SmC phase actually becomes unsatisfactory from an experimentalist's point of view. Of course, the free energy of the phase, which is often described by a Landau expansion in terms of the order parameter, cannot depend on how a certain variable is measured, but the tilt angle value obtained by X-ray diffraction is indeed very different from that obtained optically, and the optical tilt in turn depends on the wavelength chosen. In experimental work aimed at determining coefficients of the Landau expansion, different results should be expected depending on the exact choice of tilt angle definition. In this thesis, the symbol θ is reserved for denoting the tilt of the *director*, defined as the most common direction of \mathbf{m} , and thus without taking its experimental detection into account. All experimentally determined tilt-angles, optical, X-ray, or others, will be denoted by other symbols.

While tilted smectic phases are generally (weakly) biaxial [12], biaxiality does not imply that \mathbf{n} and \mathbf{k} are not parallel. Actually, the category smectic C originally referred to *biaxial*, not necessarily tilted, smectics with liquid-like in-layer order. Hence, when discussing the hypothetical biaxial smectic phase with \mathbf{n} parallel to \mathbf{k} , de Gennes called this phase smectic C_M [2], where the index M stands for McMillan, who was the first to discuss the possibility of such a phase. Today, the meaning of smectic C has shifted, and the tilt is the primary characteristic. Thus, the biaxial orthogonal smectic (the existence of which is still a controversial matter) is nowadays generally called a biaxial smectic A, often denoted SmA_b [14].

2 CHIRALITY AND POLARITY IN LIQUID CRYSTALS

O wonderful, wonderful, and most wonderful wonderful! and yet again wonderful, and after that, out of all whooping!

William Shakespeare, As you like it

OVERVIEW

The important combination of chirality and a tilted smectic geometry, and its consequences involving the spontaneous appearance of electric polarization, is the topic of this chapter. Ferro- and antiferroelectric liquid crystals are properly introduced and, in connection to the latter, the issue of how our terminology must be updated to cope with anticlinic phases is discussed. The basic dielectric properties of the SmC and SmC_a* phase are described and some attention is given to the special optical properties related to the anticlinic structure of the SmC_a* phase. Finally, the important concept of surface-stabilization is defined.*

2.1 Ferroelectric liquid crystals

If the mesogenic molecules are chiral, this may radically change the macroscopic behavior of the phase, and such a phase is therefore distinguished from the achiral one by adding a star after the letter, *e.g.* SmA*, SmC*, etc. The molecular arrangement of the chiral phase may be completely similar to the achiral version (as in SmA and SmA*) or distinctly different (as in SmC and SmC*), but the *physical properties* of the chiral phases are always different from those of the achiral ones.

The presence of chiral molecules in a layered mesophase with a non-zero tilt between the layer normal \mathbf{k} and the director \mathbf{n} , has quite dramatic consequences on the polar properties of the phase, as first recognized by Robert Meyer in 1975 [15]. This applies not only when the phase is made up of a single species of chiral molecule, but just as much to the case that a certain concentration of chiral molecules – dopants – are added to an achiral matrix. There are several tilted smectic phases formed by chiral molecules which could serve to illustrate this, but, since the most important are the different variants of the chiral smectic C phase, we will here use the ordinary SmC* as example. Of course, the results apply equally to the other chiral tilted smectic phases.

As schematically illustrated in Table 2.1, the monoclinic symmetry prevailing in tilted smectics contains only one axis of symmetry, namely a C_2 axis lying in the plane of the smectic layers and directed perpendicular to the *tilt plane*, *i.e.* the plane spanned by \mathbf{n} and \mathbf{k} . This means that the only rotational symmetry operation of the phase is a 180° rotation around this axis. In addition to the rotational symmetry, there is a hori-

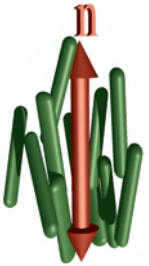
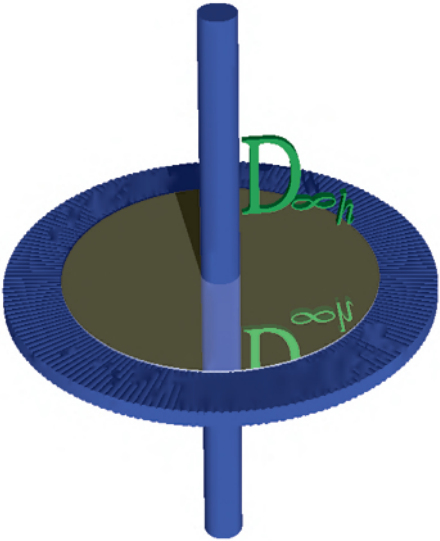
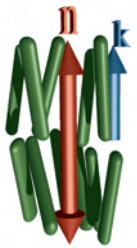
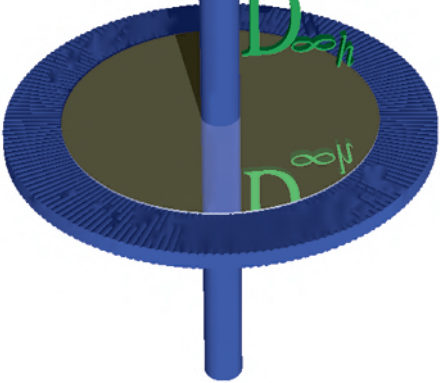
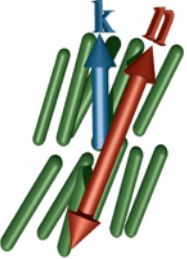
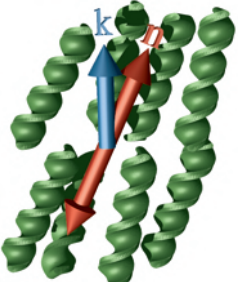
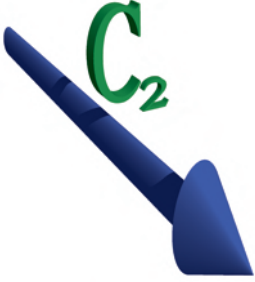
Phase	'Molecular' organization	Symmetry
Nematic (N)		
Smectic A (SmA)		
Smectic C (SmC)		
Chiral Smectic C (SmC*)		

Figure 2.1 Local symmetries of the N, SmA, SmC and SmC* phases. In the center column, the organization of the molecules, drawn as rigid rods or rigid spirals, is shown in a very schematic way, in order to define the director \mathbf{n} and layer normal \mathbf{k} . The symmetry illustrations on the right, where the axes are axes of rotational symmetry, are drawn to correspond to the geometry of the molecular system. This means that the two-fold rotation axis defining the 'vertical' direction in C_{2h} , is drawn horizontal, while the 'horizontal' mirror plane is drawn vertical. The infinite number of two-fold axes in the mirror plane of $D_{\infty h}$ are represented by a continuous ring of two-fold axes.

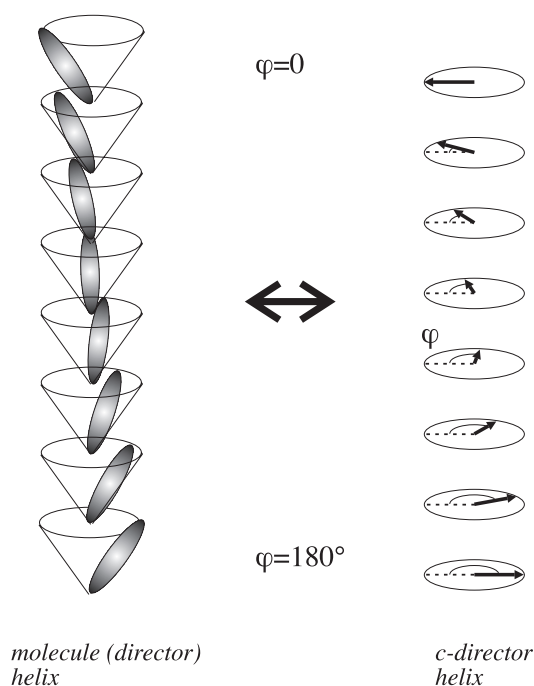


Figure 2.2 The bulk smectic C^* phase features a helical director configuration, where the helix axis is parallel to the layer normal. The tilt-angle is constant throughout the sample, but the phase-angle φ changes continuously from layer to layer. Sometimes one prefers to describe the SmC^* structure using the concept of the C -director, which is simply the projection of the director onto the layer plane (right part).

zontal¹ mirror plane containing \mathbf{k} and \mathbf{n} , in the case that we have achiral molecules (and thus an achiral phase). The point group symmetry of the SmC phase is therefore C_{2h} . However, if we introduce chiral molecules in the phase, their presence removes the mirror symmetry and we are left with the two-fold rotation axis only, *i.e.* the symmetry of the SmC^* phase is, on a local scale, C_2 . The C_2 axis is now a *polar* axis, as it has no more a mirror plane perpendicular to itself, which would reverse a polar vector along C_2 . Meyer thus concluded that the SmC^* phase is spontaneously polarized, with the polarization fixed along the C_2 direction, *i.e.* directed parallel to the layers but perpendicular to the tilt plane. Obviously, the molecules must, in addition to being chiral, exhibit some dipole moment with a component perpendicular to the long molecular axis. This is, however, almost always the case.

2.1.1 The helical bulk SmC^* structure

A phase built up of chiral molecules will, if possible, reflect the molecular chirality through some kind of chiral macroscopic structure. In the case of the SmC^* phase, this superstructure is, in general, a helicoidal modulation of the director. As a helix within the layer plane is incompatible with a layered structure², the helix axis must be oriented along the layer normal \mathbf{k} , *cf.* figure 2.2. The variable that changes helicoidally is then the phase-angle φ , *i.e.* the tilting direction precesses continuously around \mathbf{k} as one travels from layer to layer. As the spontaneous polarization has a fixed directional rela-

1. As the axis of highest symmetry always defines the vertical direction in symmetry considerations, this mirror plane will be called horizontal, despite that it in the normal picture of the smectic phases – middle column in Table 2.1 – is generally taken as vertical

2. An in-layer helix would break the layers, and therefore such a helix-structure is incompatible with the normal smectic structure. However, in certain smectic liquid crystals with very strong twisting power, the layers may actually break up and form ordered defect structures. We can see this phenomenon in the so-called TGB (Twist Grain Boundary) phases, appearing in a narrow temperature range at the high-temperature boundary of the smectic phases.

tionship to \mathbf{n} , the polarization vector will also precess around \mathbf{k} with the same periodicity as the director helix, resulting in a complete cancellation of polarization on a macroscopic scale.

The periodicity of the helix, called the *pitch* (in this thesis denoted with p), often increases somewhat with increasing temperature, but the variation might be much more complex and varies from compound to compound. In some materials there is even a helix inversion, meaning that the pitch first increases to infinity and then decreases, within the SmC* phase. This occurs when the handedness (or sense) of the helix at the low-temperature end of the SmC* phase is opposite of the one at the high-temperature end. The only way of continuously going from a right-handed to a left-handed helix is by passing through an infinitely long helix.

2.1.2 *Small-signal response of the SmA* and helical SmC* phases in planar-aligned samples*

The polarity of chiral tilted smectics renders their response to electric fields particularly interesting. An investigation of their dipolar properties by means of dielectric spectroscopy or of their electrooptic response as observed in a polarizing microscope can give much information about the molecular organization and can be very helpful in determining the liquid crystal phase. The basics of dielectric spectroscopy are given in condensed form in appendix B.2, where also the relevant terminology used in this thesis is introduced and motivated. A richer discussion can be found in my licentiate thesis [16]. In this section we will briefly discuss the influence from small-amplitude electric fields on the director tilt magnitude and direction in the SmA* and SmC* phases.

2.1.2.1 Tilt-angle fluctuations

It is a general property of second order phase transitions that the magnitude and relaxation time of the order parameter fluctuations away from the equilibrium value will diverge ('critical behavior'), the temperature dependence being characterized by a critical exponent, on approaching the transition temperature from either side. In case the order parameter couples, directly or indirectly, to an external field, the dielectric susceptibility χ describing this interaction will also diverge. In the chiral SmA*-C* system the polarization is such an order parameter, although only secondary, with the director tilt-angle θ as the primary order parameter. Any fluctuation in the polarization is thus linked to a fluctuation in the tilt-angle (and vice-versa), which in a well-aligned sample can be observed experimentally under the approximation $\theta \approx \theta_{\text{opt}}$ (the tilt of the slow axis). Note that, as the polarization is perpendicular to the director, the director tilt plane is orthogonal to the electric field. In order to obtain a visible redirection in the slow axis the field should thus be applied along the smectic layers, *i.e.* perpendicular to the sample surfaces in planar aligned samples. The angle θ_{opt} is a linear function of the field strength up to a saturation value which can be quite high, often $\sim 10^\circ - 15^\circ$ close to the SmA*-C* transition. On the other hand, the birefringence remains more or less unchanged by the effect in most SmA* phases. This field-induced collective behavior is of great importance, especially in the field of electrooptics where it is referred to as the *electroclinic effect*.

At the SmA*-C* (and SmA-C) transition, the elastic constant which constitutes the restoring force against fluctuations in the director tilt weakens, or softens, and therefore the electroclinic effect will diverge, *i.e.* the field-induced slow axis tilt will grow larger and larger, as the transition is approached. The same fluctuation can also

be observed by means of dielectric spectroscopy where it is commonly referred to as the *soft mode*. This is recognized in the dielectric spectrum as an absorption which starts to diverge in strength and relaxation time on approaching the phase transition. True critical behavior is however never observed at the SmA*-C* transition [16]. The central absorption frequency of the soft mode typically does not decrease below 1 kHz and the susceptibility seldom reaches values above ~ 100 . The soft mode is also often referred to as an *amplitudon* mode since it is connected to fluctuations in the tilt *angle* (as opposed to tilt direction).

2.1.2.2 Phase-angle fluctuations

As the spontaneous polarization can be regarded as a dipole sterically fixed perpendicular to the director, also fluctuations in the phase angle φ , *i.e.* in the tilt *direction*, will couple to an electric field. The corresponding small-signal dielectric response, present whenever the equilibrium tilt angle is non-zero, is in the SmC* phase often referred to as the ‘SmC* Goldstone mode’. However, this is a correct name only in the exceptional case of an undisturbed helix the pitch of which is infinite [16]. A better name, which is always adequate, is *phason* mode. In the general case of a helicoidal SmC* phase, this mode corresponds to a field-induced helix distortion. When referring to the phason mode in helical samples I will therefore use the term *helix distortion* mode, alternatively the abbreviation HD-mode.

An analytical expression for the susceptibility of the helix distortion mode has been developed by Levstik *et al.* [17]:

$$\chi_{HD} = \frac{1}{8\pi^2 K_\varphi} \left(\frac{P_s p}{\theta} \right)^2 \quad (2.1)$$

The parameter K_φ is the elastic constant counteracting phase-angle fluctuations, P_s is the magnitude of the spontaneous polarization, θ the equilibrium director tilt angle, and p the helical pitch. Obviously, the HD-mode susceptibility can be very high, especially in a long-pitch material, which renders the mode quite spectacular in a dielectric spectrum. The value is typically in the range 100 - 1000. Regarding the critical frequency, a similar reasoning to that of Levstik’s and co-workers’, based on elasticity theory, leads us to the expression [18]:

$$f_{HD} = \frac{K_\varphi 2\pi}{\gamma_\varphi p^2} \quad (2.2)$$

where γ_φ is the viscosity counteracting changes in the phase-angle. If one inserts typical parameter values for a SmC* compound, for instance $p = 1 \mu\text{m}$, $K_\varphi = 5 \text{ pN}$, $\gamma_\varphi = 0.01\text{-}0.1 \text{ Ns/m}^2$, one ends up with a critical frequency in the range $f_{HD} \approx 300 \text{ Hz}$ -3000 Hz. This fits well with experimentally observed critical frequencies for the mode.

In practical cases the helicoidal director configuration is disturbed even in the zero-field state, due to the presence of the sample boundaries. It may therefore be difficult to say exactly which phase-angle fluctuation gives rise to the observed response, and the term phason mode is then very useful as a general name. We will return to the issue of phason modes, in particular which types we may expect when the liquid crystal is confined in a thin sample cell, in section 6.2.

2.1.3 A comparison with solid ferroelectrics

In solid ferroelectrics, the primary order parameter, or the order parameter ‘driving the transition’, is the spontaneous polarization. The higher order of the low-temperature ferroelectric or antiferroelectric phase, compared to the high-temperature *paraelectric* phase, is manifest through a macroscopic ordering of the dipoles. In polar liquid crystals, the situation is quite different. The primary order parameter is the director tilt, not the spontaneous polarization. The polarization is rather a secondary effect – allowed by the presence of chiral molecules – of the same kind of ordering as we have in achiral SmC. The polarization is therefore often called the *secondary order parameter* of the SmA*-C* transition, and ferroelectric liquid crystals are said to belong to the class of *improper ferroelectrics*.

There is no fundamental reason why a liquid crystal could not exhibit a paraelectric-ferroelectric transition driven by the polarization, but there is a practical one: the weakness of the dipolar interaction in molecular liquids [19]. In order to form a ferroelectric state, driven by the polarization, the dipolar interaction energy must be of the order of the thermal energy, $k_B T$. But generally, the thermal energy is much higher even at the melting point, leading to crystallization before any ferroelectric liquid crystal ordering of this kind could take place. The dipolar interaction energy is limited by the relative bulkiness of the molecules, leading to a quite large average distance between dipoles. One might think that this problem could be overcome by synthesizing molecules with very high dipole moments, but it turns out that such compounds tend to form dimers with opposite directions of the spontaneous polarization [19]. In the case of smectics, the ‘dimerization’ may be across the layer boundaries. This is the case in antiferroelectric liquid crystals, discovered as a side effect of the efforts to increase the spontaneous polarization in ferroelectric liquid crystals.

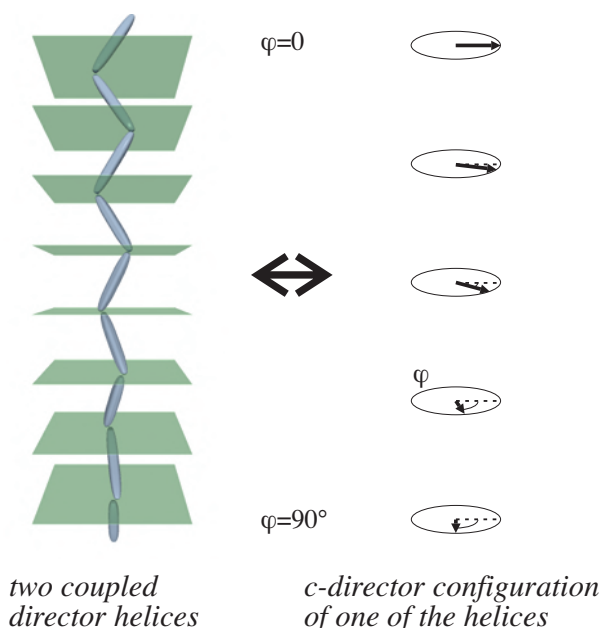
2.2 Antiferroelectric liquid crystals

When we speak of ferroelectric liquid crystals (FLCs) we refer to chiral liquid crystals which have only one type of smectic C phase: the ‘ordinary’ SmC* phase. *Antiferroelectric liquid crystals* (AFLCs) may also develop the SmC* phase, but also one or more other versions of the chiral smectic C phase. Most important, they always develop the SmC_a* phase, the antipolar properties of which has given this group of liquid crystals their name.

2.2.1 The bulk structure of the SmC_a* phase

The SmC_a* phase exhibits an anticlinic structure, *i.e.* the director tilt changes sign from layer to layer. Since the phase is chiral, there will be a spontaneous polarization in the layer plane which also changes sign between adjacent layers. The SmC_a* phase features a similar type of helical arrangement of the molecules as the SmC* phase, leading to selective Bragg reflection at optical wavelengths and strong optical rotatory power (ORP) along the helix axis. The anticlinic ordering of tilt directions will however prevail on a local scale and the resulting structure can therefore be described as a double helix consisting of two regular helices, shifted in position by one layer and in phase by slightly more than 180°, geared into each other (*cf.* figure 2.3). As the helical

Figure 2.3 The bulk chiral smectic C_a^* phase combines a local anti-clinic director structure and a macroscopic helical modulation. Such a structure can be obtained by coupling two helices, with a fixed phase-angle difference of slightly more than 180° (it cannot be exactly 180° since the phase-angle shift on going between two neighboring layers should be constant).



superstructure is locally non-polar in the SmC_a^* case, the optical periodicity is equal to half the helical pitch, as it also is in the cholesteric phase. Thus we will observe a half pitch Bragg reflection band for all angles of incidence, whereas in the SmC^* case we generally observe two reflections, corresponding to the full pitch and the half pitch, respectively. Only if the light is incident along the helix axis it will encounter the same dielectric properties in each half-period of the SmC^* helix, hence only in this special case the full pitch band vanishes.

An interesting difference between FLCs and AFLCs is that, whereas the helical SmC^* pitch in the former materials is often in the range of several microns, that of the SmC_a^* phase in pure AFLCs is always short. In the case that also a SmC^* phase appears in an AFLC material, the pitch is short in that phase as well. To the best of my knowledge, there is no single-compound SmC_a^* phase which has a stable³ pitch much longer than $0.5\mu\text{m}$, as is easily seen from the fact that they all selectively reflect light in the visible spectrum. This is most certainly related to the fact that pure AFLC compounds always exhibit very high values of the spontaneous polarization, as compared to FLC compounds. The spontaneous polarization and the helicoidal superstructure are both manifestations of the molecular chirality, so apparently the correlation between micro- and macroscopic properties is stronger in AFLCs than in FLCs.

2.3 A terminology for describing anticlinic smectics

Much of the terminology used so far has a quite long history. It was developed for the case that the order locally does not change much, as in the case of the nematic, smectic A and smectic C phases or their chiral analogs. With the discovery of anticlinic phases, where the whole geometry is rotated 180° around the layer normal every time a layer boundary is crossed, much of the terminology became more or less ambiguous. For the

3. There are a few AFLC compounds, such as MHPOBC and EHPOCBC, which exhibit a helix inversion within the SmC_a^* phase. Obviously the pitch will diverge on approaching the inversion temperature, but far away from that temperature, the pitch stabilizes at values producing visible selective reflection or even shorter, as in the case of EHPOCBC.

sake of clarity, it can therefore be wise to pause briefly and address the issue of how the basic concepts should be interpreted when discussing the new systems.

The issue of how the director should be understood in the discussion of anticlinic structures was touched upon already in section 1.4. As pointed out there, the only reasonable choice is to connect the director to the structure of a single layer, and I will use this interpretation in the following. We will use a 1, 2, 3 - coordinate system for discussions on this local scale, where the 3-axis is directed along the director and the 2-axis is perpendicular to the tilt plane, spanned by the director and the layer normal. For considerations on a mesoscopic level, we will instead use the coordinate system $\mathbf{x}, \mathbf{y}, \mathbf{z}$, where the \mathbf{z} -axis is along the layer normal and the \mathbf{y} -axis coincides with the average 2-direction.

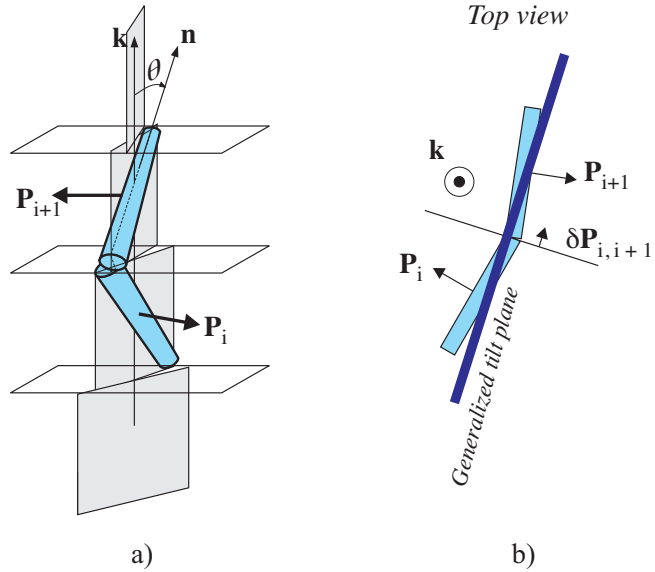
Having defined our local coordinate system, it would be practical to define also a corresponding ‘local slow axis’. However, a single smectic layer is roughly 30 Å - 40 Å thick so one may question to what extent we can attribute optical properties to such a system. The concept ‘local slow axis’ should rather be understood as describing the slow axis of the medium we would get if we replicated the selected (local) layer indefinitely in the direction of the layer normal. In principle, the local optical tilt, defined in this sense, should be roughly the same as the optical tilt that we can actually measure if we switch the SmC_a^* liquid crystal to the synclinic state. However, we cannot *a priori* know that the optical tilt measured in this way reflects the local director tilt in the anticlinic state, although we have recently been able to show indirectly that this is at least true in one case (paper 5). There may also be a difference due to the electroclinic effect, even though this would be of negligible magnitude if we avoid the discussion of the SmC_a^* phase just below a SmA^* phase.

The local optical tilt angle of the SmC_a^* phase in the relaxed state, will in this text be denoted θ_0 . In this way we can distinguish this microscopic property from the experimentally observable optical tilt of the switched synclinic state, which will be connected to the shorthand θ_s . The notation θ_{app} will stand for the apparent optical tilt. Obviously, this can be expected to vary between zero and θ_s , depending on the state of the sample observed.

It is worthwhile to discuss the relation between the optic axes and the slow axis of the biaxial systems which we mainly discuss here. It has been a fairly common practice when discussing the AFLC display principle to speak of the ‘optic axis’, actually referring to the slow axis. The reason is that in the display geometry, the anticlinic state gives a biaxial optical indicatrix in which the axial plane (containing the two optic axes) is perpendicular to the tilt plane. If the tilt plane is parallel to the cell plane, these axes are therefore seen as one, for normal incident light. This is shown in figure 5 of paper 5. Furthermore, in the switched, synclinic, state, where the two axes are not covering each other, the biaxiality is normally considered so small that it can be neglected in the discussions. However, the important thing is that in neither case is any of these two optic axes the relevant direction for the description of the electrooptic effects. Instead, this is given by the ϵ - tensor axis with the highest eigenvalue. This direction, representing the largest index of refraction, is the ‘slow axis’. In the anticlinic state it is along the \mathbf{z} direction, in the synclinic state along the director (bisecting the two optic axes). In the following we will use this name – the slow axis – remembering that it may be equivalent to the ‘optic axis’ of other texts.

Another concept which is slightly more problematic when considering anticlinic smectics is the tilt plane. In section 2.1 we could define it simply as the plane spanned by the layer normal \mathbf{k} and the director \mathbf{n} , since we then considered only the synclinic

Figure 2.4 The true, single-layer, tilt plane changes direction within the unit cell of the SmC_a^* phase (a). This also leads to an incomplete cancellation of the spontaneous polarization if one considers the ‘unit cell’ consisting of only two layers. Within this approximation, we can define the SmC_a^* tilt plane as spanned by the layer normal and the imagined residual polarization $\delta\mathbf{P}$, as illustrated in (b), where the unit cell is viewed from above, i.e. along the layer normal.



SmC^* phase where it is generally enough to consider one layer at a time. The helical superstructure has no effect on a single layer and all directions involved are thus well-defined. In the case of the SmC_a^* phase (disregarding the helical superstructure), the unit cell⁴ consists of two layers and in that case the helical twisting is present already on the unit cell level.

What we would need for an unambiguous definition of the tilt plane is a direction related to the tilt which is common to the *whole* unit cell. This may be found by considering the directions of the spontaneous polarization in the two unit cell layers, *cf.* Figure 2.4. As also the polarization direction changes direction between the layers, the cancellation of the spontaneous polarization which we would have in a non-helical SmC_a^* phase, is not complete. At the center of the unit cell, exemplified in Figure 2.4 by two layers i and $i + 1$, we can imagine a small residual polarization $\delta\mathbf{P}$, pointing in a direction right between the two single-layer tilt planes. This is the unique direction we were looking for and we can thus define the SmC_a^* tilt plane as the plane spanned by the layer normal and the residual polarization $\delta\mathbf{P}$ at the center of the unit cell. In the following, this interpretation will be used when discussing anticlinic structures. This ‘tilt plane’ is thus a generalization of the original tilt plane concept and becomes identical to it when there is no twist, *cf.* paper 5.

2.4 The consequences of the anticlinic structure for the optical properties

The macroscopic optical properties of a planar-aligned non-helical anticlinic SmC_a (or surface-stabilized SmC_a^*) liquid crystal can be worked out as a function of the local optical tilt angle on a quantitative level, as done in paper 5. The tilt plane is there considered to be in the plane of the cell, which we will refer to as the horizontal plane. By first transforming the dielectric tensors of the two local subsystems to the $\mathbf{x}, \mathbf{y}, \mathbf{z}$ frame,

4. We use the term unit cell with some hesitation. First, we do not have 3D translational order in liquid crystals, hence it is not a unit cell in the true crystallographic sense. Second, the incommensurate helicoidal modulation actually makes the system non-periodic so even in one dimension it is impossible to define a unit cell which constitutes a truly repeating unit.

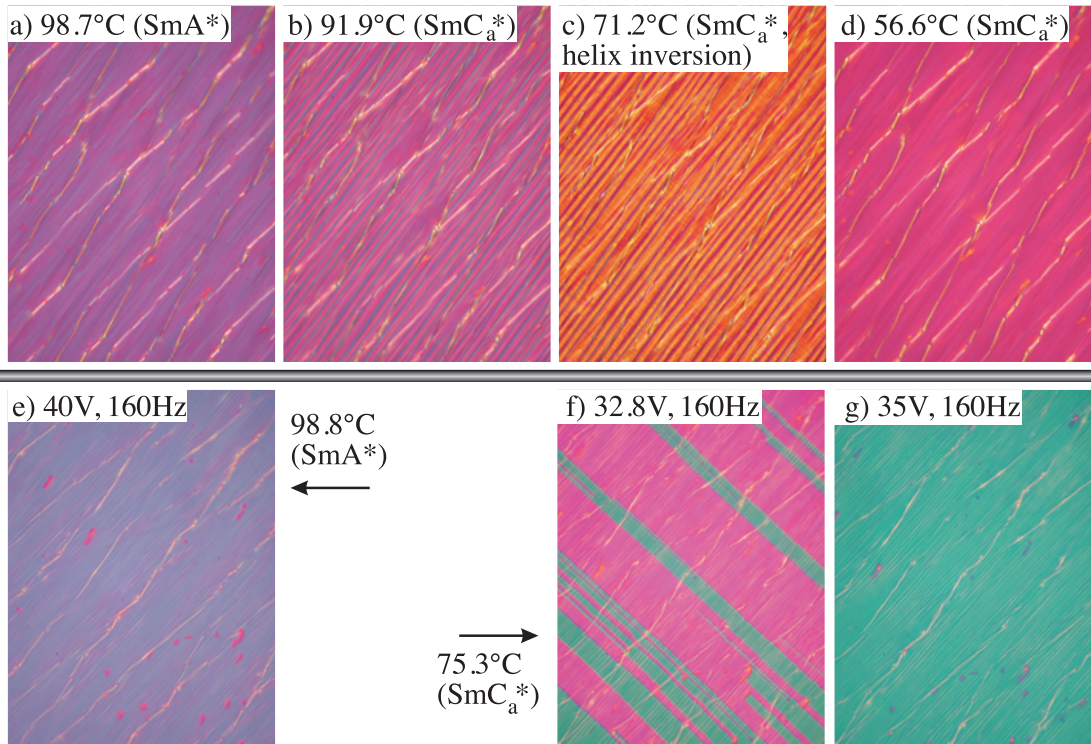


Figure 2.5 Textures between crossed polarizers of a 4 μm thick planar-aligned sample of EHPOCBC, an AFLC exhibiting a helix inversion within the SmC_a^* phase. The rubbing direction is approximately in the two o'clock, the layers in the five o'clock direction. Upper row: texture sequence on cooling from SmA^* in the absence of fields. Lower row: selected textures with electric fields applied; e: SmA^* , saturated electroclinic effect; f: SmC_a^* , field strength at the limit of switching from the anticlinic (pink) to the synclinic (bluish green) state; g: the fully switched synclinic SmC_a^* state.

the macroscopic optical properties of the anticlinic sample can be obtained simply through addition of the two tensors. This gives us the following macroscopic refractive indices:

$$\begin{aligned}
 n_x &= \sqrt{n_1^2 \cos^2 \theta_0 + n_3^2 \sin^2 \theta_0} \\
 n_y &= n_2 \\
 n_z &= \sqrt{n_1^2 \sin^2 \theta_0 + n_3^2 \cos^2 \theta_0}
 \end{aligned} \tag{2.3}$$

For moderate tilt ($\theta_0 < 30^\circ$), it turns out that $n_y < n_x < n_z$. This means that the non-helical SmC_a^* phase exhibits its lowest effective birefringence (restricting ourselves to the

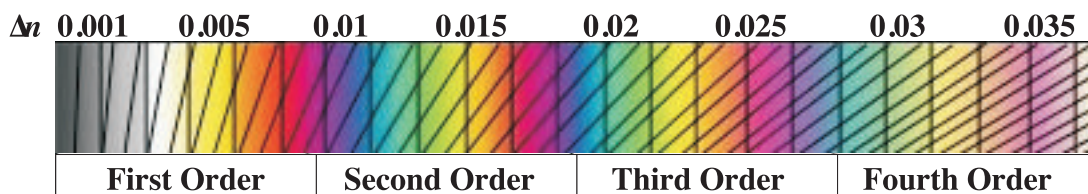


Figure 2.6 A (reduced) Michel Levy color chart showing the color of an optically anisotropic sample between crossed polarizers, as a function of the birefringence Δn .

case that the layer normal is in the plane of the sample) $\Delta n = n_z - n_x$ in this case of planar alignment. Any rotation of the tilt plane about \mathbf{z} will increase the birefringence and the maximum will occur when the whole sample is aligned with its tilt plane perpendicular to the cell plane (vertical tilt plane). In a helicoidal sample, the effective value of Δn will obviously be roughly in between these two limiting values.

These results can be easily verified experimentally in the case of the AFLC compound EHPOCBC (the chemical structure can be found in Table 1 of paper 4), which exhibits a helix inversion within the SmC_a^* phase. Textures of a $4\ \mu\text{m}$ thick planar-aligned sample with this liquid crystal are shown in Figure 2.5. The upper row shows the texture sequence as seen on cooling from the SmA^* phase. The color of the helical SmC_a^* phase (textures b and d) is not much different from that of the SmA^* texture. In contrast, the color of the unwound SmC_a^* phase, seen at the temperature of the helix inversion (c), clearly reflects a much lower birefringence (compare with the birefringence color chart in Figure 2.6). This is to be expected, since the planar boundary conditions will impose a horizontal tilt plane when the helix is unwound.

The small color change on cooling from the SmA^* into the helical SmC_a^* phase is very interesting. The corresponding small reduction in birefringence tells us that there must be a pronounced orientational disorder in the SmA^* phase, producing a decrease in Δn as compared to what would be the result of a structure where all molecules stand essentially orthogonal to the layer plane. In fact, the decrease is almost as important as that due to the helicoidal, anticlinically tilted director structure of the SmC_a^* phase. This is also confirmed by the textures obtained on switching the sample (lower row in Figure 2.5) where the birefringence increases markedly with the field-induced optical tilt. This type of orientationally quite disordered smectic organization has very interesting properties and it will be discussed extensively in the following chapter. There are actually several indications that the SmA^* phase in antiferroelectric liquid crystals in general comes closer to this type of organization than in ferroelectric liquid crystals.

2.5 The dielectric properties of the SmC_a^* phase

2.5.1 The small-signal dielectric signature

In planar-aligned bulk-like samples (thick enough for the helix and the local anticlinic structure to develop undisturbed), the dielectric spectrum of the SmC_a^* phase in its relaxed state is characterized by two modes of very low susceptibility. The weak response is to be expected considering the antipolar order of the phase. As the origin of the modes is still a slightly controversial matter, they are often distinguished by their respective critical frequencies f_c . Also this is, however, no perfect solution since the frequencies can change quite a lot within the phase temperature range, both generally increasing on heating. The critical frequency of the ‘low-frequency’ mode always follows an Arrhenius dependence of the temperature. At high temperatures, close to the SmA^* phase, the two absorptions may come very close to one another in frequency. However, far below the SmA^* phase they are usually well separated, as can be seen in the dielectric absorption spectra in figure 2.7. Five of the examples here are obtained on AFLC mixtures, the reason being that the SmC_a^* modes are usually easier to detect in mixtures. The first reason for this is the suppression of the crystallization temperature induced by mixing. At temperatures close to room temperature, where single-com-

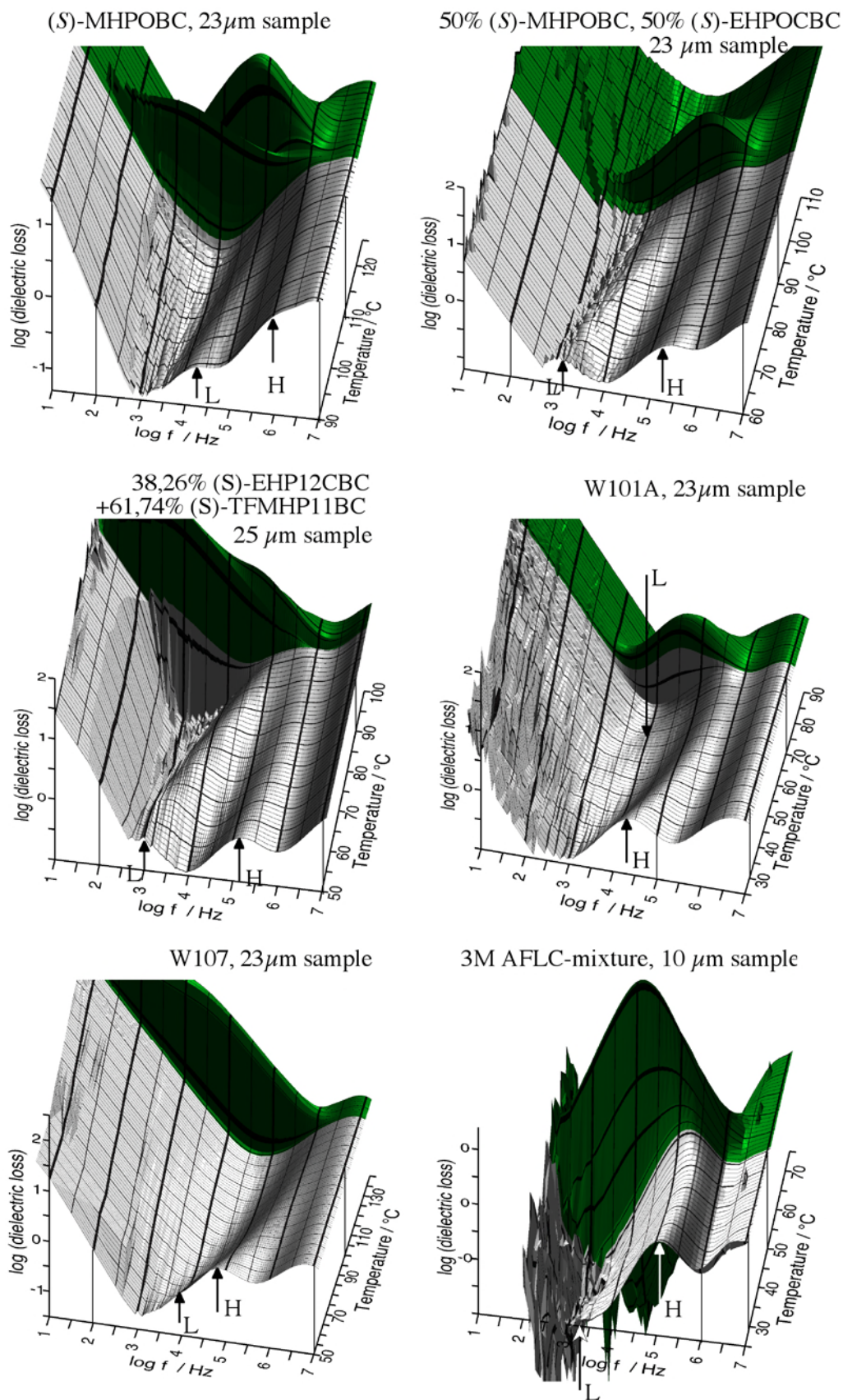


Figure 2.7 Six examples of dielectric absorption spectra from liquid crystals exhibiting the SmC_a^* phase in a broad temperature range. For clarity, the data from the other phases are plotted in a darker color. The low- and high-frequency AFLC modes are indicated with L and H, respectively. For further comments, see main text.

pound AFLCs in general are crystalline, the modes have critical frequencies typically in the range $10^3 - 10^5$ Hz and can thus easily be resolved. At higher temperatures, f_c often approaches the cut-off frequency of the sample cell and then the mode ‘vanishes’ in the spurious cut-off peak. However, the activation energy of the modes changes between different materials, so there is no general (non-compound-specific) relation between the frequencies and the absolute temperature.

In the single-compound antiferroelectric liquid crystal MHPOBC (SmC_γ^* , SmC_β^* , SmC_α^* and SmA^* above SmC_α^* , see chapter 5 for a description of the first three of these phases), shown at the top left in figure 2.7, both modes are visible but they are weak. In the first two mixtures, MHPOBC + EHPOCBC (only SmA^* above SmC_α^*) and EHP12CBC + TFMHP11BC (SmC^* and SmA^* above SmC_α^*), both modes are much easier to see and, in particular in the latter case, the Arrhenius temperature dependence of the low-frequency mode is also quite clear. Going to the multi-component mixture W101a (direct SmA^* - SmC_α^* transition), developed by the Dabrowski group (Warsaw), the high-frequency mode is strong and its typical ‘curved’ temperature dependence of the critical frequency, stabilizing on approaching the SmA^* phase, is easily seen. But the low-frequency mode is here much more difficult to see, mainly because of its unusually low value of f_c . Only close to the transition to the SmA^* phase does the mode exit from the low-frequency ionic contribution (see appendix B.2), but its susceptibility is then also very low.

The next example is also from a multi-component AFLC mixture from the Dabrowski group, W107 (SmC^* and SmA^* above SmC_α^*), a material which exhibits a first-order SmA^* - C^* transition and an exceptionally high saturation tilt angle ($\theta \sim 45^\circ$), *cf.* paper 5. Here the low-frequency mode is even more difficult to detect, but this time due to its relatively *high* value of f_c , in addition to the susceptibility being rather low. At the low-temperature end of the SmC_α^* phase, the critical frequency is only slightly below that of the high-frequency mode. On further heating, f_c should increase further according to the Arrhenius behavior. Hence, it will disappear in the high-frequency mode, and later in the spurious cell cut-off absorption. Indeed, one can even imagine that the two SmC_α^* modes actually cross each other in this mixture, such that the ‘low-frequency’ mode has a higher critical frequency than the ‘high-frequency’ mode close to the SmA^* phase, but this is impossible to verify. One could speculate that this unusual behavior is related to the exceptionally high director tilt.

The last example, an AFLC mixture to be discussed in section 3.4 (direct SmC_α^* - SmA^* transition), is very interesting. The difficulty in observing the low-frequency mode is in this case really due to an unusually weak response of the mode, as its frequency is actually in the best range for separating it from the high-frequency AFLC mode as well as the cell cut-off. At room temperature, the relatively low value of $f_c \approx 1$ kHz makes it slightly disturbed by the ionic conduction absorption, but on heating the critical frequency increases according to the Arrhenius behavior, hence getting more and more free of the spurious peaks. As described below, the origin of the low-frequency mode is probably related to reorientations of the longitudinal molecular dipoles. The experimental results described in section 3.4 indicate that the molecules in this compound aggregate pairwise in an anti-parallel fashion. Obviously, in such a configuration the molecular longitudinal dipoles will cancel each other and the effective dipole along the reorienting ‘rod’ will be essentially zero, leading to the unusually weak susceptibility of the low-frequency mode.

Summarizing, we can say the following about the two SmC_α^* dielectric modes:

Table 2.1 The characteristics of the SmC_a^* small-signal dielectric modes.

	<i>Low-frequency mode</i>	<i>High-frequency mode</i>
Critical frequency	Follows Arrhenius dependence of temperature. Typical range: 10^3 - 10^5 Hz	Increases on heating at low temperature, but the rate falls off on approaching the SmA^* phase. Close to this phase, the value changes very little with temperature and it often even starts decreasing just before the transition. Typical range: 10^4 - 10^6 Hz
Susceptibility	$\chi \sim 1$ or lower. In certain compounds, it can be much lower, to the limit of almost not being detectable.	$\chi \sim 1$. Usually this mode is the stronger of the two.

2.5.2 The types of fluctuations behind the SmC_a^* dielectric absorptions

The Arrhenius behavior on temperature of the critical frequency of the low-frequency mode suggests that it is non-collective in nature, *i.e.* it is related to the fluctuations of the molecules on a local level and not to the macroscopic structure of the phase. Generally, the mode is interpreted as reflecting the reorientation of the molecules around their short axes [20], as schematically illustrated in figure 2.8 *a*. The reason why this fluctuation would contribute to the dielectric permittivity ϵ is that the molecules generally have a non-zero dipole moment along the molecular long axis. In the presence of an electric field directed in the \mathbf{x} -direction, the molecular orientations $\mathbf{m} \parallel \mathbf{x}$ and $\mathbf{m} \parallel -\mathbf{x}$ will therefore have slightly different energies, and thus the reorientations around the short axis between these two states should be slightly biased, leading to a (weak) induced polarization.

Obviously, the average direction of \mathbf{m} must have a component along \mathbf{x} in order for this process to contribute to ϵ , *i.e.* in perfect planar alignment the mode should be invisible. For this reason, there has been some objection to the short axis reorientation

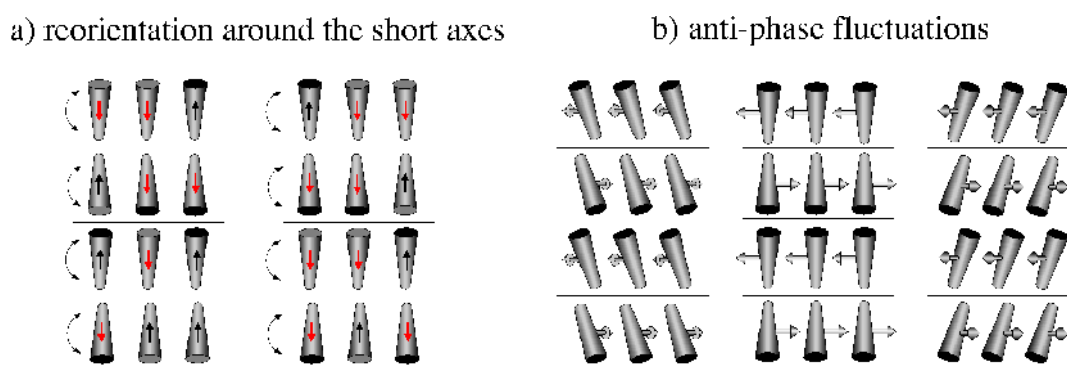


Figure 2.8 Schematic illustrations of the two fluctuations suggested to be responsible for the dielectric absorptions in the SmC_a^* phase. The paper plane is equivalent to the cell plane, *i.e.* the measuring field is directed into the paper. Reorientation around the short molecule axes (*a*) probably gives rise to the low-frequency absorption, while fluctuations in the tilt direction, in opposite sense in adjacent layers (*b*), are likely to be the reason for the high-frequency absorption. For clarity, orientational fluctuations are completely neglected, *i.e.* the molecules are drawn as if they all adopt the average (director) orientation.

interpretation, since the mode is normally observed also in planar-aligned samples [21, 22]. However, this objection neglects the fact that a perfectly planar-aligned SmC_a^* sample is almost never seen. In most dielectric spectroscopy experiments one uses cells thick enough for the helix to develop rather undisturbed, and so the average direction of \mathbf{m} will have a component out of the substrate plane except in two layers per period of the helix. In case of a surface-stabilized sample, we generally do not achieve the ideal geometry, with a tilt plane exactly in the plane of the cell and so we normally see the mode also in that case.

The origin of the mode with higher frequency is most probably fluctuations in tilt direction, *i.e.* phase angle φ , in opposite senses in adjacent layers, as depicted in figure 2.8 *b*. As the spontaneous polarization in each layer is perpendicular to the director, a fluctuation in the tilt direction will give rise to the same fluctuation in polarization direction. If the fluctuations are in opposite sense in adjacent layers, this will effectively lead to a fluctuating magnitude, and eventually sign, of the residual polarization $\delta\mathbf{P}$ (*cf.* figure 2.4). In the case of a tilt plane which on the average is vertical, as depicted in the center of figure 2.8 *b*, the fluctuating residual polarization will be directed along the measuring field and thus contribute maximally to ϵ . As illustrated in the two ‘fluctuation cases’ of the figure, this mode is also coupled to a change in effective slow axis direction as well as an increase in effective birefringence. In contrast to the reorientation mode, this mode will therefore be not only dielectrically, but also electrooptically active. In paper 7 we showed how a careful study of the magnitudes of the two SmC_a^* modes can actually give us information on the structure of a SmC_a^* sample.

2.6 Surface-stabilization of polar phases

– *bringing the local properties to the macroscopic scale*

The presence of a spontaneous polarization is one of the characteristics of ferroelectricity, and Robert Meyer therefore called compounds exhibiting the SmC^* phase Ferroelectric Liquid Crystals (FLCs). In order to call a medium ferroelectric, the polarization should however be macroscopic, and it should be switchable between two stable directions. The bulk SmC^* samples studied by Meyer and co-workers in their early experiments did not fulfill this requirement, because of the helicoidal superstructure which leads to cancellation of the polarization on a macroscopic scale. Bulk SmC^* samples should thus not be called ferroelectric in the true meaning of the word, but rather *helicelectric* or *helical antiferroelectric* [23]. Due to the helicoidal structure, the *global* symmetry of the bulk SmC^* phase is D_∞ and not C_2 . The phase thus has the same symmetry as the non-polar N^* or SmA^* .

In specific geometries and under the influence of strong surface action, the helix may however be suppressed, giving the SmC^* liquid crystal a spontaneous macroscopic polarization which may be switched between two stable states [24]. Such a sample, which is called a *Surface-Stabilized Ferroelectric Liquid Crystal* (SSFLC), fulfills the requirements to be called ferroelectric, and as such it is extremely interesting for numerous applications. The bistable macroscopically polar state can easily be verified since any ferroelectric sample will spontaneously form domains of polarization up and polarization down. As these domains in an SSFLC sample by necessity have different orientations of the slow axis, they will look different in the polarizing microscope. If

one applies a triangular wave electric field over such a cell one will also see the typical ferroelectric response (*cf.* figure 5.1 *c*). Usually, the geometrical constraint for achieving the SSFLC state is that the cell thickness is of the order of the helical pitch.

Also the SmC_a^* helix may be suppressed by surface interactions. We then obtain a *Surface-Stabilized AntiFerroelectric Liquid Crystal* (SSAFLC). By applying an electric field we will see the tristate switching characteristic of this phase (*cf.* figure 5.1 *b*). Also in a thicker cell one will see a similar response at low frequencies ($f < 50$ Hz) since the helix may be unwound by the electric field at a lower voltage than the threshold for switching to the ferroelectric state. At higher frequencies the relaxation back to the antipolar state ($E = 0$) is however far too slow, and then the response for the antiferroelectric will approach that of an SSFLC sample.

3 THE SMA-C TRANSITION AND THE ISSUES OF TILT AND LAYER THICKNESS IN SMECTICS

This approach to the problem has the advantage that it appears to work, whereas the other one did not.

Adriaan de Vries [25]

OVERVIEW

This chapter is devoted to matters which at first may seem to be completely uncontroversial, but actually turn out to be not at all so simple, yet extremely important for our understanding of smectic A and C liquid crystal phases. First of all, we will address the issue of the internal structure of the smectic layers and what variables influence their geometry. This will bring us to the question of what actually happens on a molecular level when we go from an orthogonal to a tilted phase. These nuances of the ordering processes in smectics were discussed lively some 25 years ago but then much of the discussion faded into oblivion. Recently, however, the questions raised at that time have been brought into the spotlight again, and many of the answers which have been accepted for such a long time are doubted. The main reason for the renewed attention is that it has become clear that these matters are not only of interest on an academic level, but actually of vital importance for the success or failure in commercialization of devices based on polar liquid crystals. Their importance for the phase sequence of antiferroelectric liquid crystals (see chapter 5) is also being more and more recognized. The main topic of the chapter is the de Vries diffuse cone model of the SmA-C transition, which can explain the appearance of director tilt without layer shrinkage.

3.1 The mysteries of the ‘orthogonal’ smectic A phase

As pointed out in section 1.3.1, the orthogonality of the SmA phase refers to the orientation of the director \mathbf{n} with respect to the layers. It is tempting, and indeed quite common, to simplify this situation to the view that the molecules on the average are oriented with their long axes \mathbf{m} parallel to \mathbf{k} . From such a point of view, it is a troublesome fact that the layer spacing d measured in the SmA and SmA* phases is almost always substantially smaller than the length l of the molecule in its maximally extended conformation, as first noticed by Diele and co-workers [26]. The typical behavior is that d in the SmA phase increases slightly, more or less linearly, on cooling through the phase, reaching a maximum value – still smaller than l – at the low-temperature boundary of the phase [27].

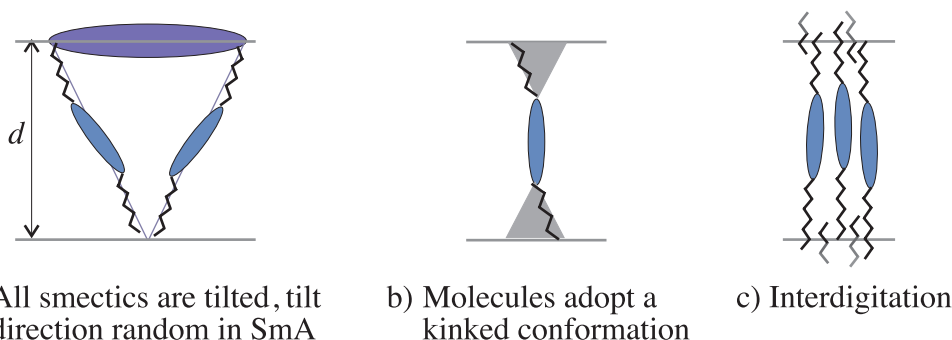


Figure 3.1 The three different model schemes proposed for explaining the fact that the SmA layer spacing d normally is smaller than the length of a fully extended molecule l ; a) the most common molecular orientation is in all smectic phases tilted with respect to the layer normal, but in SmA the direction of tilt is uniformly distributed, b) the molecules adopt a kinked conformation with the cores orthogonal to the layers but the end chains tilted, c) there is a substantial degree of molecular interdigitation across the layer boundaries.

In the beginning of the 1970s, there was a lively discussion aimed at explaining how the molecules could fit in the SmA layers, which apparently were ‘too small’. A few quite different models of the molecular organization in smectic phases were proposed, and we will now describe the three basic ideas, graphically illustrated in figure 3.1. The question of the relation between smectic layer thickness and molecular length is of interest not only to the SmA phase, but it has important implications also for the behavior of the tilted smectic C phases, as we will see in section 3.2.

3.1.1 *Adriaan de Vries, Alan Leadbetter and the idea of a SmA phase with tilted molecules*

During the approximately fifteen years over which he was devoted to the discussion, the Kent State University X-ray crystallographer Adriaan de Vries presented several models for explaining the mysteries of the SmA (and SmC) layer structure. Apart from an initial model where the nature of the layer boundaries played an important role (see section 3.1.5), they all shared the basic important assumption that the molecules on the average exhibit a substantial inclination with respect to the layer normal in the SmA phase. With tilted molecules, the d -value would be expected to be closer to that measured in SmC than to the length of a fully extended molecule, and such a situation was indeed quite often encountered. The exact nature of the molecular tilt and the origin of the SmA uniaxiality in spite of a substantial tilt angle, varied between his different models. Most important is clearly the *diffuse cone model*, of which he also presented several modifications as he developed it over time, but we will start to look at the precursor to this description, a model which I refer to as the *non-correlation model*.

3.1.2 *The non-correlation model*

Adriaan de Vries first presented the idea of tilted molecules in the SmA phase in an effort to explain the fact that the orthogonal SmA phase is never miscible with the tilted SmC phase, while the orthogonal and tilted SmB phases¹ were found to be misci-

1. With today’s classification scheme, neither the smectic SmB phase nor the soft crystal B phase is tilted (*cf.* section 1.3.3). It is not clear what the tilted smectic B phase de Vries discusses would be called today, but probably it is the soft crystal H phase.

ble with each other [28]. His suggestion was that the main difference between the SmA and SmC phases was that there is a coupling in tilt directions across layer boundaries in the SmC phase whereas this is absent in SmA. Without explicitly stating it, de Vries here implied that the molecules in SmA as well as in SmC exhibit a well-defined and uniform (within the layer) tilt with respect to the layer normal and that the difference in macroscopic properties is solely due to the presence or absence of a macroscopically uniform tilt direction.

This idea became completely clear in a short paper from 1977 [29] where the non-correlation model was first presented in its entirety. However, the model was not suggested to describe all SmA phases, as implied in [28], but de Vries now made a very clear distinction between two types of SmA-C transitions; those coupled to a shrinkage of the layer thickness d , with orthogonal molecules in SmA and tilted molecules in SmC, and those occurring without affecting the d -value. The latter were proposed to follow the non-correlation model, with a molecular tilt fixed at a permanent value throughout the A and C phases – de Vries suggested a tilt angle of $\sim 15^\circ$. In the SmA phase the layers are “stacked in a random fashion”, leading to a macroscopically uniaxial phase with the director parallel to the layer normal, but in the SmC phase the correlation length in tilt direction gradually increases along \mathbf{k} , producing a continuously increasing effective director tilt. In addition, he proposed that the non-correlation type of SmA-C transition is always a first-order transition, while the ‘normal’ transition type is of second order. However, the only motivation for this was the experimental observation of an unusually large SmA-C transition enthalpy for the single compound – among the ones discussed in the paper – having a fixed d -value throughout the SmA and SmC phases, while most other compounds show an unmeasurable transition enthalpy at the onset of macroscopic tilt. De Vries presented no fundamental reason to why the correlation \leftrightarrow non-correlation transition should be first order, but reading the earlier article [28] it is clear that he considered the long-range coupling of tilt direction to be associated with a term in the total free energy which he apparently assumed cannot go continuously to zero.

3.1.3 *The diffuse cone model*

In his reports on the experimental determination of distribution functions in liquid crystals using X-ray and neutron scattering [30, 31], the Exeter-based crystallographer Alan Leadbetter pointed out that the orientational disorder in the SmA phase actually leads to a substantial most probable molecular tilt, and that this in itself can explain the relation between layer spacing and molecule length. In [31] he writes:

This shows that even for a smectic A phase the orientational distribution of the long axes will result in the layer spacing (d) being significantly less than the molecular length (l) irrespective of any effects of internal conformation and it is indeed very common to find $d < l$ for these phases.

Inspired by the observations of his British colleague, de Vries realized that the – rather far-fetched – idea of layers with uniformly tilted molecules but without correlation in tilt direction across the boundaries, was not at all necessary. The non-correlation model – together with several other models for the SmA phase – was therefore rejected by de Vries, Ekachai and Spielberg in 1979 in a paper entitled ‘*Why the molecules are tilted in all smectic A phases and how the layer thickness can be used to measure orientational disorder*’ [32]. The ideas of Leadbetter were here developed into what de Vries called the *diffuse cone model* (although the name was not introduced until somewhat

later [33]), and it seemed the question of the $d - l$ discrepancy was to a large extent solved since the new model required no special, hard-to-motivate, properties of the SmA phase. As is clear from the title, de Vries thus no longer saw any need to distinguish between two different types of SmA-C transition, although he would do so again in later work (see section 3.2.1.2).

Today the idea of an SmA phase with tilted molecules is mainly connected to de Vries, although it is a strange historical fact that the description of his which seems to have survived the best is the older and much less general non-correlation model, not the diffuse cone model. This is indeed difficult to understand, because when reading de Vries' and Leadbetter's papers, it is obvious that the diffuse cone model to a large extent *must* be correct and apply to *all* smectic phases, since its basis is nothing but the recognition of the orientational disorder which undoubtedly is present in smectics. The non-correlation model, on the other hand, attributes properties to the SmA phase which cannot be regarded as generally present, rendering non-correlation SmA phases – if they exist – a very special case. Nevertheless, the consequences of this model are interesting, in particular in the case of the chiral SmA* phase. It is worth to stress, however, that a simple equivalence between the non-correlation model and de Vries' view of SmA phases is not historically correct, and that there is no reason to classify a compound as a 'de Vries SmA' material, defined as something different from 'ordinary SmA', just because the layer thickness in the SmA phase does not correspond to a phase where all molecules stand up along the layer normal. If one should discuss 'de Vries materials' as a special case of liquid crystals (even though a better name should certainly be used) it should, as will become clear in section 3.2, instead be materials where the *transition* between SmA and SmC occurs without affecting the layer thickness.

A graphical illustration of the diffuse cone model is given in figure 3.1 *a*. The model is to a large extent a merger of the observations of Leadbetter with de Vries' non-correlation model. To understand Leadbetter's reasoning, we start by introducing the *orientational distribution function* (ODF), $f(\beta)$, which is essentially a Boltzmann distribution:

$$f(\beta) \sim e^{-\frac{V(\beta)}{kT}} \quad (3.1)$$

where $V(\beta)$ is the potential as a function of the angle β . We may understand the ODF as describing the preference of a molecule to tilt the angle β relative to \mathbf{n} . It has its maximum value for $\beta = 0$ and then falls off continuously and rather rapidly for increasing values of β . However, as no other degrees of freedom than β are considered, $f(\beta)$ could only describe the orientational distribution in two dimensions. The 3D case can be modelled by considering all possible molecule orientations as spanning a hemispherical² state space with \mathbf{n} as the north-south axis. A certain point on the surface corresponds to \mathbf{m} aligned along the line from the origin to that point. The probability to find a molecule with a certain angle β relative to \mathbf{n} is proportional to the value of the ODF for this angle, but also to the total density of states with this $\mathbf{m} - \mathbf{n}$ inclination. With the aid of figure 3.2 we see that a molecule orientation restricted to an inclination between β and $\beta + d\beta$ and an inclination direction between φ and $\varphi + d\varphi$ takes up an area in state space given by $Rd\beta \cdot R\sin\beta d\varphi = \sin\beta d\beta d\varphi$, where we in the last step set the

2. The director sign invariance makes the southern hemisphere degenerate with the northern.

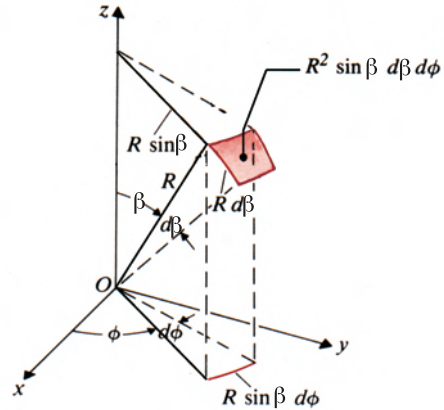


Figure 3.2 Graphical illustration of how to calculate the area of a surface element on a sphere of radius R .

state space hemisphere radius to unity. In the SmA phase we have full degeneracy in φ so all tilt directions must be considered, giving us a total area $2\pi \sin\beta d\beta$ in state space which corresponds to a certain inclination β . We can thus conclude that the true probability of an $\mathbf{m} - \mathbf{n}$ inclination between β and $\beta + d\beta$ in three-dimensional space is proportional to $f(\beta)\sin\beta$ rather than to $f(\beta)$ alone.

Typical examples of the two functions, calculated using an approximation [32] based on the Maier-Saupe model for the orientational distribution in nematics and with a value of the nematic order parameter $S = 0.8$, are given in figure 3.3, illustrating that they have quite different shapes. Most important, the orientational probability function $f(\beta)\sin\beta$ is zero rather than maximum for $\beta = 0$, illustrating the density of states minimum occurring for this inclination angle. The maximum of the function is instead found at $\beta \approx 15^\circ$ and the average value $\langle\beta\rangle$, calculated using $f(\beta)\sin\beta$ as weighting function, is normally around 20° [32]. It is thus clear that the picture of the molecules standing approximately normal to the layers in the SmA phase is quite far from the truth. Realizing this, de Vries and Leadbetter pointed out that the observation of a layer spacing smaller than the molecule length is indeed what should be expected in any SmA phase.

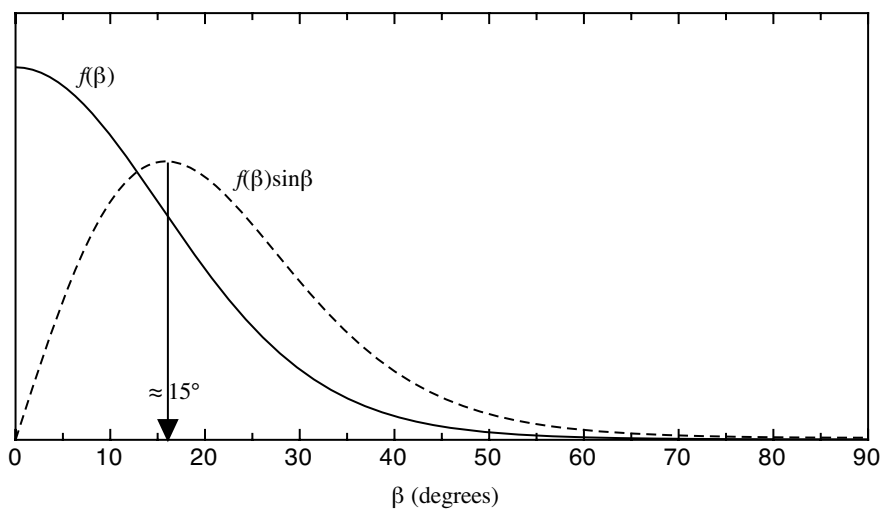


Figure 3.3 Typical examples of the (2D) orientational distribution function $f(\beta)$ and the (3D) orientational probability function $f(\beta)\sin\beta$, calculated for the case $S = 0.8$. The curves are drawn with arbitrary units on the y-axis.

To make this absolutely clear, consider an SmA phase consisting of orientationally disordered rigid rods of length l . In this case the smectic layer spacing d is described by the average:

$$d = l \langle \cos \beta \rangle \quad (3.2)$$

where β , as usual, denotes the inclination angle between the rod and the director, which in the SmA case of course coincides with the smectic layer normal \mathbf{k} . Let us now expand equation (3.2) to second-order in β :

$$d \approx l \left(1 - \frac{\langle \beta^2 \rangle}{2} + \dots \right) \quad (3.3)$$

This can be compared to the corresponding expansion of the nematic order parameter, described in chapter 1:

$$S \approx 1 - \frac{3}{2} \langle \beta^2 \rangle + \dots \quad (1.2)$$

We can now eliminate $\langle \beta^2 \rangle$ and obtain:

$$d \approx \frac{l}{3} (2 + S) \quad (3.4)$$

which in the limit $S \rightarrow 1$ describes how d depends on the orientational order parameter S .

Equation (3.4) shows that the layer spacing equals the rod-length l in the case of perfect orientational order, $S = 1$, only. In any case of orientational disorder ($S < 1$) d is reduced in comparison to l . With typical SmA values of S , we have to expect smectic layer spacings that are 7 - 10 % reduced with respect to l just as is usually the case. On the other hand, an observation of d being equal to l should be considered extraordinary indeed!

A consequence of the diffuse cone model is that, dynamically, the smectic layer spacing is not everywhere, and all the time, the same: due to the orientational disorder, the molecules must sometimes (somewhere) stand close to perpendicular to the layers, imposing a large layer spacing, sometimes (somewhere) be very much inclined, demanding a much smaller layer thickness. The average layer spacing is still quite well-defined at each temperature but one must allow for local fluctuations in d , as well as layer boundaries which are wavy rather than straight.

3.1.4 The zig-zag model

After having discussed the intermolecular order / disorder, the question which may next be addressed is what type of *intramolecular* order prevails in smectics, *i.e.* how does the 'rigid rod' behave internally? It is difficult to object to de Vries' reasoning for the SmA phase on a general level, as it is clear that the orientational order in liquid crystals is indeed far from perfect, but one may ask if it is really the molecules as a whole that define the low orientational order, or if different parts are more ordered than

others. It is well known that the mobility of the terminal chains is much larger than that of the rigid mesogenic core, and that there is quite a large degree of freedom in the angle which the end chains on the whole make to the core. One may therefore contemplate that the rigid cores are much more ordered than the general orientational order parameter suggests, while the flexible terminal chains exhibit much larger fluctuations and may also have a different average orientation.

Among the first to address the relation between the SmA layer spacing and the length of the molecules were the chemists in Halle. Diele *et al.* [26] suggested that the molecules exhibit a kinked conformation with their cores orthogonal but the end chains tilted in the SmA phase, as illustrated in figure 3.1 *b*. This gives the phase the observed uniaxial properties but at the same time a layer spacing d smaller than the length of the fully extended molecule l . This view of the SmA phase is sometimes referred to as the ‘zigzag’ model. It appeared in many different modifications and was one of the main competitors to the ideas of de Vries. Today it seems quite clear that one must consider several aspects of the smectic ordering, and that the zigzag model can – and should – easily be incorporated into the diffuse cone model rather than seen as a competing description. It is more a question of how much disorder should be attributed to the core, and how much to the tails.

The balance between the order of the cores and that of the terminal chains may to a large extent explain the different macroscopic behavior seen in different SmA^(*), SmC^(*) and SmC_a^(*) compounds. For instance, as the optical properties are mainly dictated by the internal structure and dynamics of the core, a study of the birefringence of a compound tells us much about the order of the cores. The chiral smectics studied in papers 1 and 2 exhibit a clearly field-dependent birefringence in the SmA* phase (such compounds are unusual, but a few other cases have also been identified, see *e.g.* [34]), a behavior which is a clear indication that the cores of the molecules, not only the end chains, are substantially disordered in the relaxed, field-free state. (We will describe these experimental results in more detail in section 3.4.4.) In contrast, the more common case of a fairly field-independent birefringence suggests that the orientational order of the mesogenic cores should be higher (even though, strictly speaking, the only conclusion one can draw from this behavior is that the electric field does not influence the orientational order of the cores).

3.1.5 The effect of molecular interdigitation on the smectic layer structure

Up to now we have been discussing different aspects of the orientational order of smectics, but also the type and degree of *positional* order may have a large impact on the SmA layer geometry. If one allows for a relatively large degree of molecular interdigitation between adjacent layers in the SmA phase, *cf.* figure 3.1 *c*, a layer spacing which is smaller than l may result. This was actually de Vries’ first proposal for explaining the $d - l$ discrepancy [35] but he later rejected it when he realized that the diffuse cone model could explain the situation in a less *ad hoc* way [32]. However, molecular interdigitation is always to a certain extent present, and it can have important consequences. Not only does it still occur in the modern discussion of the layer spacing of chiral SmA*-C* materials [36, 37], but we will see in chapter 5 that there are many indications that interdigitation can actually influence the whole phase sequence of smectics.

3.2 The molecular origin of the optical SmC(*) tilt

– *tilting transitions with and without layer shrinkage*

With the awareness that the SmA phase cannot be regarded simply as a layered phase where all molecules stand orthogonal to the layers, the nature of the director tilt present in *e.g.* the SmC phase becomes a much more complex matter than one may first anticipate. In fact, the origin of the optical tilt has been a constant matter of debate since the early 1970s, when it was first discovered that a compound exhibiting SmA and SmC phases generally has a temperature dependent optical tilt angle θ_{opt} [38]. The view that had been prevailing earlier was that the SmC phase had a more or less constant and rather large tilt, as observed in the compounds with a direct transition from the nematic to the smectic C phase. Was the ‘new’ SmC phase, with a tilt which continuously increased from zero below the second order phase transition from SmA, saturating at a value of $\theta \approx 30^\circ$, of a different kind than that observed in compounds without an SmA phase? Was the molecular organization in the smectic layers different in the two cases?

3.2.1 The diffuse cone model descriptions of the onset of tilt

3.2.1.1 The asymmetric diffuse cone model SmA-C transition

One can view the transition from the orthogonal SmA phase to the tilted SmC phase in two ways. One way is to imagine that the molecules, for some reason, strive towards a non-zero inclination relative to \mathbf{k} in SmC. In other words, the orientation of energy minimization, around which the molecules fluctuate (more or less) symmetrically, is tilted away from the layer normal, and the director \mathbf{n} therefore exhibits a certain tilt relative to \mathbf{k} . This view of the tilting transition, which we will describe in more detail in section 3.2.1.2, will in general be connected to a shrinkage of the average layer thickness. The higher degree of order in SmC as compared to the SmA phase (*cf.* section 1.3.2) is perhaps not so obvious – the ‘attractor direction’ of the fluctuations has merely been shifted. The choice of the director tilt angle θ as the order parameter of the SmA-C transition may then seem not so well motivated.

There is however another, quite different, way of viewing the SmA-C transition. As in the nematic phase, the cylindrical symmetry of SmA allows order only in the angle β , expressing the inclination of the long molecular axis with respect to the director (which in SmA coincides with the layer normal \mathbf{k}). In the smectic C phase, the cylindrical symmetry is removed, allowing ordering also in the azimuthal angle φ . If we keep the direction of the layer normal, \mathbf{k} , as the ‘attractor direction’ of the orientational fluctuations, but introduce a biasing of the azimuthal angle towards a certain inclination direction φ_0 , we also end up with the geometry of the SmC phase. The average molecular long axis orientation, *i.e.* the director \mathbf{n} , is tilted a certain angle θ away from the layer normal, in a well-defined direction φ_0 .

We will keep the interpretation of the angle β as the deviation from the *director*. In many cases in the treatment of smectics, we are however more interested in the deviation from the *layer normal*, and as $\mathbf{n} \neq \mathbf{k}$ in SmC this deviation is not expressed by β . In order to discuss the molecular tilt with respect to the layer normal for all smectic phases, we introduce the angle θ_s , the (instantaneous) single-molecule tilt. This will in many cases take the role of β in the following.

In the second view of the origin of the director tilt, which by de Vries was given the name ‘asymmetric diffuse cone model SmA-C transition’ [39], it is quite obvious that

the appearance of director tilt θ reflects an increased orientational order, namely in the reduced fluctuations in the azimuthal angle φ . In the spirit of A. Wulf's theoretical description of the diffuse cone model SmA-C transition [40], we may express this formally by introducing a new order parameter r , defined by:

$$r = \frac{\theta}{\langle \theta_s \rangle} \quad (3.5)$$

where $\langle \theta_s \rangle$ is the root mean square molecular inclination with respect to \mathbf{k} . The director tilt θ can only be equal to $\langle \theta_s \rangle$ if the azimuthal ordering is perfect. The new order parameter r also reaches its maximum value $r = 1$ in precisely this situation. On the other hand, at complete azimuthal disorder, the director tilt will vanish and so will r as defined in equation (3.5).

Within this description of the director tilting, the order in the inclination angle θ_s is not *per se* affected by the transition, which means that the average inclination $\langle \theta_s \rangle$ can be the same in SmC as in SmA. Hence the layer spacing d , related to $\langle \theta_s \rangle$ through equation (3.2), can also remain unaffected. What makes de Vries' diffuse cone model so interesting is thus not that it can explain the discrepancy between d and l in the SmA phase, but rather that a transition to a tilted phase can occur without any layer shrinkage. Actually, the model described so far predicts that the SmA-C transition *always* occurs at constant layer thickness. But it is experimentally well confirmed that this is the exceptional case, while a decrease in d on cooling through the SmC phase is much more common. When taking the step from the simpler SmA case [32] to the SmC phase, de Vries therefore introduced additional degrees of freedom, in terms of new tilt angles, in the model [27, 33, 39]. The number of different tilts which have to be kept apart now approaches the limit of confusion. In order to minimize this, the different tilt definitions occurring in the discussion are summarized in Table 3.1.

The new tilt angle introduced with the asymmetric diffuse cone model is the *preferred tilt* or *tilt of minimum energy*, and is (here) denoted θ_p . This is different from the *spatial average* tilt, *i.e.* the director tilt θ as defined in section 1.4. At first sight, one would think that it instead is equivalent to the root mean square tilt $\langle \theta_s \rangle$, *i.e.* the tilt obtained when the tilt *direction* is not considered in the averaging, but de Vries makes a difference even between these tilts. He suggests that the actual value of $\langle \theta_s \rangle$ will reflect a balance between the strive towards energy minimization by tilting the angle θ_p , and the equally present wish to align along the cone axis, which has the role of an 'attractor' direction around which the molecular orientations are distributed. This direction is most easily defined by the introduction of yet another tilt angle, which I denote θ_a . In the asymmetric diffuse cone model, this angle is always identically zero.

3.2.1.2 The tilted diffuse cone model SmA-C transition and the skewed cybotactic nematic phases

In the asymmetric diffuse cone model, which was de Vries' first attempt to model the SmC phase and the SmA-C transition, the cone axis coincided with the layer normal. Later on [39], de Vries divided the SmC phases into two classes. The older model applied to the case that the smectic, positional, order is much stronger than the nematic order. If instead the latter, orientational, order is the stronger, as one may expect in the case of a direct nematic to smectic C transition, via skewed cybotactic clusters, de Vries instead suggested that the whole cone axis tilts. The distribution of molecular

Table 3.1 Different types of tilt angles considered in the discussion. Note that they are all defined as strictly positive, $0 < \text{tilt} < 90^\circ$, i.e. in order to describe the tilt direction, the phase angle φ has to be specified.

	Symbol	Name	Zero direction	Meaning
Non-measurable	θ_s	Single-molecule tilt angle	\mathbf{k}	Instantaneous value of the inclination of a particular molecule with respect to the layer normal \mathbf{k} .
	$\langle \theta_s \rangle$	Root mean square tilt	\mathbf{k}	Average of the <i>magnitude</i> of the molecule long axis tilt. The directions in which the molecules tilt are not considered.
	θ_p	Preferred tilt angle	\mathbf{k}	The value of θ_s which would best correspond to the smectic layer spacing. This is supposed to be the energy-minimizing tilt.
	θ_a	Attractor tilt angle	\mathbf{k}	The inclination of the diffuse cone axis.
	θ	Director tilt angle	\mathbf{k}	<i>Spatial</i> average of the tilt. The direction of the tilt is considered when performing the average.
Measurable	β	Director deviation angle	\mathbf{n}	The angle β is special in the sense that it is not necessarily measured with respect to the layer normal \mathbf{k} in the smectic phases, but to the director \mathbf{n} . This is the only difference to θ_s , so these two angles are the same except for a constant offset. In SmC this offset is approximately equal to θ_p , i.e. $\beta(\text{SmC}) \approx \theta_s - \theta_p$, while in the SmA and nematic phases the offset is zero, i.e. $\beta(\text{N, SmA}) = \theta_s(\text{N, SmA})$.
	θ_{opt}	Optical tilt angle	\mathbf{k}	The inclination of the optic slow axis, i.e. the direction of maximum refractive index, with respect to the layer normal.
	θ_{SAXS}	Small-angle X-ray tilt angle	\mathbf{k}	The angle fulfilling the relationship $\cos \theta_{\text{SAXS}} = \frac{d_{AC}}{d_C}$. See section 1.4.
	θ_{WAXS}	Wide-angle X-ray tilt angle	\mathbf{k}	This tilt angle essentially corresponds to the spatial average angle between the axis of inertia of the molecules and the layer normal, i.e. it is probably the best experimental approximation for the director tilt θ . See section 1.4.

orientations is now, as in the SmA phase, supposed to be cylindrically symmetric around the cone axis, but this axis is inclined with respect to the layer normal, i.e. $\theta_a \neq 0$, in this *tilted diffuse cone model*.

This view of two different types of SmC phases, differentiated by the type of SmA-C transition and the behavior of the tilt, is still well accepted [41]. Today we know that a first-order transition to the SmC phase, which we always have in the case of a direct N-SmC or (less common) isotropic-SmC transition, and in a few cases also at an SmA-C transition, results in a large, fairly temperature-insensitive tilt-angle ($\theta \sim 45^\circ$), while

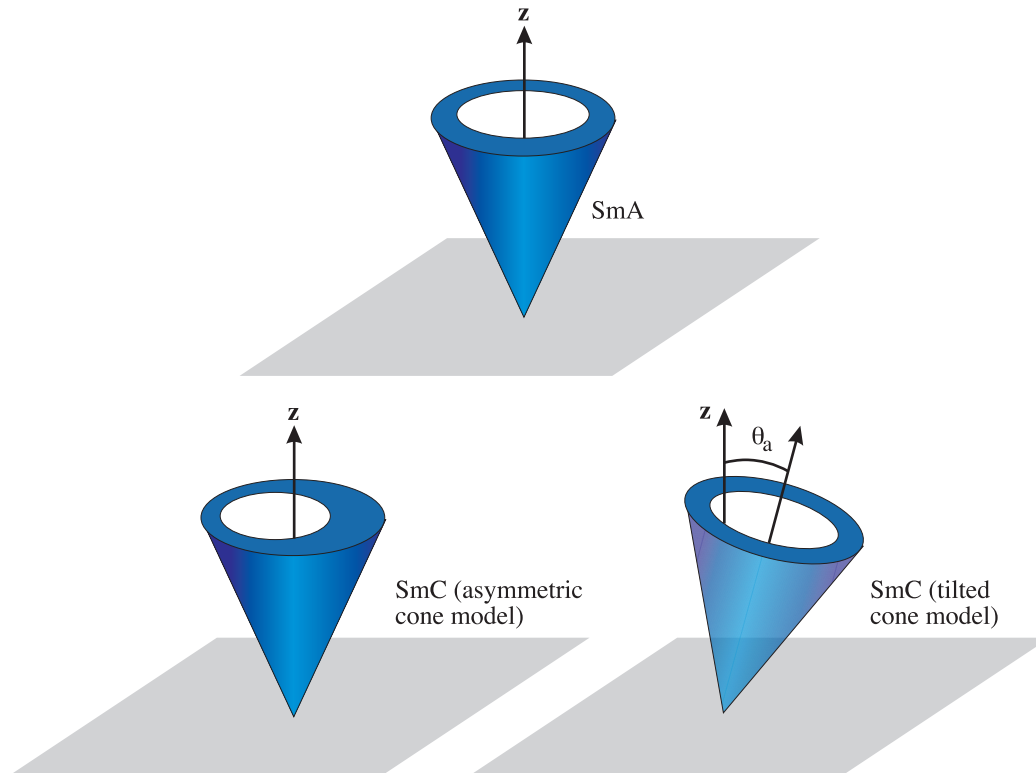


Figure 3.4 Three smectic phases as described within the diffuse cone model. The cylindrically symmetric SmA phase (top), the asymmetric cone SmC (bottom, left) and the tilted cone SmC phase (bottom, right). The thickness of the cone surface in a certain direction is proportional to the probability of finding molecules tilted towards this direction. Redrawn from de Vries [39].

ature and seldom reaches values larger than $\sim 30^\circ$ [42]. The fact that the tilt can vary with temperature when the SmC phase is preceded by SmA at higher temperatures, was reported as something quite unexpected when it was first described by Taylor *et al.* [38]. The subdivision of the SmC phase into two classes is today not connected to the diffuse cone model descriptions, but such a connection is not difficult to do. For instance, the moderate limiting tilt value below the second order transition is easy to understand within the asymmetric diffuse cone model, as the tilt is here limited by the very origin of the diffuse cone, namely the orientational disorder. Typical order parameters correspond to average tilts of $\sim 20^\circ$ so a considerably larger value of the director tilt without tilting the cone would require an unrealistically low order parameter.

The two versions should not be seen as the only possibilities for the SmC phase, but rather as two extremes, as also pointed out by de Vries in [39]. The biasing of the azimuthal fluctuation will probably induce a slight tilt of the cone and it is difficult to imagine a complete rotational symmetry around a tilted cone axis. Thus, all smectic C phases probably have components of both descriptions. It is, however, obvious that a tilting of the cone axis must have larger impact on the layer spacing, so a non-layer shrinkage SmA-C transition must come much closer to the asymmetric than to the tilted description.

The connection between the asymmetric diffuse cone model and high smectic order parameter, and the tilted model and high nematic order parameter is interesting from a modern perspective. It is quite likely that the balance between the processes involved in producing the tilt (cone axis tilt or azimuthal biasing) is affected by the

extent to which we can treat the smectic layers as individual systems, *i.e.* by the smectic order parameter. In the case of weak smectic order, where molecules in one layer are much affected by steric interaction with molecules from the neighboring layers (interdigitation), the orientational (nematic) order, may be expected to be higher. The azimuthal biasing may then play a much smaller roll than in the case of high smectic order where the ordering is more two-dimensional. As there are many indications that antiferroelectric liquid crystals have a higher smectic order than ferroelectric liquid crystals, it is thus not unlikely that the diffuse cone model aspect of the description of smectic phases is more important among the former materials. For instance, in the famous AFLC compound MHPOBC, the decrease in layer thickness measured when heating the compound from the high-ordered SmI_a^* phase to SmC_a^* [43], clearly suggests that the lower degree of order in the high-temperature phases has an important effect on the smectic structure. Also, the polar non-layer shrinkage materials described in section 3.4 have high smectic order but very weak correlation across the layer boundaries. One of them is also clearly antiferroelectric.

3.2.1.3 Shortcomings of the diffuse cone model SmC descriptions

Although the simplicity of the basic diffuse cone model description of the onset of tilt makes it attractive and useful, it is not difficult to find it problematic in various ways. By extending the original diffuse cone model to include the preferred tilt angle θ_p , de Vries could account for all types of experimental data observed at SmA-C transitions, but this was at the cost of rendering the model much less transparent and weaker in many respects. Not only does the introduction of all the different tilt angles make the model quite confusing, but de Vries also makes several approximations which may be questioned. For instance, despite the fact that the cylindrical symmetry is lost at the onset of tilt, the preferred tilt angle θ_p is supposed to be independent of the phase angle φ . Is it realistic to consider a φ -independent θ_p if we no longer have degeneracy in φ ? In the case of the tilted diffuse cone model, de Vries instead assumes cylindrical symmetry around the tilted cone axis. We here touch upon the acceptability of the uniaxial approximation of the SmC phase, introduced in section 1.4. For the optical properties it seems that the approximation is clearly acceptable to first order, but it is not obvious what the consequences are of bringing this approximation into the modelling of the onset of tilt.

Furthermore, the probability that θ_s takes a certain value in the de Vries' model is supposed to be proportional to $e^{K \cos^2(\theta_s - \theta_p)}$, where K is a factor containing the nematic order parameter. The problem with this function is that it is symmetric in θ_p , *i.e.* a tilt larger than the preferred tilt is just as probable as the same deviation towards smaller tilt. But the average tilt $\langle \theta_s \rangle$ is supposed to be a result of a balance between forces pulling the molecules towards the θ_p orientation on the one hand, and towards θ_a on the other, so these situations must then be very different and have very different probabilities. The deviation towards smaller tilt seems quite likely, since the tilt then ends up between the two limiting values θ_p and θ_a , but fluctuations towards tilt angles above θ_p must be considered to be much less probable, in contrast to the probability function proposed by de Vries.

Finally, there is good reason to ask what actually attracts the molecules to the direction of the cone axis in SmC as well as in SmA. The most natural explanation seems to be that the cone axis corresponds to the energy-minimizing direction, at least in the SmA and tilted diffuse cone SmC phases, but de Vries explicitly states that this

is not the case [27]. Wulf proposed that alignment along the cone axis direction (which in his model was restricted to the layer normal) may instead be favored by translational entropy and intralayer van der Waals attraction [40], but gave no further explanation or motivation. The origin of the preferred tilt angle θ_p is also a strange story. The magnitude of θ_p is supposed to be set by the smectic layer spacing d [27], but the whole basis for the diffuse cone model is that d is a function of the average tilt $\langle\theta_s\rangle$ which, in turn, is a function of θ_p in the models for the SmC phase. In other words, in the development of the diffuse cone model to fit all kinds of experimental data, de Vries ends up in a circular reasoning!

It is beyond the scope of this thesis to digress further into these problems, so I will restrict myself to point out that the diffuse cone models, although attractive in many respects, suffer from a number of shortcomings. Nevertheless, there are no smectic C or smectic A phases where one can neglect the orientational disorder, and thus the models must to a certain extent be considered.

3.2.2 Other ways of explaining a non-layer shrinkage SmA-C transition

– conformational changes and variations in interdigitation

Just like the diffuse cone model is not the only possible explanation for the SmA layer thickness, it is also not necessarily the correct explanation of an SmA-C transition occurring without a shrinkage of the layers. Following the zig-zag model, one can imagine that some sort of change in the molecular conformation occurs at the SmA-C transition, such that the effective length of the molecules is increased just by the amount needed to compensate for the director tilt. Bartolino *et al.* [44] suggested a kinked conformation, similar to that proposed for the SmA phase by the Halle group (described above), but instead for the SmC phase. The end chains were here supposed to be orthogonal to the layers and the cores tilted. In the SmA phase, on the other hand, they assumed that the molecules are fully elongated and orthogonal. Such a scheme cannot explain a constant layer spacing, since already the tilting of the cores will reduce the effective length, but well a layer spacing which varies much less than would be expected from the magnitude of the optical tilt angle. Combining this model with that of the Halle group, assuming fluctuating tilted end chains in both phases, but with decreasing magnitude of end chain tilt and fluctuations in the SmC* phase, Buivydas *et al.* [45] constructed a model which in principal could explain a constant layer spacing. This of course approaches de Vries' ideas to a large extent, but the orientational disorder is here restricted to the tails.

Two things should be pointed out regarding this 'conformational change' model for SmA-C transitions without layer shrinkage. First, it seems quite a coincidence that the change in effective molecule length exactly compensates the tilt. Second, it is difficult to explain a second-order NLS transition, since a conformational change can hardly be regarded as continuous.

Finally, a tilting transition without affecting the d -value can also be imagined to result from a change in the degree of molecular interdigitation across the layer interfaces. If one adopts the interdigitated view of the SmA phase described in section 3.1.5, but assumes sharper layer boundaries in the SmC phase, a layer spacing not affected by the tilting of the molecules may result [35, 37].

A graphical overview of the different suggested mechanisms for the SmA-C transition at constant d is given in figure 3.5.

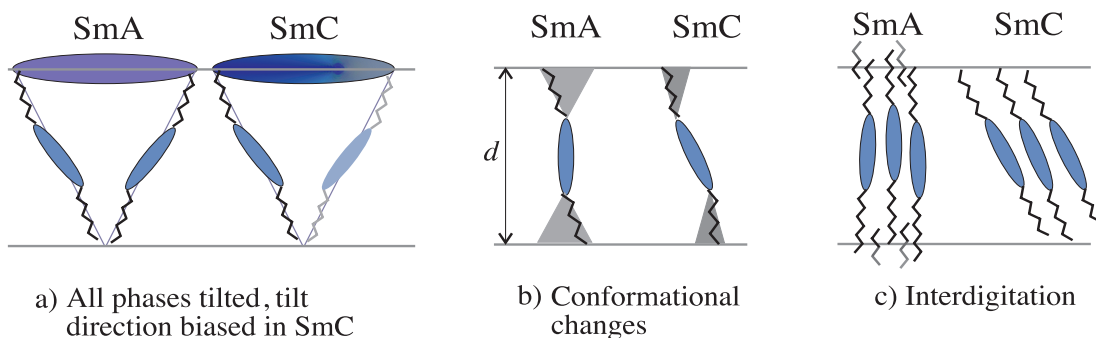


Figure 3.5 Different mechanisms proposed for a smectic A - smectic C transition occurring at constant layer thickness d .

3.3 The electroclinic effect and the de Vries SmA* models

– an update to polar liquid crystals

As mentioned in section 3.1.4, the idea of a substantial average tilt of the molecules will have important consequences for the optical properties of the phase, as long as the tilt is not restricted to the terminal chains but applies also to the mesogenic cores. The first obvious consequence is that any type of increased orientational order will increase the birefringence of the medium. Whereas the electroclinic effect in its simplest definition (*cf.* section 2.1.2.1) just means a tilting of the director, it is in the de Vries views of the SmA* phase obviously also connected to a biasing of the orientational fluctuations, *i.e.* a field-induced increased orientational order. Hence, the slow axis tilt induced by the applied field must also be connected to a corresponding increase in effective birefringence. Selinger *et al.* [34] have formalized these general observations in a theoretical model, where the molecules are treated as rigid rods, *i.e.* the cores exhibit the same tilt as the molecule as a whole. In addition to the obvious field-dependence of Δn , the model predicts that changes in Δn observed within the SmA* or SmC* phases of the de Vries type, are a function of the optical tilt angle θ_{opt} only.

The field-dependence of the birefringence and the Δn - θ_{opt} relation provide us with an easy means of experimentally detecting SmA* phases that can be described either by the diffuse cone or the non-correlation model, but how do we tell these two models apart? While the predictions regarding the electrooptic properties are in principal the same for the two models, it turns out that it is actually very difficult to explain the temperature dependence of the electroclinic effect within the non-correlation model. Yet, observation of a non-correlation SmA* phase, denoted ‘SmC_R’ ($R = \text{Random}$) has been claimed [46]. If each layer is uniformly tilted, and the randomization is strictly related to low correlation across the layer boundaries, each layer must exhibit virtually the same local spontaneous polarization P_s as in the SmC* phase. By applying only a weak electric field (without interlayer correlations there is no obvious strong restoring force, in contrast to helical SmC*, where the helix has to be unwound, or the antiferroelectric SmC_a*, where the antiferroelectric state has to be broken) the tilt directions should be organized on a macroscopic scale. The necessary field strength, and the

resulting optical effect, should in principle be independent of the temperature in the SmA* phase. But this is in complete conflict with the strong temperature dependence always observed for the electroclinic effect.

If a non-correlation chiral SmA* phase will ever be found – which must be regarded as unlikely – it should thus be easily recognized by its unique temperature independence of the electroclinic effect. A non-layer shrinkage chiral smectic which exhibits a ‘normal’ electroclinic effect should, on the other hand, rather follow the diffuse cone model, *i.e.* the mechanism behind the field-induced director tilt must be a biasing of the nematic order fluctuations. An important consequence of this result is that we have a distribution not only in tilt directions φ , but also in tilt magnitudes, θ_s . In all models developed [34] or used [46, 47] recently for explaining the macroscopic properties of chiral de Vries type non-layer shrinkage compounds, the randomization is supposed to occur only through fluctuations in φ , while θ_s has a more or less fixed value throughout the SmA* and SmC* phases. This oversimplification may be the reason for the inability of the models to quantitatively describe the optical properties of the investigated compounds.

3.4 Two examples of tilting transitions without layer shrinkage

– experimental evidence of diffuse cone model SmA-C* and SmA*-C_a* transitions*

Almost all FLC and AFLC materials exhibit a pronounced layer shrinkage when cooled from SmA* to the SmC* / SmC_a* phase. The structural defects generated by this variation in d has turned out to be the main obstacle for a successful large-scale commercialization of polar liquid crystal electrooptic devices. As the layers are positionally anchored at the surfaces, the decrease in d will induce a buckling of the layers into a chevron geometry which is the only one compatible with the new combination of surface and bulk conditions [48]. Accompanying the development of the chevron structure is the formation of so-called ‘zig-zag’ defects and a reduction in effective optical tilt angle, effects which seriously degrade the quality of any electrooptic device.

A few examples of ferroelectric liquid crystal materials displaying virtually constant smectic layer spacing have however been identified [36, 49, 50] and these compounds have therefore come to receive a considerable interest from industry as well as academia. In paper 1 we report on a new non-layer shrinkage FLC material with several peculiar properties and in paper 2 we describe the behavior of a mixture based on that compound. To the best of my knowledge, this is the first observation of an antiferroelectric liquid crystal without layer shrinkage. These two works will be summarized in the following.

3.4.1 Determination of the phase sequence

The two liquid crystals studied by us were supplied by Dr. Marc Radcliffe of the 3M company. The chemical constitution of the FLC single-compound, code-named 8422[2F3], is given in figure 3.6. The high degree of fluorination of one of the terminal chains of the molecule seems to play an important role for the properties of the material, as we will show below. Unfortunately, it also makes the compound a poor X-ray

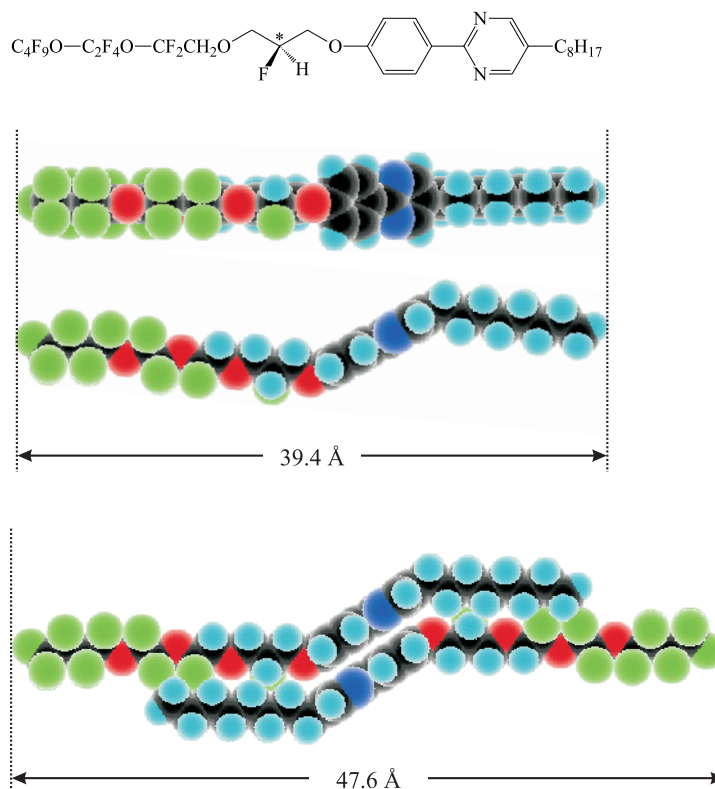


Figure 3.6 Chemical constitution of the non-layer shrinkage FLC compound 8422[2F3]. The length l of a single maximally extended molecule, as well as that of an aggregate consisting of two anti-parallel oriented molecules in this conformation, as suggested by Rieker and Janulis [51, 52] for similar compounds, are also given.

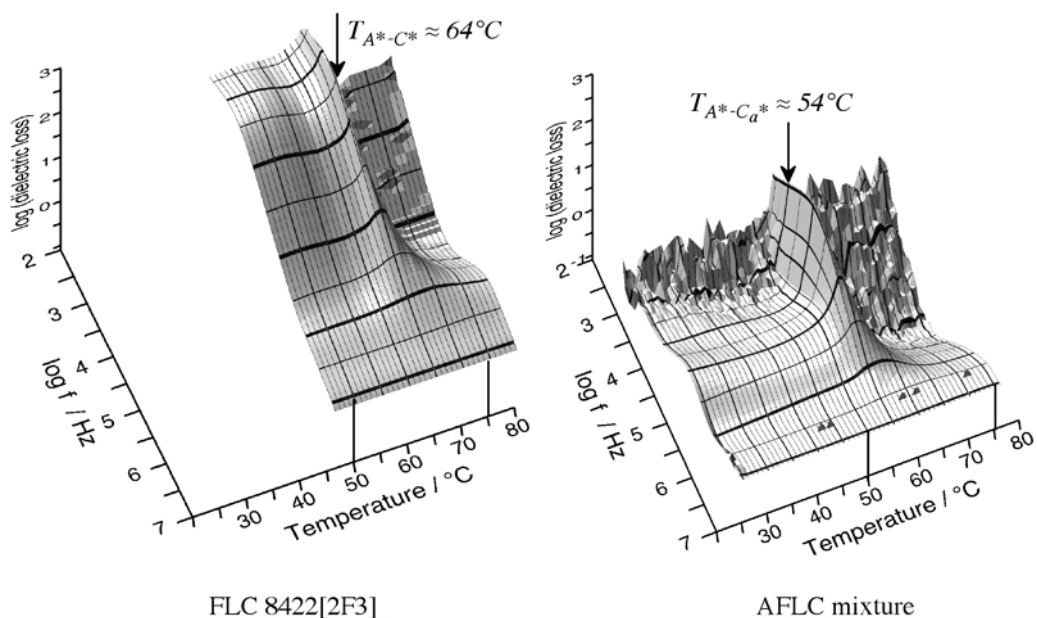


Figure 3.7 Dielectric absorption spectra, obtained on cooling, for the 8422[2F3] (left) and the mixture based on 8422[2F3] (right) in 10 μm thick planar-aligned samples. Both diagrams are plotted on the same scale, with the absorption axis logarithmic. Because of the crystallization of 8422[2F3] above room temperature, the measurement on the pure compound was not extended as far down in temperature as that of the mixture.

scatterer in the wide-angle regime, and the diffraction images obtained are therefore not as intuitively descriptive as for many other liquid crystals. Nevertheless, by evacuating the camera and prolonging the X-ray illumination, images good enough for quantitative analysis were obtained.

Both compounds develop helical macrostructures in bulk samples. In case of the pure compound, the resulting selective reflection in the quasi-homeotropic geometry (*cf.* appendix II.3. 2) was measured to be 404 nm [53], corresponding to a helical pitch of approximately 270 nm (assuming an average refractive index of ~ 1.5).

One of the best ways of determining the phase sequence in polar liquid crystals is by carrying out dielectric spectroscopy measurements on planar-aligned cells [16]. We performed such experiments on both liquid crystal materials and the results, as obtained on cooling, are illustrated in figure 3.7. The single-compound, 8422[2F3], exhibits a prominent absorption at temperatures below the SmA* phase, clearly indicating that the phase here is the polar SmC* phase. The absorption is typical of a phason mode, *i.e.* fluctuations in tilting direction which, due to the steric coupling between director and spontaneous polarization, couple to the measuring electric field. In contrast, the absorption spectrum of the mixture was almost featureless below the soft mode peak at the transition from SmA*. Here only two weak modes are active, one of them (barely) visible only towards the low-temperature end of the spectrum. This is the typical dielectric signature of the antiferroelectric SmC_a* phase [16].

The phase sequences of the two compounds can now be summarized, taking observations from DSC and optical microscopy into account in addition to the dielectric spectroscopy results.

Table 3.2 Phase sequence of 8422[2F3].

Crystal	\leftrightarrow	SmC*	\leftrightarrow	SmA*	\leftrightarrow	Isotropic
	43.1°C		64.5°C		91.0°C	

Table 3.3 Phase sequence of the AFLC mixture. (*RT = Room Temperature.*)

Crystal	\leftrightarrow	SmC _a *	\leftrightarrow	SmA*	\leftrightarrow	Isotropic
	$\sim -18^\circ\text{C}$		52°C		$\sim 78^\circ\text{C}$	

In the mixture case, it is impossible to give definite values for the melting and clearing points, since the first-order nature of these transitions in a mixture lead to extended temperature regions of two-phase coexistence.

3.4.2 Measuring the orientational distribution

The de Vries types of SmA-C transition can easily be recognized by tracking the evolution of the orientational distribution function (ODF) $f(\theta_s)$ (note the change $\beta \rightarrow \theta_s$, necessary since $\mathbf{n} \neq \mathbf{k}$) while cooling from the SmA to the SmC phase. If this remains unaffected by the transition, the average molecular inclination is constant and the transition must follow one of the de Vries scenarios. We investigated $f(\theta_s)$ in the SmA* and SmC* phases of the single-compound FLC, 8422[2F3], by wide-angle X-ray scattering (WAXS) experiments on samples uniaxially aligned in a moderate magnetic field (~ 1 Tesla). Selected examples of the diffraction patterns are shown in Figure 3.8.

At small scattering angles, the diffraction patterns of both phases exhibit very sharp first- and second-order (pseudo-) Bragg peaks along the meridian (defined by the direction of the aligning field, vertical, along $q_{||}$, in Figure 3.8). These peaks clearly show that the smectic layers were well-aligned with their normals, \mathbf{k} , along the mag-

netic field. As motivated in section 1.3.1, the diffuse scattering in the wide-angle regime exhibits a directional intensity modulation which reflects the orientational order of the rod-like molecules in the scattering volume with respect to the aligning field direction. Since \mathbf{k} coincides with the field direction, the intensity profile $I(\chi)$ directly probes $f(\theta_s)$, the orientational distribution function of the rod-like molecules relative to \mathbf{k} .

As expected, $I(\chi)$ measured in the SmA^* phase (left image, upper row in figure 3.8) exhibited a maximum on the equator (q_{\perp} , *cf.* figure 1.2). Much more surprising was the observation that the diffraction pattern did not change at all by cooling the sample into the SmC^* phase (right image, upper row). In sharp contrast to what is most often observed at smectic A-C and $\text{A}^*\text{-C}^*$ transitions [8], neither a splitting of the layer reflection, indicating a tilt of \mathbf{k} , with \mathbf{n} fixed in the magnetic field direction (*cf.* figure 1.3 *d*), nor a broadening along χ of the diffuse wide-angle maximum, indicating a tilt of \mathbf{n} , with \mathbf{k} fixed by the magnetic field, was observed. We can thus conclude that the total orientational distribution of the 8422[2F3] molecules in the scattering volume is not affected by the $\text{SmA}^*\text{-C}^*$ transition. Such a scenario is just what is to be expected at a de Vries type transition from SmA^* to helical SmC^* . In SmA^* we have rod-like molecules tilted by a certain average angle $\langle\theta_s\rangle$, all possible tilt directions φ being equally probable. Below the transition to SmC^* , $\langle\theta_s\rangle$ remains unchanged but

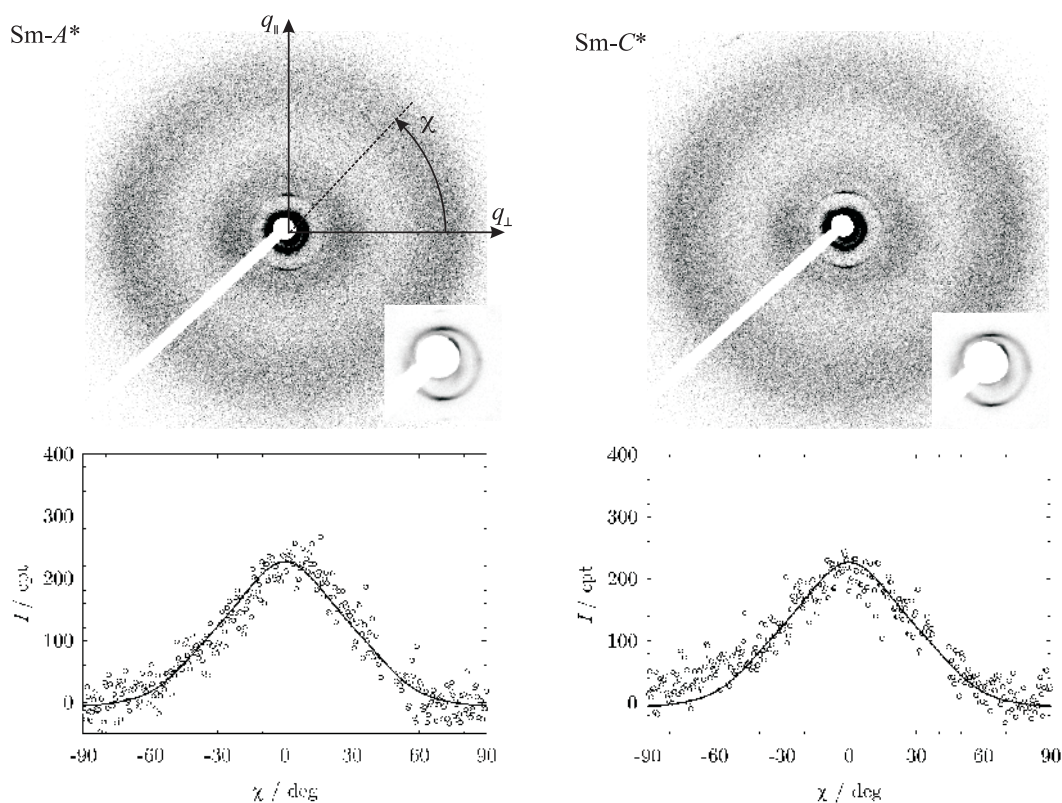


Figure 3.8 Upper row. X-ray diffraction patterns in the SmA^* (left) and SmC^* (right) phases of 3M 8422[2F3]. The magnetic field is oriented vertically (meridional direction). Since the scattering intensities in the small- and wide-angle regimes are very different, the layer spacing peaks are reproduced with lower contrast in the insets. Lower row. The directional scattering profile $I(\chi)$, as obtained by radial integration over the wide-angle regime in the diffraction patterns. The continuous curves are best fits of equation (3.6) to the experimental data obtained in the SmA^* phase.

the tilting becomes biased towards a certain direction φ_0 . As we have a chiral SmC* bulk phase, the preferred direction of tilt φ_0 spirals helically along \mathbf{k} . Integrated over a full pitch length, we therefore observe, like in SmA*, all possible values of φ with the same probability. As long as $f(\theta_s)$ remains unchanged, and the helical pitch is smaller than the dimensions of the scattering volume, the two configurations, SmA* and helical SmC*, cannot be distinguished by the X-ray experiment and thus produce identical diffraction patterns.

The striking similarity between the SmA* and SmC* diffraction patterns in Figure 3.8 directly gives a qualitative indication of the absence of change in the orientational order at the A*-C* transition. In addition, we investigated the orientational distribution function by a numerical analysis of the scattering profile obtained for the SmA* phase. Following a procedure developed by Davidson, Petermann and Levelut [54], we write an expansion for the scattering profile $I(\chi)$:

$$I(\chi) = \sum_0^{\infty} f_{2n} \frac{2^n n!}{(2n+1)!!} \cos^{2n} \chi \quad (3.6)$$

This is fitted to the experimental scattering data with the f_{2n} as fitting parameters. We can then obtain the ODF $f(\theta_s)$ through the following expression:

$$f(\theta_s) = \sum_0^{\infty} f_{2n} \cos^{2n} \theta_s \quad (3.7)$$

The best fit of equation (3.6) to the SmA* data of 8422[2F3] is shown as a solid line in Figure 3.8. The curve is actually drawn in both lower diagrams in order to illustrate how well the ODF determined for the SmA* phase describes also the SmC* data. In figure 3.9 we have plotted the orientational *probability* distribution function $f(\theta_s)\sin\theta_s$. As seen from the maximum in the curve, the most probable inclination angle of the molecules in the SmA* and SmC* phases of 8422[2F3] is fairly high, slightly above 25°.

Knowing $f(\theta_s)\sin\theta_s$, we can use the general averaging:

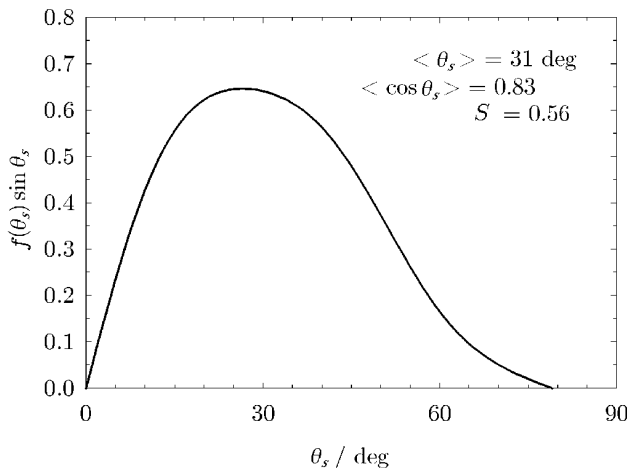


Figure 3.9 The function $f(\beta)\sin\beta$ as obtained from the experimental wide-angle scattering data, $I(\chi)$, and the corresponding average molecular tilt $\langle\beta\rangle$, average molecule length projection factor $\langle\cos\beta\rangle$ and orientational order parameter $S = \langle P_2 \rangle$.

$$\langle X \rangle = \frac{\int_0^{\pi/2} X f(\theta_s) \sin \theta_s d\theta_s}{\int_0^{\pi/2} f(\theta_s) \sin \theta_s d\theta_s} \quad (3.8)$$

to (numerically) calculate any expectation value $\langle X \rangle$ of a certain property X related to the probability distribution. With $X = \theta_s$ we obtain the average SmA* and SmC* inclination angle $\langle \theta_s \rangle = 31^\circ$. Such a large molecular inclination points towards a substantial orientational disorder in the smectic phases of the compound. Indeed, the orientational order parameter S , calculated by using equation (3.8) with $X = (1/2)(3 \cos^2 \theta_s - 1)$, was found to be only 0.56, about 20 - 30 % lower than the typical $S = 0.7 - 0.8$ observed in ordinary SmA^(*) phases.

3.4.3 The correlation between orientational distribution and smectic layer spacing

The layer spacing as a function of temperature was measured with high accuracy using small-angle X-ray scattering on unaligned samples. The results are shown in figure 3.10. After a non-negligible increase on cooling through the SmA* phase (in particular observed in the AFLC mixture), d decreased marginally after the onset of tilt in SmC* or SmC_a*. The decrease was of the same, very small, magnitude in the two materials: the minimum value, observed ~ 15 K and ~ 8 K, respectively, below the transition temperature, was only 0.3 Å less than the layer spacing measured at the low-temperature border of the SmA* phase. On further cooling, d again increased and at room temperature the value of the pure compound had actually regained the value 38.7 Å observed at the onset of optical tilt. With such small variations in layer spacing,

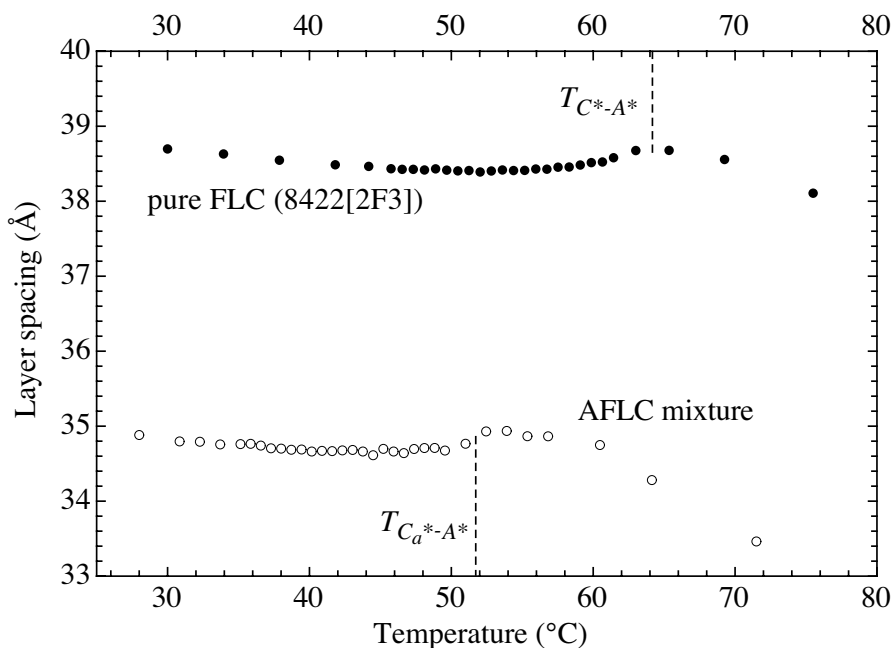


Figure 3.10 Layer spacing of the pure FLC compound 8422[2F3] and the AFLC mixture based on this compound, as a function of temperature. The data were obtained from small-angle X-ray scattering (SAXS) measurements on cooling from SmA*. Note that the variation in d within the tilted phase (SmC* or SmC_a*) is only 0.3 Å in both cases.

it is clearly reasonable to regard both materials as non-layer shrinkage smectics. An interesting question to contemplate, of course, why d increases in the SmA* phase on approaching the transition. As d , strictly speaking, increases from either side, the onset of macroscopic tilt seems to entail some subtle change in the aggregation of molecules, perhaps connected with appearing helical order.

Considering the relation between the smectic layer spacing d and the orientational order, equation (3.2), it is interesting to compare the SAXS and WAXS results for the pure compound by setting $X = \cos\theta_s$ in equation (3.8). We thus obtain the value $\langle \cos\theta_s \rangle = 0.83$ (for the SmA* as well as the SmC* phase of 8422 [2F3]) showing that d is about 17 % reduced with respect to the length of the ‘rods’ building up the layers. With $d \approx 38.7 \text{ \AA}$ we can then estimate the rod-length to:

$$l_{rod} = \frac{d_{SAXS}}{\langle \cos\theta_s \rangle} \approx 47 \text{ \AA} \quad (3.9)$$

However, the length of the 8422[2F3] molecule has been calculated to be only $l = 39.4 \text{ \AA}$ (*c.f.* figure 3.6). Our $l_{rod} \approx 47 \text{ \AA}$ therefore suggests that the smectic layers in this compound are composed by aggregates of more than one molecule. Rieker and Janulis [51, 52] have studied semifluorinated liquid crystals which in many respects resemble 8422[2F3] and presented experimental evidence that the molecules form aggregates such that the fluorinated chain of one molecule pairs with the non-fluorinated one of its neighbor. Such an aggregate will for the case of 8422[2F3] have a length l in the range 47 - 48 \AA , fitting very well with our experimentally determined value of l_{rod} .

Whether the same aggregation occurs in the AFLC mixture is impossible to say at present since we have not yet performed WAXS measurements on this material. The $\sim 4 \text{ \AA}$ decrease in layer spacing, as compared to the pure FLC compound, suggests either that the aggregation does not occur, or that the orientational disorder is even higher in the mixture, a conclusion which is not unreasonable.

3.4.4 The optical evidence for the validity of the diffuse cone model in the SmA*, SmC* and SmC_a* phases

3.4.4.1 The peculiar natural textures

An investigation of the sample texture as a function of temperature and cell gap gave clear evidence of several unique properties of 8422[2F3]. In figure 3.11, the texture at $8.5 \mu\text{m}$ cell gap during cooling from the SmA* phase is shown. The sample was initially rotated to the extinction orientation of one domain (horizontal, along top image border). The SmA* texture, (a), had a first-order pink birefringence color. Directly after the phase transition, (b), a quasi-periodic modulation along the layer normal appeared, revealing that the liquid crystal tried to adopt a helical structure. While the helix developed fairly well in some areas, others were clearly non-helical, *i.e.*, in these areas the sample was (quasi-) surface-stabilized. On further cooling, the helix was expelled in more and more regions, leaving only a few domains with the slow axis along \mathbf{k} in the texture at 50°C (c).

A most interesting observation was that the color of the helical regions was very similar to that of the SmA* phase texture, in contrast to the color of the non-helical regions which were first dark blue close to the transition, then turned cyan at lower

temperatures. In other words, the birefringence of the helical SmC* state was approximately the same as in SmA* while in the non-helical state it was considerably higher (see the birefringence color chart in figure 2.6). This is quite different from what one usually expects to see at a SmA*-SmC* transition, in which case the spacial averaging of the optical properties, resulting from the helix formation, radically decreases the birefringence in the helical state (see, *e.g.*, [55]). In the surface-stabilized state, one may expect a very small increase of birefringence also in regular SmC* materials, due to the transition from uni- to biaxiality³, but the magnitude of this change is far too small to explain the observed color change, see, *e.g.*, [56, 57]. On the other hand, this behavior fits very well with a de Vries type SmA*-SmC* transition. As this is a transition from random to ordered molecular tilt, an increased effective birefringence must be expected as the optical tilt increases from zero in non-helical SmC* samples. But if the helix develops, the periodic modulation in φ has the same averaging effect as in the SmA* with random tilt direction (assuming a short helical pitch as in the present case, *i.e.*, $p \sim 0.3 \mu\text{m}$), leading to identical birefringence and slow axis direction in both phases.

The many peculiar characteristics of the SmC* textures formed by 8422[2F3] actually constitute unusually clear evidence of an extremely weak correlation of the tilt direction across the layer boundaries in this compound. The occurrence of surface-stabilization of a compound with a $p \sim 0.3 \mu\text{m}$ helical pitch at $8 \mu\text{m}$ cell gap is quite extraordinary. In fact, the helix does not form unobstructed even at cell gaps as large as $20 \mu\text{m}$. In such thick samples, a twisted structure, where the director rotates *within* each layer around a twist axis directed along the cell substrate normal, instead tends to develop. If the correlation in φ across the layer boundaries is very weak, the forces maintaining the helical structure along the layer normal are easily overcome by the influence of the cell surfaces, which – disregarding the polar interactions – promote a uniform director structure. At small and intermediate cell gaps (below $\sim 10 \mu\text{m}$), surface-stabilized ferroelectric domains (SSFLC domains, *cf.* section 2.6) will therefore appear. By increasing the cell gap, the energy cost of adopting the in-layer twist goes down, and such structures will then form.

An even more striking evidence is found in studying the shapes of the domains which form in the SSFLC state, *cf.* figure 3.12. In contrast to the usual SSFLC domain types, which have approximately equal size along and across the layers, many of the domains in 8422[2F3] have a very small area with an in-layer extension considerably larger than that across the layers. This gives rise to a very large amount of boundaries between domains, which at first seems surprising, as boundaries always cost energy. However, almost all boundaries run *along* the layers and will therefore, in the case of weak interlayer φ -correlation, cost much less energy than the boundaries occurring within layers. Hence, the equilibrium area of the domains is in 8422[2F3] much smaller than in usual FLC materials, and the domain structure has a striking layered character.

The reason for the weak interlayer correlation in φ may well be found in the two-molecule aggregate making up the building-block of the layers, *cf.* section 3.4.3. As

3. In the biaxial surface-stabilized SmC* state, the ordinary refractive index depends on how the index ellipsoid orients with respect to the plane of the cell. Usually, it is the smallest axis (n_1) which, together with the largest axis (n_3), aligns in the plane of the cell, giving a slight increase of the effective sample birefringence, as compared to the uniaxial SmA* phase, where the rotational symmetry corresponds to an averaging of n_1 and n_2 , the two smallest axes of the SmC* index ellipsoid.

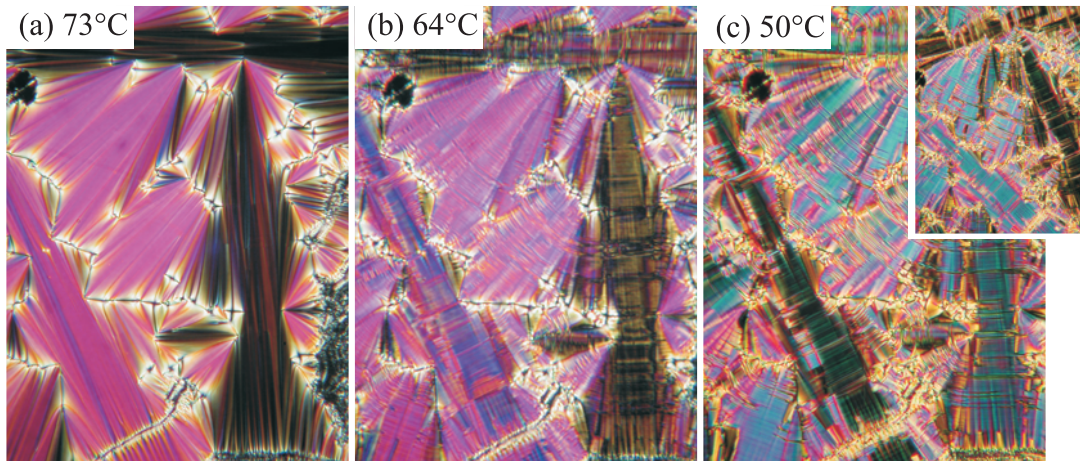


Figure 3.11 Textures of 8422[2F3] at $8.5 \mu\text{m}$ cell gap on cooling from the SmA^* phase to the SmC^* phase: a) SmA^* ; b) SmC^* just below the transition; c) SmC^* . In the main images, the sample is aligned relative to the polarizers such that the horizontal domain along the top edge is black in the SmA^* phase, i.e. in this domain the layers are approximately vertical. In the inset of c), the sample has been rotated to the new extinction orientation of this domain, 19.5° from the initial orientation. The existence of an orientation with good extinction indicates that the (quasi-) surface-stabilized state is not one where the slow axis rotates from one substrate to the other, as it does in the so-called splayed polarization state.

seen in figure 3.6, both ends of the aggregate end with fluorine atoms. This means that the contact between molecules in adjacent layers is mediated via fluorine-fluorine interactions only, whereas in most liquid crystals these interactions are mediated via hydrogen atoms. This probably leads to weaker induction and dispersion forces interacting between two adjacent smectic layers and may thus explain the unusually weak interlayer correlations observed in 8422[2F3].

These observations naturally direct the thoughts to de Vries' non-correlation model, and it may seem that this is the most reasonable description in this case. However, the temperature-independent electroclinic effect expected for a non-correlation type SmA^* phase, as described in section 3.3, was not observed in 8422[2F3], and we

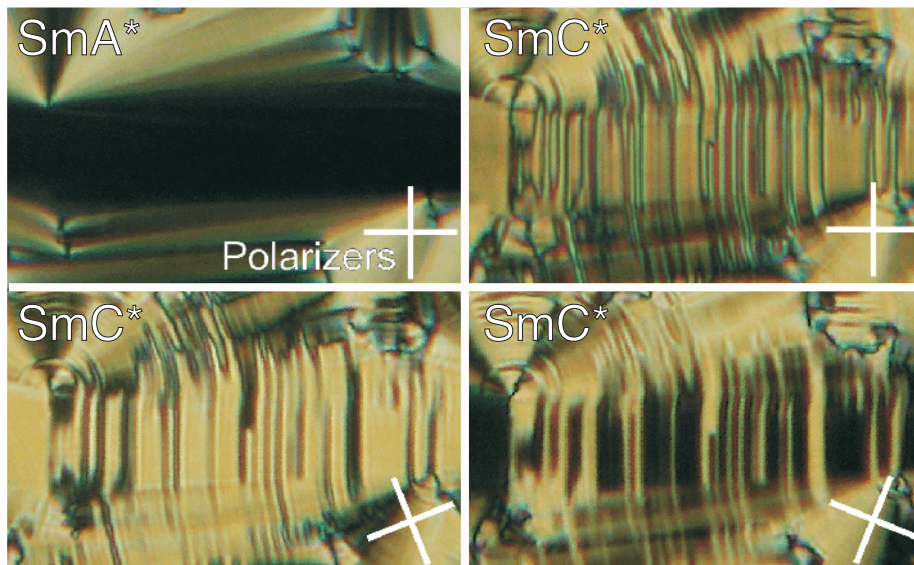


Figure 3.12 The peculiar type of ferroelectric domains appearing in surface-stabilized 8422[2F3], observed at $5 \mu\text{m}$ cell gap.

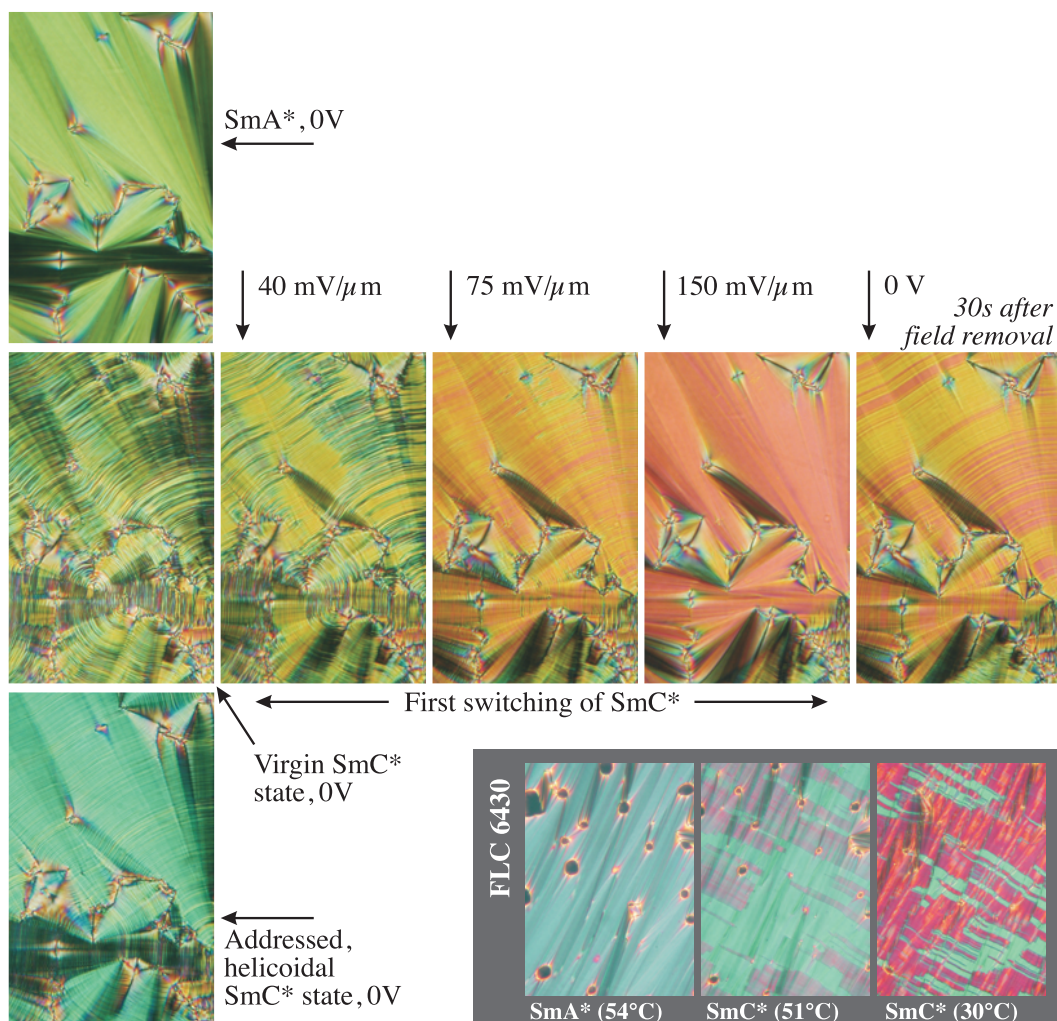


Figure 3.13 Textures of the FLC compound 8422[2F3] at 12.8 μm cell gap in the SmA^* and in the SmC^* phase, with and without electric fields applied. For comparison, textures of the ‘normal’ FLC mixture 6430 (Roche), exhibiting layer shrinkage, are also shown. For explanations, see main text.

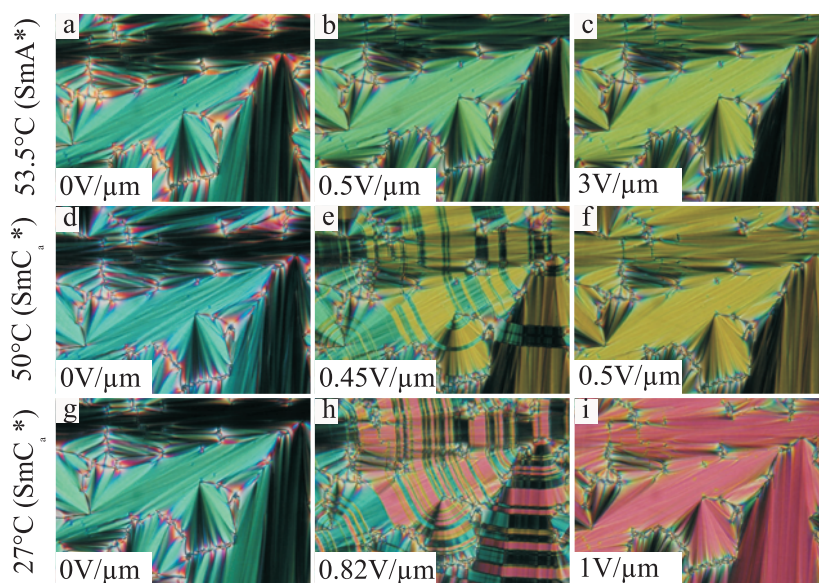


Figure 3.14 Textures of the AFLC mixture in a 10 μm thick planar-aligned cell at different temperatures and electric field strengths.

therefore believe the asymmetric diffuse cone scenario to best model the SmC* phase of this compound. On the other hand, the strength of the interlayer correlations should probably have an impact on the average orientational order observed in macroscopic volumes. The unusually low value $S = 0.56$ may therefore to a large extent have its origin in the molecular aggregation. We may even contemplate that the origin – whatever it is – of the biasing of azimuthal fluctuations responsible for the director tilt, always exhibits only a weak correlation across layer boundaries. A tilt transition that can be completely described by the diffuse cone model will then not only occur without layer shrinkage, it can also be recognized by very weak director correlations along the layer normal in the SmC(*) phase. In the end, it may thus be that the requirements for the development of an asymmetric diffuse cone model SmC* phase are very similar to the case of the non-correlation model, and the two descriptions may thus in some sense need to be merged.

3.4.4.2 The effects of an electric field on the optical properties

By applying electric fields over the samples, the special electrooptic properties predicted for polar liquid crystals of the de Vries type (*cf.* section 3.3) could be verified in both materials under study. The textures in the SmA* and SmC* / C_a* phases, in the relaxed state and with electric fields of various strengths applied, are shown in figures 3.13 and 3.14. In the case of the 8422[2F3] series of textures (figure 3.13), obtained using a 12.8 μm sample, the helical SmC* state did not form spontaneously on cooling, but instead the virgin SmC* texture was characterized by a quasi-periodic large-scale modulation of the director tilt, as seen at the left end of the middle row. Comparing with the SmA* texture, it is obvious that the slow axis direction has shifted, indicating that the sample is not helical. By addressing the sample with an a.c. electric field, and bringing down the amplitude slowly, a quite homogeneous helical state could, however, be obtained, shown in the lower picture in figure 3.13. The lower horizontal domain has almost the same extinction as in SmA*, indicating that the slow axis is again along \mathbf{k} . The color of this helical texture is close to the color of the SmA* phase, with a slight shift towards the blue indicating that the helix decreases the effective birefringence slightly more than the orientational disorder in SmA*.

If we instead apply d.c. fields of increasing strength to the virgin SmC* state, the process shown in the middle row is observed. The first step is an unwinding of the (quasi-) helical regions, producing a smoother, yellow texture, reflecting a higher birefringence. This can almost be stabilized across the whole sample area at a field strength of $\sim 60\text{mV}/\mu\text{m}$, but at higher fields the end of the switching process is reached via a quite distinct step. The yellow birefringence color is replaced by orange in the fully switched state, which thus has a yet higher birefringence reflecting a maximum in orientational order. After releasing the field, the relaxation is very slow and occurs along the layers, as can be seen in the final picture of the middle row series. These processes are very reminiscent of the typical AFLC switching and relaxation. Note also that the relaxed state is the yellow intermediate state, not the helical dark green one.

For comparison, three textures from a 4 μm sample with the ‘normal’ FLC mixture 6430 from Roche, in the absence of fields, are shown at the bottom right of the figure. The first is taken in the SmA* phase, the two other in the SmC* phase, close to and far below the transition, respectively. The pitch of the SmC* phase is rather short but at 4 μm cell gap, the helix is partially unwound. Below the SmA*-C* transition, regions where the helix develops change color: the SmA* cyan is replaced by a purple color, turning more red on further cooling. The SSFLC regions, in contrast, keep roughly the

same cyan color as in the orthogonal phase. If one applies an electric field over the sample, all remains of the helix are unwound and the whole sample acquires approximately the same color as the SSFLC texture. The birefringence of the unwound SmC* phase is thus approximately the same as that of SmA*, while the helix produces a considerable decrease of birefringence due to the variation of the slow axis direction on a scale smaller than the optical resolution. This is the behavior we can expect in a SmC* phase which is *not* described by the asymmetric diffuse cone model.

Going to the AFLC sample, we may first of all notice that the zero-field texture is almost identical throughout the phase sequence. There is no trace of the defects typically generated in the case that the layer spacing changes and the birefringence seems to be identical in the SmC_a* and SmA* phases. Both these observations are strong indications that the material is well described by the diffuse cone model scenario. The birefringence, Δn , also increases markedly when a field is applied, both in the SmA* and in the SmC_a* phase, as seen in the distinct color changes. As expected from the fact that the orientational order must increase with decreasing temperature, the difference in color continuously increases on cooling. The typical finger-like switching between the anti- and synclitic states can easily be seen in the textures at intermediate field within the SmC_a* phase.

The special optical properties described here on the basis of the textures, were confirmed on a quantitative level by means of high-accuracy electrooptic measurements. These are described in papers 1 (*cf.* figures 8 and 9) and 2 (figures 5, 6 and 7). We also verified that the 8422[2F3] compound indeed exhibits the special $\theta_{\text{opt}} - \Delta n$ behavior predicted by Selinger *et al.* [34] for diffuse cone model SmA*-C* phases (*cf.* figure 9, paper 1).

3.5 First- and second-order transitions to the SmC^(*) phase

3.5.1 Observations and predictions regarding the order of the non-layer shrinkage tilting transition

Most of the early non-layer shrinkage materials showed an unusually high transition enthalpy at the SmA-SmC transition (*e.g.*, [29, 58]) and this led many to believe that such smectics always exhibit a first-order transition between orthogonal and tilted phases. Such a conclusion would fit well with a conformational change (Figure 3.5 *b*) which can hardly be imagined compatible with a continuous phase transition. Later on, however, reports of materials with a second-order A-C transition without layer shrinkage appeared [49, 50]. It thus seems that one cannot make any direct connections between the order of the phase transition and the temperature dependence of d .

If one considers the – today generally accepted – division between first-order transition \leftrightarrow high saturation tilt, and second-order transition \leftrightarrow low saturation tilt smectic C^(*) phases, the conclusion should rather be the opposite of the initial suggestion, *i.e.* that a non-layer shrinkage transition in general is connected to a *second*-order SmA-C transition. Among the diffuse cone model variants, it is clearly the asymmetric version that is compatible with a constant layer spacing, while the tilted diffuse cone model must represent the high saturation tilt SmC phases, connected to either a smectic A or a nematic phase via a first-order transition. This also correlates well with the opinion of

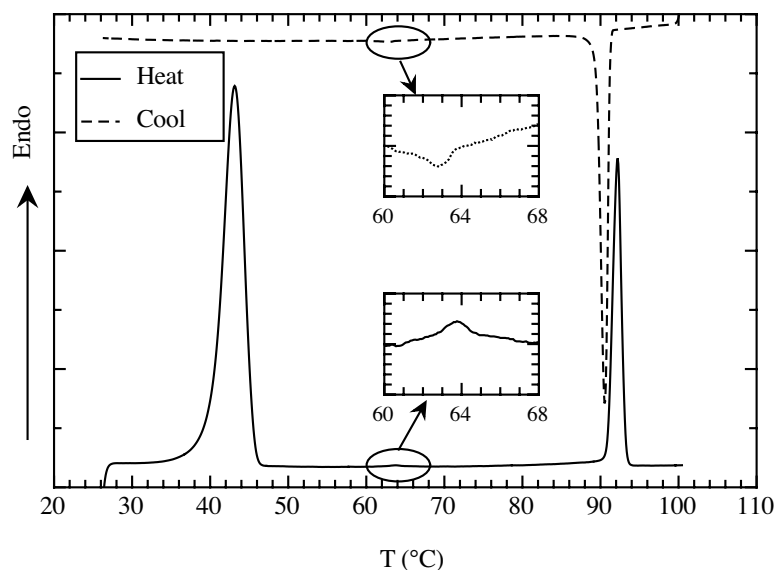


Figure 3.15 Heat flow on heating and on cooling (5 K / min.) of 8422[2F3]. The insets show magnifications of the region in which the second-order SmA*-SmC* transition takes place.

Wulf in his theoretical work on the diffuse cone and non-correlation models, where he concluded that the non-correlation model was less realistic and at least not compatible with a first-order transition [40, 59].

3.5.2 The thermodynamics of the transitions in the 3M materials

In Figure 3.15, the DSC thermogram obtained for 8422[2F3] is shown. The weak non-resolved peak above the baseline close to 64°C indicates a second-order SmA*-SmC* transition, an observation which conforms well with the optical measurements described in section 3.4.4. The second-order nature of the SmA*-SmC* transition is clearly indicated in the Δn and θ_{opt} diagrams of paper 1. Neither in the field-free measurement data nor in those taken while switching the sample is there any sign of discontinuity in any of the observables. The behavior of the AFLC mixture was very similar (see paper 2) illustrating that also the SmA*-C_a* transition at constant layer thickness is second order.

The compounds should thus in the first instance be compared with other second-order transition NLS materials. Among these, the compound studied by Radcliffe *et al.* [50], denoted 8/422, is an achiral smectic with a molecular structure very similar to that of 8422[2F3]. It turned out that the key element in producing the NLS properties of 8/422 is the fluoroether tail, as homologues where this tail had been replaced by fluoroalkyl showed lower d -values in SmC than in SmA. This is yet another indication that the molecule aggregation occurring in 8422[2F3] is important for generating the temperature-independent layer spacing.

On the other hand, the core structure of 8/422 could be modified without losing the desired properties. The compound is thus in this respect very different from the first-order transition NLS materials studied by Mochizuki *et al.*, where the naphthalene component of the core structure is the essential building block. The other known second-order NLS material, 9HL [49], is a non-fluorinated FLC belonging to a homologous series where the $d(T)$ behavior changes very much with end chain length, thus again

Chapter 3

indicating a large importance of the end chain geometry for the non-layer shrinkage properties.

4 ELECTROOPTIC MECHANISMS OF POLAR LIQUID CRYSTALS

Do not use the Ultradisc2000 as a projectile in a catapult
Warning label on a CD player

OVERVIEW

By means of dielectric spectroscopy combined with texture monitoring, one can get a good picture of unwinding and switching mechanisms possible in the SmC and SmC_a* phases. Such reorientation processes often give rise to a characteristic strong, low-frequency dielectric absorption. I will start by discussing the dynamics of the helix unwinding in both phases, and then the switching of surface-stabilized samples will be described.*

4.1 Quadratic and linear field effects

The switching between the dark and the bright states in (almost all) commercial liquid crystal displays, based on nematic liquid crystals, is a *dielectric* process originating in the dielectric anisotropy of the medium. The director \mathbf{n} tends to align parallel to the electric field if the dielectric permittivity is the largest along the director, hence this is the minimum energy state in the presence of a field. In dielectric switching, the sign of the applied field has no importance: the system wants to align with \mathbf{n} parallel to the field, but as \mathbf{n} has no sign, it does not matter if the field points upwards or downwards.

The situation is very different in polar liquid crystals. Here, it is the coupling of the *spontaneous polarization* \mathbf{P}_s to the electric field which decides the equilibrium state. As \mathbf{P}_s does have a sign, the liquid crystal will in general react very differently depending on if the electric field is applied upwards or downwards. The sensitivity on the electric field sign is characteristic of the *linear polar* switching as opposed to the *quadratic* dielectric switching observed in non-polar liquid crystals. In a SmC* or in a SmC_a* phase, which have a spontaneous polarization \mathbf{P}_s , there is a torque $\mathbf{P}_s \times \mathbf{E}$, linear in the field \mathbf{E} , which has no counterpart in a nematic liquid crystal. Simultaneously there is also a torque $\sim \mathbf{E}^2$ from the dielectric anisotropy. At fields \mathbf{E} of low strength we normally neglect this quadratic part, but at higher fields it will eventually grow important and even dominate the linear torque.

If we apply a field to a helical SmC* or SmC_a* phase, the coupling to \mathbf{P}_s will start to unwind the helix. This process has no threshold and the macroscopic polarization induced by the field grows from zero in a linear fashion at small fields. Thus the helix

unwinding is a dielectric process. It is, however, of a rather different nature in SmC_a^* , compared with the corresponding process in SmC^* .

This chapter is devoted to the electrooptic mechanisms observed in the SmC^* and SmC_a^* phases, and how we can recognize them in dielectric spectra. It relates mainly to papers 6 and 7.

4.2 Electric helix unwinding in the SmC^* and SmC_a^* phases

In bulk samples, the SmC^* and SmC_a^* phases exhibit a helicoidal superstructure. Not only the director \mathbf{n} but also \mathbf{P}_s spirals around the layer normal. Obviously, if one applies a field perpendicular to the helix axis, it will couple with the polarization, inducing first a distortion of the helix and, finally, complete unwinding. However, the difference between the two phases, the ordering being syn- and anticlinic, respectively, will lead to quite different response to the applied field and the helix unwinding process looks quite different in the two cases.

4.2.1 Unwinding a SmC^* helix

– *dielectric spectroscopy and texture signatures*

In a planar-aligned SmC^* sample, thick enough for the helix to develop unobstructed in the bulk, the helix axis is in the plane of the cell, along the layer normal. In case the helical pitch is short, on the order of $0.5 \mu\text{m}$, the details of the helix cannot be resolved visually and the optical properties of the sample will reflect an average of the local variations along the helix. This means that, in the relaxed state, the slow axis will be directed along the helix axis, *i.e.* along the layer normal, and the birefringence Δn will be reduced with respect to the non-helical state at the same temperature.

If a weak electric field is applied over the sample, directed perpendicular to the helix axis, it will couple to the spiraling layer polarization and the helix will start to distort. The regions where \mathbf{P}_s points along the electric field will expand, while those where it points in the opposite direction will contract. Instead of a continuous variation in polarization direction we will have uniform regions, the ‘happy layers’, separated by ‘walls’ in which the $\mathbf{n} - \mathbf{P}_s$ couple makes a 360° turn, as schematically depicted in the two intermediate pictures of figure 4.1. The regions in which the rapid twist takes place are often referred to as spatial solitons. As is clear from figure 4.1, there will be one soliton per period of the helix for small values of the field.

As the unwinding of the helix means the lining up of permanent dipoles, it obviously polarizes the medium and corresponds to a large contribution in the dielectric permittivity. In a dielectric spectroscopy experiment the process corresponds to the helix distortion mode (HD-mode), introduced in section 2.1.2.2. The ease in distorting the SmC^* helix and the fairly large magnitude of the spontaneous polarization which we may encounter in FLCs and, in particular, in AFLCs, give the mode a high susceptibility. On the other hand, the quite large collective reorientations involved limit the speed of the response and we will therefore typically observe an absorption maximum due to the helix distortion mode at frequencies in the range $10^3 - 10^4 \text{ Hz}$ [16].

Since the changes are still on a scale below the limit of visible resolution, the optical effect will simply be a slight increase of birefringence and a tilting of the slow axis

away from the layer normal. As long as the fields are small, the effect is linear and can in principle be utilized in electrooptic devices, in which case it is often referred to as the *Deformed Helix Mode*. A display working in the deformed helix mode is sometimes referred to as a DHF-LCD (Deformed Helix Ferroelectric Liquid Crystal Display) [60]. Such displays have never been commercialized, mainly because the useful modulation width is limited by the fact that the medium behaves quite differently if the field strength approaches the region where removal of solitons starts, *i.e.* where *unwinding* of the helix, rather than simple distortion, commences. Such unwinding immediately leads to unwanted hysteretic effects. We investigated this mode by means of dielectric spectroscopy and simultaneous texture monitoring in paper 6. The example given here is from the same measurement series but at a slightly higher temperature.

The deformation of the bulk helix can be divided into two regimes:

- the *elastic* mode, corresponding to the small-signal response described above where there is one soliton per helix period. On release of the field the helix quickly rebuilds again without any memory of the distorted state, and this regime is therefore the interesting one for DHF-LCDs.
- when the field strength reaches a certain threshold level, we enter the *plastic* regime. This is where neighboring uniform regions merge, *i.e.* where solitons are expelled from the sample. Once this has started, the rebuilding of the helix is substantially slower. On further increase of the field strength, the number of solitons is rapidly reduced, reaching zero in the fully unwound state.

In planar samples, we may also distinguish a third surface-stabilized regime. Here the helix is fully unwound in bulk, but the director rotates on the surface of the smectic

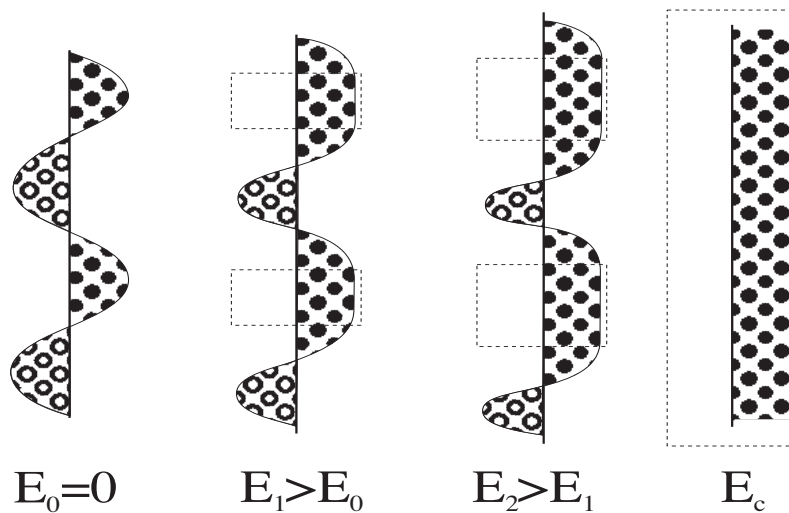


Figure 4.1 On applying an electric field perpendicular to the SmC^* helix axis (*i.e.* along the smectic layers) the helix will distort into a structure with discrete translational symmetry and (initially) with the same period as the initial helix. At regular intervals the director will twist 360° in a confined region. In between these periodic ‘spatial solitons’ the director will be homogeneously directed. These uniform regions are enclosed in a dashed box in the figure. When the field-strength increases, the uniform regions grow and the twisted ones diminish in size, up to the limit where solitons start to unwind. The different cases are illustrated through the projection of the director on the paper plane, with the filled circles corresponding to a net polarization along the field, and the empty circles to a net polarization against the field. At a critical field E_c the last solitons have been squeezed out and the medium is homogeneously polarized.

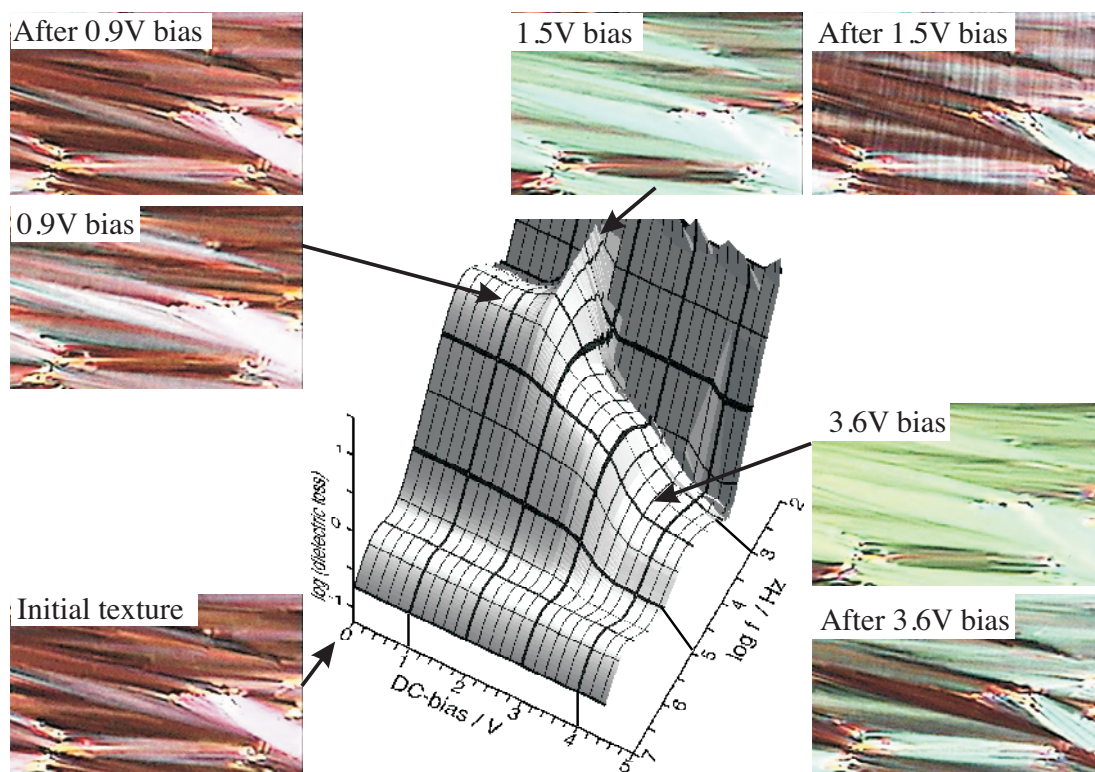


Figure 4.2 The different steps of the SmC^* helix unwinding process, as seen optically and dielectrically in an $8.5 \mu m$ sample of the AFLC compound (*S*)-11F1M7. Below $\sim 1 V$ dc-bias, the process is in the elastic, deformed helix mode regime, and relaxes fully after release of the field. Between $\sim 1 V$ and $\sim 3.5 V$ dc-bias, we see the plastic regime within which the deformation caused by the electric field will not disappear immediately after the field is released. Finally, at dc-voltages above $\sim 3.5 V$, the director structure is essentially uniform within the cell. On releasing the field, the sample stays non-helical for a very long time.

cone on going from one substrate to the other. Hence the polarization exhibits a splay - bend and the director a twist-splay-bend deformation. The reason for this ‘twisted SmC^* ’ state is the polar surface anchoring, inducing a tilt in opposite directions at the two surfaces, *cf.* section 6.2. This regime is characterized by fluctuations in the polarization splay-bend structure and ends when the voltage is large enough to switch the director at the surface imposing the ‘wrong’ – in the point of view of the field – anchoring. Once this state is reached, the rebuilding of the helix after switching off the field can be extremely slow.

In figure 4.2, dielectric absorption spectra and polarizing microscopy textures from these three regimes in the unwinding process of the SmC^* helix of the AFLC compound (*S*)-11F1M7 (*cf.* paper 3 or 6 for chemical constitution) are shown. The sample is $8.5 \mu m$ thick, with planar-aligning surface treatment, and the temperature is $86^\circ C$. The helix is unwound by applying a larger and larger dc-bias in intervals of $0.3 V$ while carrying out the dielectric spectroscopy scans. For bias-voltages up to $\sim 1 V$, we are in the elastic regime. The texture shows no sign of helix unwinding, only a slight change in slow axis direction and birefringence color, reflecting the distortion of the helix. After releasing the field, the initial helical state reforms immediately. When the dc-bias reaches the border of the plastic regime, at around $1.2 V$, a strong absorption at very low frequency appears (the frequency is in the order of Hertz; it is very far from a ‘pure’ Debye-type mode, so a value of f_c cannot be attributed to the absorption). This mode, which reaches its maximum at $1.5 V$ dc-bias, is most likely related to fluctuations in the soliton walls which are almost unwound at this dc-voltage. When releasing

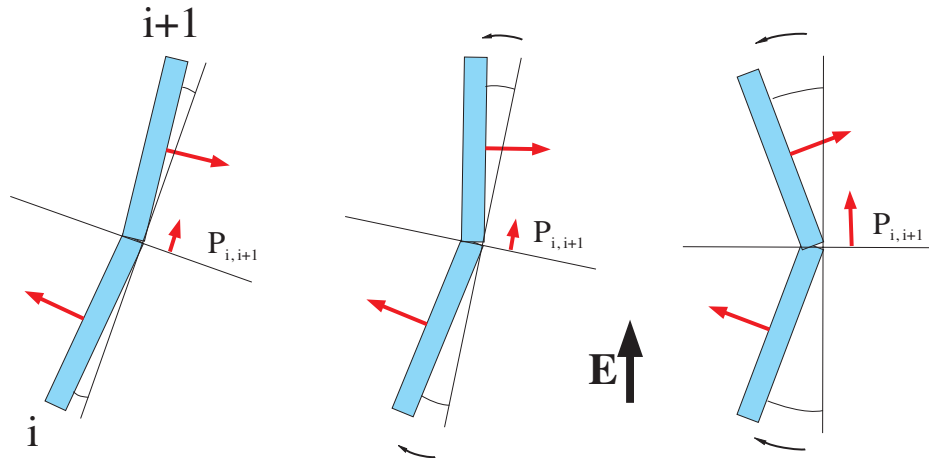


Figure 4.3 An electric field applied to a SmC_a^* phase couples to the spontaneous polarization within each layer. Due to the antipolar structure, the field will induce a tilt direction reorientation, in opposite senses in adjacent layers, affecting the residual polarization. In the end state, the generalized tilt plane aligns with the field, provided that the system remains in the anticlinic state, *i.e.* as long as the threshold for switching into the synclinic state is larger than the field necessary for unwinding the helix.

the field, the helix now does not reform immediately everywhere, but the unwound state stays in many areas, leading to a metastable soliton structure persisting at zero field. At yet higher dc-bias, the low-frequency absorption disappears, indicating that all solitons are expelled, but there is still a reasonably strong absorption present. This is due to fluctuations in the polarization splay-bend structure, *i.e.* we are now in the third regime described above. The susceptibility of the mode decreases continuously with increasing dc-bias and finally, at a dc-voltage of ~ 3.5 V, also the twisted structure is unwound. This is seen in the decrease in dielectric loss and in the change of color, from bluish green to a more yellowish tone within the second birefringence order (*cf.* figure 2.6). After switching with this high voltage, the helix does not reform at all on releasing the field, as is obvious from the green post-switching texture, with an inclined slow axis.

4.2.2 The helix unwinding process in the SmC_a^* phase

Also in the SmC_a^* phase, the driving mechanism for the helix unwinding is the coupling between the electric field and the spontaneous polarization within the layers. However, as the phase is antipolar, the unwinding takes place in a very different manner from the unwinding in the SmC^* phase. As the adjacent layers have essentially opposite polarization directions, and these are firmly coupled, the dipoles of one layer cannot turn into the field direction without the neighbor layer dipoles moving out of it. The final result of the unwinding is therefore the situation illustrated to the right in figure 4.3, where the individual dipoles of all layers are almost perpendicular to the applied field. Thus, no \mathbf{P}_s belonging to a single layer is along the field, but only the resulting dipole $\mathbf{P}_{i,i+1}$ belonging to a layer pair. As the $\mathbf{P}_{i,i+1}$ direction defines the generalized tilt plane, the unwinding can also be described as the rotation of all local tilt planes into the field direction. This process is described in detail in section III of paper 7.

In figure 4.4, the process of aligning the SmC_a^* tilt plane with the field is shown for the case of an almost pitch-compensated AFLC mixture (EHP12CBC +

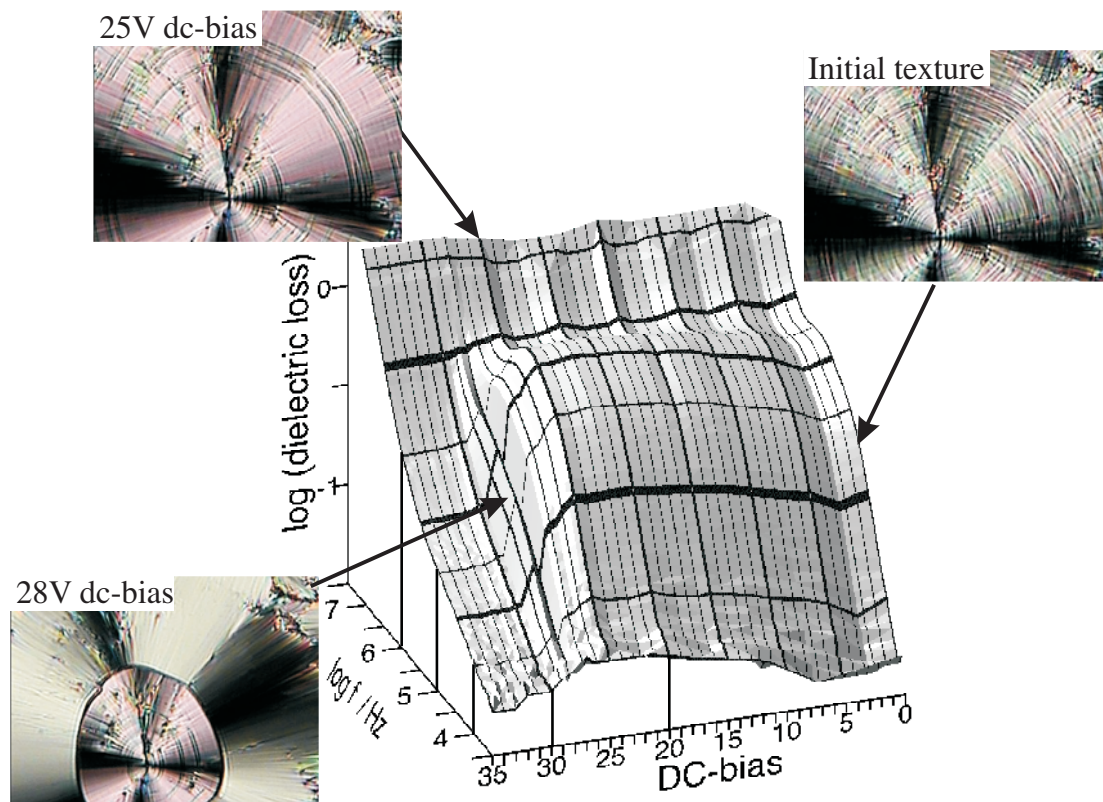


Figure 4.4 The process of aligning the tilt plane in the SmC_a^* phase (dc-bias ~ 25 V), followed by switching it to the synclonic state (dc-bias ≥ 28 V), as seen in dielectric spectroscopy and polarizing microscopy. The sample is an almost pitch-compensated AFLC mixture in an $18 \mu\text{m}$ thick planar-aligning cell.

TFMHP11BC in the ratio $\sim 40:60$) in an $18 \mu\text{m}$ planar-aligned sample. The temperature is 96°C , which is roughly 5°C below the SmA^* phase. The fairly large sample thickness places the texture color in the fourth birefringence order. In the zero-field texture, the long pitch of the phase is obvious from the heavily striped texture. Essentially two colors are visible, pale green and pale pink. In the dielectric spectrum, both SmC_a^* modes are clearly visible, but not very easy to separate at this temperature (lower temperatures could not be used as then the maximum dc-bias of the dielectric bridge used for the experiment was not enough to induce the final switching into the synclonic state). In figure 2.7, where the dielectric absorption spectrum of this sample is shown as a function of temperature instead of dc-bias, the two modes are easier to distinguish.

As the dc-voltage is increased, the green stripes are more and more expelled and at ~ 25 V, the texture is almost uniformly pink. We can thus conclude that the pink color reflects the maximum birefringence of the phase in its anticlinic state, observed when the tilt plane is vertical, along the field. As motivated in section 2.5.2, this geometry is also the optimal for detection of the SmC_a^* modes and, consequently, the dielectric absorption spectrum exhibits a maximum at this voltage. Increasing the voltage further, the transition to the synclonic state takes place, as clearly seen in the 28 V texture. The center ring is still in the anticlinic state, with the same extinction direction, everywhere along the layer normal, as in the 25 V picture. In contrast, the outer areas exhibit an extinction direction which is tilted with respect to the layer normal by the synclonic tilt angle. The color has also changed to white reflecting the increase in birefringence connected to the change of state.

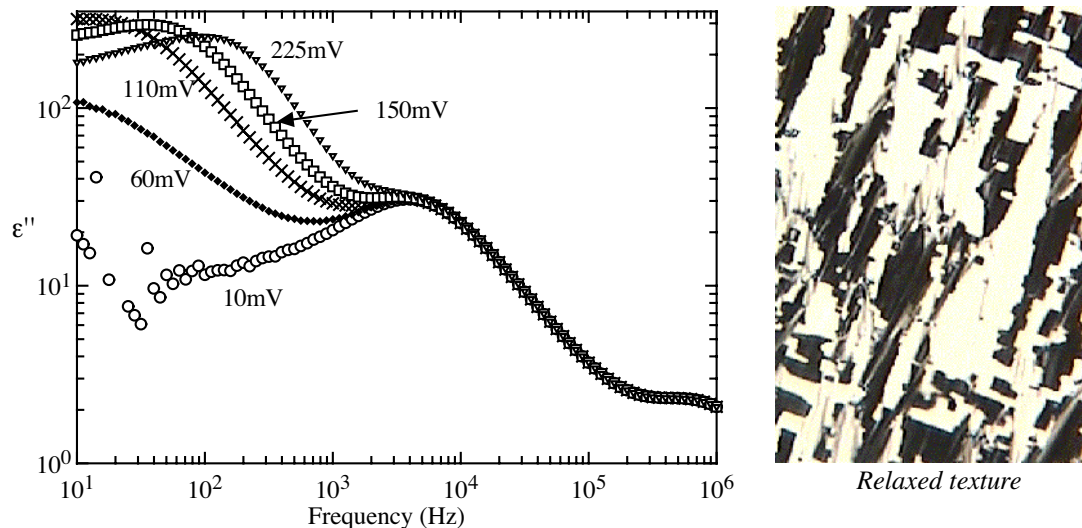


Figure 4.5 The dielectric response of an SSFLC sample (the AFLC mixture 40 % (S)-EHP-nCBC-12 + 60 % (S)-TFMHPnBC-11 in the SmC^* phase, $2 \mu m$ cell gap) at varying measuring field strengths. With a weak measuring field, the spectrum reflects fluctuations mainly in the zero-field structure, exhibiting a strong absorption at $f_c \approx 5$ kHz. On increasing the field strength, this absorption remains, but now the domains with the polarization pointing against the field start switching, giving rise to a very strong, very low-frequency absorption. At measuring fields above 225 mV, the contribution to the dielectric permittivity is so high that the dielectric bridge gets overloaded, and measurements are then no longer possible.

4.3 The dielectric signatures of switching non-helical, surface-stabilized, samples

4.3.1 Switching an SSFLC sample

Whereas the helix unwinding process (as opposed to helix distortion alone) can in general only be studied dielectrically by applying a dc-bias while doing the measurement, the switching of a surface-stabilized ferroelectric SmC^* sample (SSFLC) can often be triggered by the measuring field alone. This gives a very strong and characteristic response in the absorption spectrum, as depicted in figure 4.5 for the case of the AFLC mixture 40:60 EHP12CBC + TFMHP11BC in its SmC^* phase. This mixture is essentially pitch-compensated in the SmC^* as well as in the SmC_a^* phase. The cell gap is $2 \mu m$, assuring that the helix is completely unwound by the surfaces, as easily verified by looking at the texture, which displays the characteristic SSFLC UP and DOWN domains.

At very weak measuring field strengths, ~ 10 mV, the dielectric spectrum is dominated by an absorption centered around $f_c \sim 5$ kHz. The origin of this is most certainly polarization fluctuations within the SSFLC domains, occurring below the threshold for switching between the two states. Increasing the measuring field to 60 mV, a much stronger absorption appears at very low frequencies. The reason is most likely that the measuring field now is strong enough to influence the borders between the UP and DOWN domains, thus commencing the SSFLC switching mechanism. The fluctuation in sample polarization coupled to this mechanism is huge and we can only increase the

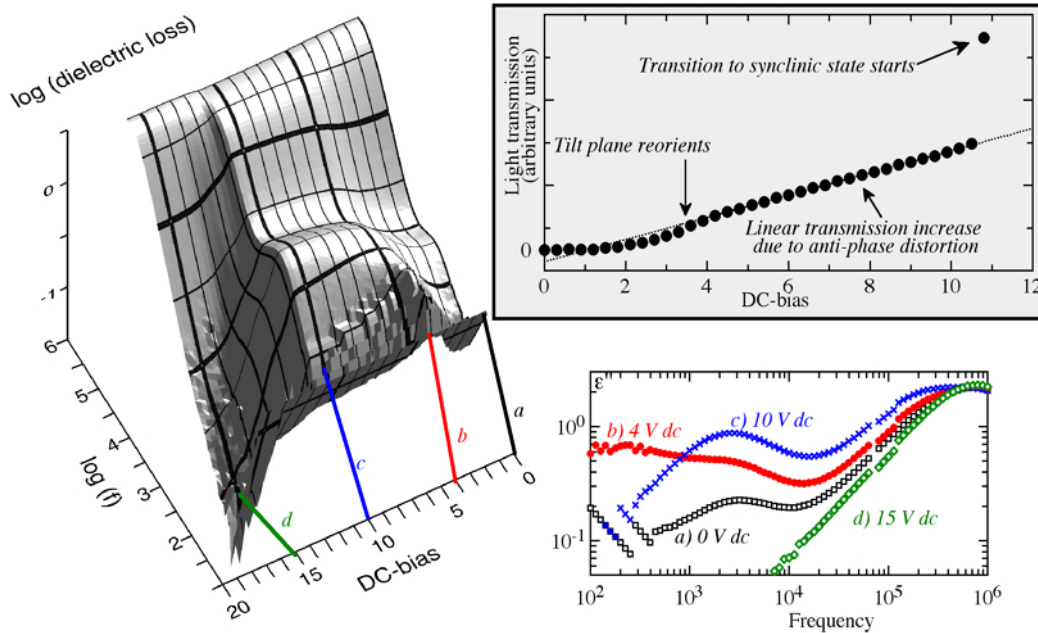


Figure 4.6 The SSAFLC Frederiks transition as witnessed by dielectric spectroscopy and simultaneous light transmissivity measurement. The reorientation of the tilt plane at a dc-voltage of ~ 4 V is recognized by the additional low-frequency dielectric absorption. From then on, the light transmission increases linearly with the dc-voltage until the transition to the synclonic state occurs at voltages above ~ 11 V.

measuring field up to 225 mV before the response is too large for the equipment: the dielectric bridge is overloaded. The SSFLC fluctuation mode detected at the weakest field strength is still present, essentially unaffected by the new mode, but the latter now completely dominates the dielectric spectrum.

4.3.2 The SSAFLC Frederiks transition

– fluctuations in the tilt plane alignment studied with dielectric spectroscopy

In a surface-stabilized SmC_a^* phase (an SSAFLC sample), the helix is unwound by the influence of the closely spaced cell surfaces. In general, one assumes that the planar-aligning surfaces induces an alignment of the tilt plane in the plane of the cell, but in the case of an anticlinic structure, where the extinction direction (in general) is in the same direction regardless of tilt plane orientation, this is not an obvious thing to verify optically. However, as the tilt plane orientation has a large impact on the contributions of the SmC_a^* dielectric modes, dielectric spectroscopy actually gives us a means of verifying the tilt plane alignment. This was shown in paper 7 for the case of the orthoconic AFLC (this special class of antiferroelectric liquid crystals and their optical properties are described in section *iv.A* in the paper) material W107 where the tilt plane alignment can actually be verified optically as well. It turns out that a horizontal tilt plane is generally *not* what we spontaneously get in SSAFLC samples. Here we will briefly discuss another, related, example from that paper, describing how we can follow the Frederiks transition in an SSAFLC sample in a dielectric spectroscopy experiment.

We again study the pitch-compensated AFLC mixture 40:60 EHP12CBC + TFMHP11BC in the $2 \mu\text{m}$ cell discussed above. As in the SmC^* phase, the helix is

completely expelled also in SmC_a^* in this cell, *i.e.* the cell is an SSAFLC sample. From a dielectric spectroscopy scan in the absence of bias fields (curve *a* in the 2D dielectric spectrum in figure 4.6), we conclude that the tilt plane is close to, but not exactly in, the ideal horizontal condition, since both SmC_a^* modes are weakly active. On applying a dc-voltage, there will be a conflict between the surface interaction, imposing an essentially horizontal tilt plane, and the electric field, imposing a vertical tilt plane (*cf.* section 4.2.2). There will thus be a threshold voltage where the two interactions are of roughly the same strength, and where the fluctuations in the tilt plane alignment become very large. This voltage is in our case ~ 4 V and at this dc-bias level the dielectric spectrum reveals a strong low-frequency mode the origin of which is the fluctuations of the tilt plane (curve *b* in the 2D diagram). The normal SmC_a^* modes have also increased in intensity, reflecting the increasing deviation from the horizontal tilt plane condition. On further increase of the bias voltage, the tilt plane fluctuation mode disappears around ~ 5 V, where the tilt plane is aligned vertically, and the SmC_a^* modes increase in strength, reaching their maxima just before the transition to the synclinic state at ~ 11 V.

The reorientation from a horizontal to a vertical tilt plane in a surface-stabilized AFLC sample is actually a Frederiks transition [61, 62]. Below the transition voltage, the electric field has essentially no effect, but once the Frederiks voltage is reached, the reorientation takes place rather quickly. This can be tracked also electrooptically, as described in the case of applied ac electric fields in paper 7. In the dc-field case studied dielectrically, the threshold voltage will be slightly different. However, during the dielectric spectroscopy experiment, the texture at each dc-voltage level was photographed and by integrating the intensity we can obtain an electrooptic curve for the dc-field case, reproduced in the upper right of figure 4.6. Extrapolating the linear increase in light transmission down to the 0 V level, we can see that the threshold voltage in this case is roughly 1 V. Once the tilt plane is aligned vertically, the light transmission increases linearly with the voltage, expressing the effective optical tilt angle increase resulting from the field-induced anti-phase-angle distortion (*cf.* section 2.5.2).

5 THE SUBPHASES OF ANTIFERROELECTRIC LIQUID CRYSTALS

'Curiouser and curiouser!' cried Alice

Lewis Carroll, *Alice's Adventures in Wonderland*

OVERVIEW

... are there ferroelectric liquid crystal phases?

5.1 A brief history of antiferroelectric liquid crystals *– the early years*

Antiferroelectricity in liquid crystals was discovered more or less as a byproduct of an effort to develop ferroelectric liquid crystals with very high polarization. During the latter part of the 1970's and throughout the 1980's, reports on a new chiral tilted smectic phase with unusual behavior became more and more common (the early development is described for instance in [23]). Understanding these observations was however not so easy and it was not until 1989 that French and Japanese groups independently presented the first proofs of the major new phase having an anticlinic structure and exhibiting antipolar properties [63]; Galerne, 1989 #409; Takezoe, 1989 #412]. The first antiferroelectric liquid crystal to be properly characterized was MHPOBC (4-(1-methylheptyloxycarbonyl)phenyl-4'-octyloxybiphenyl-4-carboxylate, see Table A.2, on page 105 for chemical constitution), which is still today often regarded as the prototype AFLC compound.

It was early recognized that AFLC materials exhibit not only the anticlinic phase, designated SmC_a^* , but also three other subphases, the characteristics of which were much more difficult to establish. It was also clear that these subphases disappear from the phase diagram, in favor of the ordinary, synclinic SmC^* phase, by decreasing the optical purity [64, 65], *i.e.* adding larger and larger amounts of the enantiomer with opposite handedness. In the racemate, only SmC_a and SmC prevail. Since then many efforts have been made, both experimental and theoretical, to find out which subphases may exist, which type of molecular organization prevails in each subphase and why the subphases vanish, thus are not thermodynamically stable, on reducing the purity. This work has proved to be very difficult and instead of approaching a general consensus, the first years of AFLC research produced a large number of more or less conflicting reports and models. The different subphases have been attributed varying polar properties, not seldom incorrectly or at least with little motivation, and this has led to a very disturbing terminology where phases are denoted by names suggesting properties

which they do not have. Before going on with the detailed discussion of the various antiferroelectric phases, we will therefore briefly clarify the meaning of some important concepts used for describing polar properties.

5.2 Ferro-, ferri- and antiferroelectricity

– *what do the concepts really mean?*

All materials can be polarized by an electric field but most materials have no polarization when the field is switched off. The exceptions to this, *i.e.* materials which have a non-zero spontaneous polarization \mathbf{P} in the absence of an electric field, are called either *pyroelectric* or *ferroelectric*. Whereas the polarization of the former cannot be changed substantially by applying a field, the latter may be switched between *two stable states* by applying an electric field. The states are differentiated by the sign (or direction) of \mathbf{P} , and they are stable in the sense that the sample stays in the one to which it was last switched, even after the field has been switched off.

At higher temperatures the ferroelectric normally has a phase of higher symmetry which more or less reacts like a normal dielectric on applying a field. However, on approaching the transition temperature T_c from above, the dielectric susceptibility usually grows to become very large and seems to become infinite at T_c . In this case we call the high-temperature phase *paraelectric*. Its distinction from a normal dielectric lies in the very large and strongly temperature dependent dielectric susceptibility. Paraelectricity is thus, as we will soon realize, on the threshold to being a collective phenomenon.

An *antiferroelectric* material also has no measurable polarization in the absence of a field but, locally, antiferroelectrics do have a non-zero spontaneous polarization. However, these materials are made up of two sublattices, in which the directions of the polarizations are opposite, resulting in a cancellation of dipoles and a macroscopic polarization which is zero. We may therefore refer to antiferroelectrics also as *antipolar* materials. When applying an electric field one will see the standard weak linear (dielectric) response in the beginning, but on passing a threshold value of the field, one sublattice flips over to the direction of the other and we thus obtain the so-called *field-induced ferroelectric state* of the antiferroelectric material. The possibility to switch

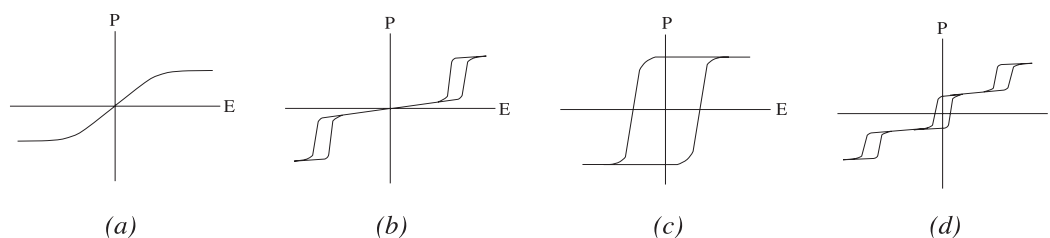


Figure 5.1 Response of polar dielectrics, *i.e.* materials which contain permanent dipoles, to an external electric field. The dielectric or paraelectric (a) response is linear in the field, the antiferroelectric (b) is distinguished by a double hysteresis loop: two loops at non-zero field values but only one stable state, and the ferroelectric (c) has two stable (zero field) states and shows a large hysteresis when switching. The ferrielectric response (d) has characteristics of the two latter and thus shows a triple hysteresis loop: one loop at zero field and two around the threshold fields (positive and negative) for switching to the ferroelectric state. A helielectric has no threshold and corresponds to (b) or (c) where the hysteresis loop shrinks to a single line.

the medium to this state is a characteristic of antiferroelectrics. There are antipolar media which cannot be classed as antiferroelectrics because it is impossible to switch them to a polar state.

Ferrielectricity represents a different order, and is in a way something in between ferro- and antiferroelectricity. This term applies for a material with two sublattices, as in antiferroelectrics, but where the polarization magnitude of the sublattices is not the same. It equally well applies to a material with three sublattices of equal \mathbf{P} -value, which can be switched independently. The response of such a system is drawn in figure 5.1 *d*. Both these systems have an incomplete cancellation of polarization in the ground state, so just like ferroelectrics we have a *bistable zero-field state*, but with a lower value of macroscopic polarization. On switching a ferrielectric, we again flip the different sublattices, and hence we get hysteresis loops at non-zero voltages as well. The typical ferrielectric response is thus very similar to a combination of the ferroelectric and the antiferroelectric.

In order to conveniently discuss the polar properties of liquid crystals, we will in the following use the term *mesoscopic* polarization, as opposed to the microscopic spontaneous polarization of a single layer and the macroscopic spontaneous polarization of the phase as a whole (or a full period of the macroscopic helix for that matter). As the name suggests, the mesoscopic polarization falls in between these two scales, referring to the polarization of the unit cell of the phase. It is the vectorial sum of the spontaneous polarization vectors of the different layers in the repeating unit of the phase. As for the two chiral smectic C phases described so far in this thesis, the SmC^* phase, with a single-layer unit cell, obviously has a mesoscopic polarization equal to the spontaneous polarization, whereas the SmC_a^* phase has no mesoscopic polarization (neglecting the small residual polarization due to the helicoidal modulation).

5.3 What is the repeating unit in the subphases?

– *Can we define a ‘unit cell’ for each subphase?*

Despite almost fifteen years of intense research on the matter, our understanding of the chiral smectic C subphase structures is still far from satisfactory. The structure of the subphase appearing at highest temperature, the SmC_α^* phase, is a controversial matter indeed, and in principal the only characteristics which we can attribute to the phase for sure is that it is optically uniaxial (when looked upon along the layer normal) and that it is weakly polar. As for the structure giving rise to these properties, the most common idea is that it is a tilted phase, but with a very small value of the tilt-angle, and with an extremely short helical pitch; only 5 - 10 layers.

Our understanding of the other two subphases, SmC_β^* and SmC_γ^* , is slightly better. Both are helielectric, characterized by a long helical pitch (typically $p \sim 2 - 3 \mu\text{m}$) and optically biaxial unit cells. With a biaxial unit cell and a pitch $p \geq \lambda$ they show an easily measurable rotatory power along the helix axis. The SmC_β^* phase, occurring between SmC_α^* and SmC_γ^* in temperature, is best recognized by its absence of mesoscopic polarization. In this sense, it behaves much like the SmC_a^* phase, *e.g.* producing the same essentially absorption-free dielectric response. The SmC_γ^* phase, on the other hand, has a non-vanishing mesoscopic polarization and is in a dielectric spectroscopy experiment recognized through a quite strong absorption, usually located at a

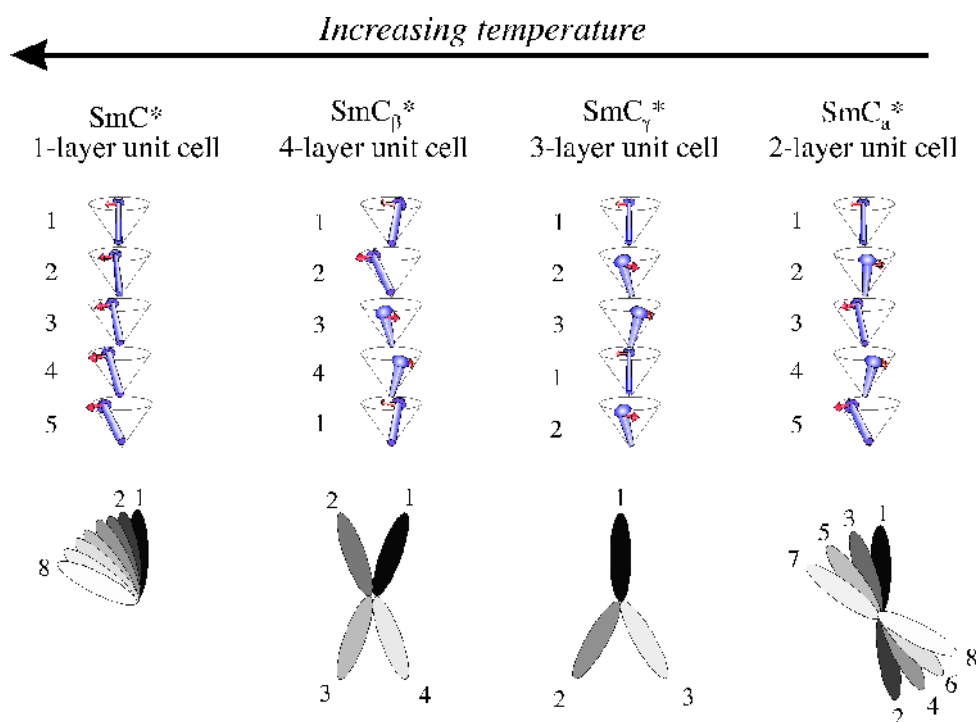


Figure 5.2 The proposed distorted clock structures of the SmC_β^* and SmC_γ^* subphases, compared with the structures of the ordinary SmC^* phase and the anticlinic SmC_α^* phase. In the lower part, darker molecules are below lighter ones.

rather low frequency. The structural pictures for these two phases have gotten clearer the last few years, much due to resonant X-ray and ellipsometry experiments carried out at Brookhaven and in Minnesota, respectively [66-69]. There now seems to be a general consensus that the directors in the basic repeating unit in neither case is restricted to a single plane, and that the unit size is four layers in SmC_β^* and three layers in SmC_γ^* . From two extreme pictures of the unit cells, a symmetric clock (xy) model [70, 71] on one hand and an Ising-like, single-tilt plane model [72] on the other, the discussion now seems to converge towards an intermediate distorted clock model picture, where SmC_β^* has an X-like and SmC_γ^* a Y-like director configuration within the unit cell, viewed along the layer normal. This picture seems to fit with most experimental data but it is still not clear which interactions could give rise to such structures. In both cases, the phase-angle change between neighboring layers is not constant. Furthermore, in the SmC_γ^* phase, different layers will have different neighborhoods: the director in the ‘vertical layer’ of the Y will have a large phase-angle difference to both surrounding layers, while the two other layers will have a small shift in one direction and a large in the other [73]. Obviously, this would be different if one considers the case that every second unit cell is inverted with respect to the next, *i.e.* Y is followed by Λ .

The present-day ‘standard’ structural picture of the different chiral smectic C phases, with the exception of SmC_α^* , is summarized in figure 5.2. This figure is not to be interpreted as depicting the correct structures, just the best structures proposed so far. The helical superstructure has also been omitted in the case of SmC_β^* and SmC_γ^* . It is obvious from this picture that these two phases also have a distorted helicoidal structure within the unit cell. There is thus a certain handedness present in these phases

even on the unit cell level. Cady *et al.* reported that the twisting sense within the ‘unit cell’ of the SmC_β^* phase of one compound (MHDDOPTCOB.) was the same as that of the macroscopic, ‘optical’, helix [69]. At first sight it might seem natural that this should always be so, at least if the two different helices have a common origin, but this cannot always be the case. If it were, the very common event of a helix inversion within a subphase [74-76], or at its border, as observed in the study described in paper 3, would imply a rather drastic change in unit cell structure over a very small temperature range. The unit cell would have to go from a distorted clock of one handedness, via an Ising-like structure, to a distorted clock of the opposite handedness. However, the two different helices actually have no inherent coupling, as illustrated in figure 5.3. This figure schematically shows the cases of left- and right-handed macroscopic helices superimposed onto the same right-handed unit cell for each phase. It is obvious that a change of handedness of the macroscopic helix requires only a minor structural change, essentially not affecting the unit cell structure.

5.3.1 The subphase terminology problem

Many names have been given to the SmC^* subphases, and the notation situation is today rather confused. Not seldom, the SmC_β^* and SmC_γ^* subphases are referred to as the ‘ferrielectric’ phases, and two corresponding abbreviations, $\text{SmC}_{\text{FI1}}^*$ and $\text{SmC}_{\text{FI2}}^*$ are often encountered. This is a most unfortunate naming scheme since it is completely misleading: SmC_γ^* may be, SmC_β^* is definitely *not*, ferrielectric. The SmC_β^* phase is actually also often referred to as the ‘AF’ phase, reflecting its antiferroelectric properties. But this is also a very bad choice since, first of all, such a name does not show that

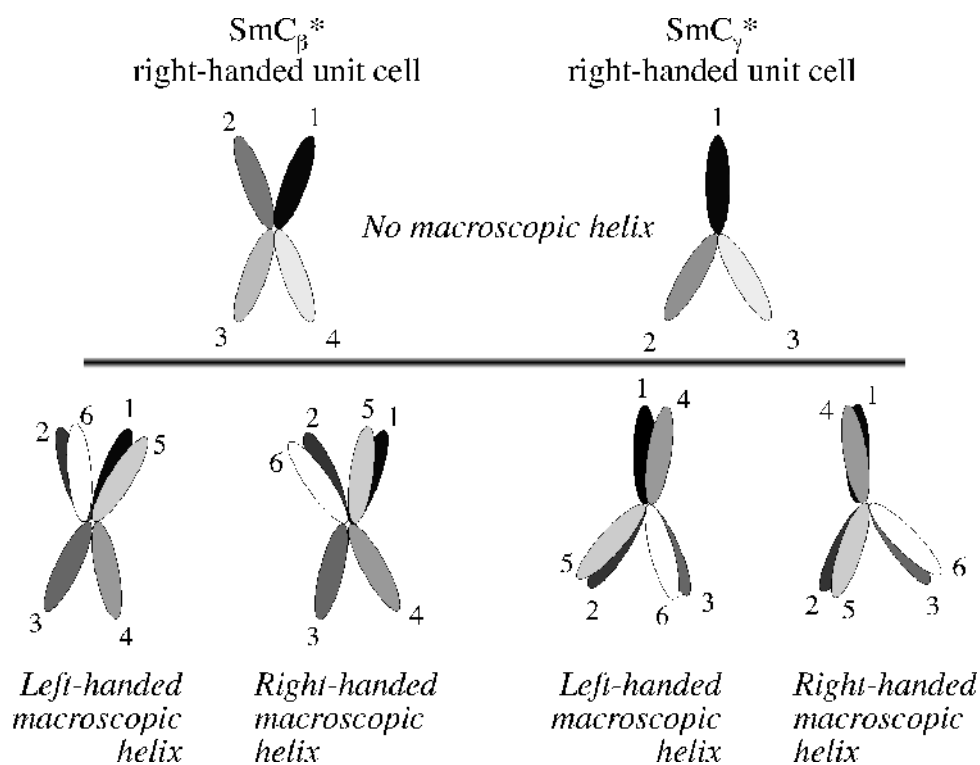


Figure 5.3 An illustration of how the macroscopic helical superstructure can change from left- to right-handed without affecting the handedness of the unit cell helix. In all cases the unit cell helix is right-handed.

the phase is a member of the smectic C* family, and second, it indicates that antiferroelectricity would be something unique for this phase. The SmC_a^* phase is the phase normally called antiferroelectric and this is the phase of applicational interest when speaking of antiferroelectricity in liquid crystals.

The naming scheme used in this thesis is actually the original scheme proposed by the Fukuda school at the time of the early studies of MHPOBC. The emerging phases on cooling in this compound were designated Isotropic-SmA*- SmC_α^* - SmC_β^* - SmC_γ^* - SmC_A^* . The nature of the middle subphase, SmC_β^* , has taken particularly long time to clarify. It was for a long time thought to be equivalent to the ordinary SmC^* phase [64, 77] and hence the notation SmC_β^* seemed superfluous. However, more careful studies showed that the behavior of the SmC_β^* in MHPOBC differed from that of SmC^* , at least in samples of high optical purity. Several investigators first attributed ferroelectric properties to the phase [78-81], but as discussed and experimentally shown in paper 4, the phase is actually the four-layer unit cell antiferroelectric subphase described above. With the realization that also MHPOBC exhibits this subphase, and that it was actually the phase which initially had been called SmC_β^* , the nomenclature problem could easily be solved by simply going back to the Fukuda scheme. We find this to be the simplest and most natural choice, with the small exception that we prefer to write SmC_a^* rather than SmC_A^* for the ordinary antiferroelectric, anticlinic, phase. We thus have a scheme which is logical and free from insinuations of any particular properties for any of the subphases.

As the size of the unit cell seems to be well established in the case of SmC_β^* and SmC_γ^* , another possibility is to base the names on this information and it was therefore suggested to call these phases $\text{SmC}_{1/3}^*$ and $\text{SmC}_{1/4}^*$ [23], where the index describes the magnitude of the wave vector corresponding to the unit cell, *i.e.* the reciprocal of the number of layers in each unit cell. In paper 3, we used this scheme, which is in line with the reasoning of the early Ising models [10], where the wavevector magnitude is called the *q*-value of the structure. But the scheme is rather awkward so when the possibility to go back to the initial terminology appeared, this solution seemed much more appealing.

5.4 Experimentally verified properties of the subphases

– *Which properties can we with certainty attribute to the subphases and how can we distinguish the phases experimentally?*

The three subphases generally develop at rather high temperatures, often in the range 80°C - 120°C, and the temperature intervals in which they are stable are always very small (typically between 0.5 K and 5 K). In compounds presenting all subphases, the SmC_α^* phase always lies highest in temperature. Its neighbor phase at higher temperature is always the SmA* phase, so SmC_α^* is actually the highest-temperature chiral smectic C phase in general. The SmC_β^* phase is stable at temperatures below SmC_α^* but above SmC_γ^* , which is thus the ‘coldest’ subphase. In many cases, the SmC_β^* phase does not follow directly after SmC_α^* on cooling, but the compound may develop the ordinary SmC^* phase in between. In contrast, the SmC_β^* and SmC_γ^* phases, when both exist in the phase sequence, always follow directly after one another. Another

important difference between the subphases is that there is no example of a direct transition $\text{SmA}^*-\text{SmC}_\beta^*$ or $\text{SmA}^*-\text{SmC}_\gamma^*$, while the direct $\text{SmA}^*-\text{SmC}_\alpha^*$ transition is frequent among optically pure AFLC compounds. The bunching together of SmC_α^* , SmC_β^* and SmC_γ^* into the collective concept ‘subphases’ is thus somewhat unfortunate, as it is clear that the former phase must be discussed separately from the two latter. In the following description of the subphase characteristics, we will start by discussing the SmC_α^* subphase on its own, and then treat the SmC_β^* and SmC_γ^* subphases together.

5.4.1 The SmC_α^* phase

– the odd chiral smectic C subphase

The SmC_α^* phase is in many respects very similar to the SmA^* phase and thus the transition between these phases can be very difficult to detect. Indeed, with many techniques it is difficult to at all realize that the phase is SmC_α^* , in particular as so many different reports of the SmC_α^* behavior exist. There are however a few more or less distinct signatures of the phase, allowing us to determine with certainty whether or not a phase is SmC_α^* .

5.4.1.1 The SmC_α^* dielectric signature

In the case of a compound exhibiting the SmC_α^* phase but not SmC^* , the former phase can be recognized quite easily by means of dielectric spectroscopy. As the phase below SmC_α^* is then generally¹ either SmC_β^* or SmC_a^* , both non-polar, the weakly polar response of the SmC_α^* phase stands out fairly clearly in a dielectric absorption spectrum. In figure 5.4, the subphase regions of heating and cooling dielectric absorption spectra of a $46\ \mu\text{m}$ sample with (S)-10F1M7 are shown. The response of each phase is here plotted with a separate color, making it easy to distinguish the different phases. The SmC_α^* phase response, plotted in green, is in this compound similar to a ‘mirror image’ of the soft mode on the other side of the transition $\text{SmA}^*-\text{SmC}_\alpha^*$, in the sense that its susceptibility decreases and critical frequency increases on leaving the transition temperature. The soft mode usually drops off much more rapidly on the low-temperature side of the transition [82], so the relatively slow decrease in susceptibility shows that there is some polar response attributable to the SmC_α^* phase. This is even more clear from the sudden decrease in absorption at the transition to the non-polar SmC_β^* phase. In other compounds, the SmC_α^* mode can be slightly stronger and more constant over the temperature range of the phase [83].

The origin of the SmC_α^* dielectric absorption is not completely clear since the local structure of the phase is not yet resolved. If one considers the picture of a small-tilt, tight-pitch SmC_α^* phase, the natural assumption is that the mode is a type of helix distortion mode. However, as the elastic constant of such a tightly twisted structure should be quite high, the susceptibility of the mode should be very low and its critical frequency high [17, 18]. As there are SmC_α^* phases exhibiting a considerably stronger

1. Reports of direct $\text{SmC}_\alpha^*-\text{SmC}_\gamma^*$ transitions exist (see for instance.[72]), but if such a transition really exists it is certainly very unusual.

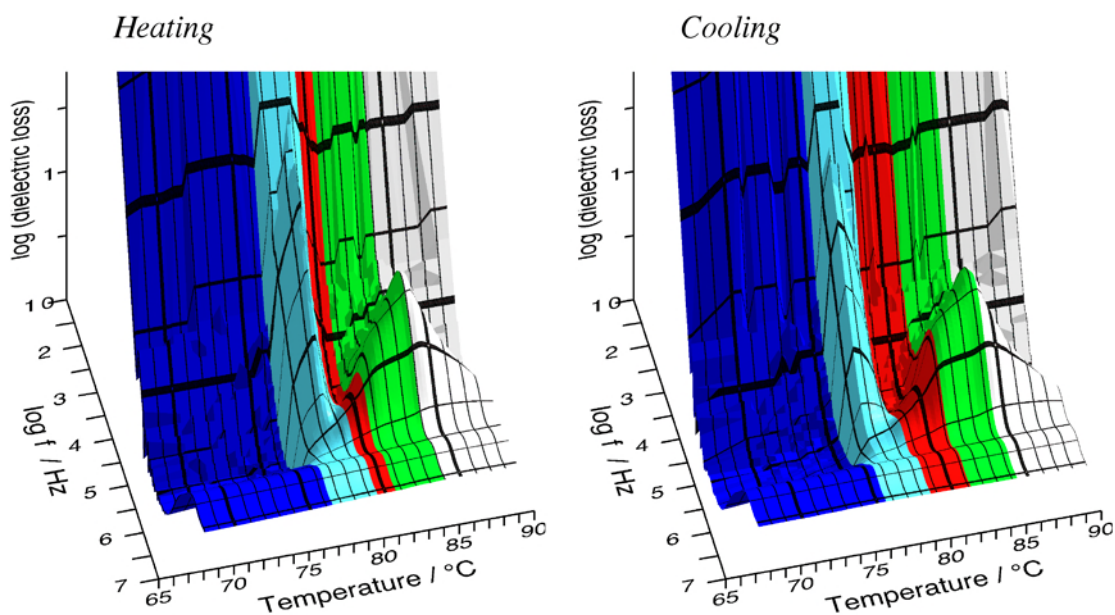


Figure 5.4 Dielectric absorption spectra of (S)-10F1M7 in a $37\ \mu\text{m}$ sample. The phase sequence is SmC_a^* (dark blue), SmC_γ^* (light blue), SmC_β^* (red), SmC_α^* (green) and SmA^* (grey).

absorption than in 10F1M7, it seems questionable if a five-ten layer pitch is a general property of the phase.

5.4.1.2 The birefringence of a planar SmC_α^* sample

By performing a dielectric spectroscopy experiment with simultaneous visible monitoring of the sample texture, it is easy to track how the optical properties change as the sample is cooled or heated through the different subphases. We will again use the

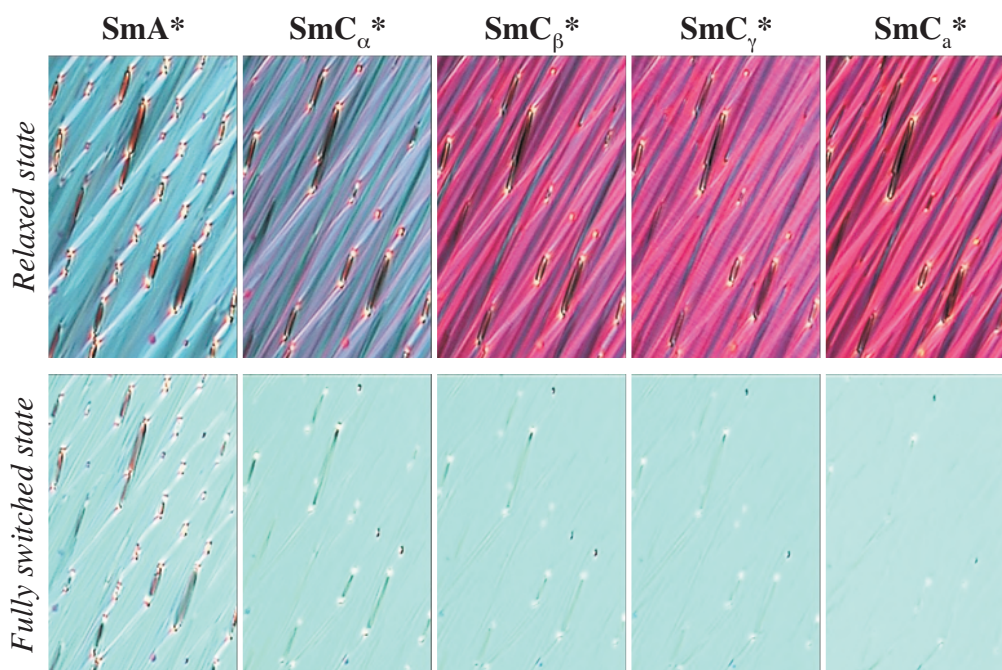


Figure 5.5 Textures of a $4\ \mu\text{m}$ sample with 10F1M7 during a dielectric spectroscopy experiment carried out on cooling. The phase at each temperature has been determined from the dielectric spectrum. Planar alignment with rubbing direction toward the upper right corner. Crossed polarizers.

example of 10F1M7, an AFLC compound which displays essentially the bulk phase sequence also in relatively thin cells (the large influence from surfaces on the AFLC phase sequence is the topic of chapter 6). We need to use a thin sample since we want to study the birefringence color in detail.

In figure 5.5, a texture from the relaxed state and one from the fully switched state is shown for each liquid crystal phase of this compound. We first of all notice that the change in the birefringence Δn on switching the SmA^* phase is very small, and the switched state has essentially the same color throughout the phase sequence. This is quite different from the case of the direct SmA^* - SmC_a^* AFLC compound EHPOCBC (figure 2.5), where the switched SmA^* state has a clearly larger birefringence, and where Δn in the switched state increases further on cooling. On cooling into the SmC_α^* phase, the color changes from bright blue to a more purple blue color, showing that Δn has decreased. This decrease indicates that the SmC_α^* phase is indeed a phase with a non-zero director tilt and a helical modulation of the tilt direction. The other possible explanation for the decrease in birefringence would be that the orientational order would decrease, but this is just opposite of what we would expect on cooling.

5.4.2 The SmC_β^* and SmC_γ^* phases

In addition to verifying the size of the SmC_β^* and SmC_γ^* repeating units, the resonant X-ray experiments [66, 67] indicated that the directors within these units cannot be coplanar in either phase, requiring some sort of clock model for a correct description. On the other hand, the ellipsometry investigations [68] showed that both phases were biaxial, which would not be the case if the unit cells were described by a completely regular, symmetric, clock model. Hence, the distorted clock model picture described above developed.

In a quasi-homeotropic sample placed between crossed polarizers, the two phases look very similar. They are both distinguished by a very long pitch, giving rise to a colorless *schlieren* texture, similar to the texture of a SmC^* or SmC_a^* phase in the case of a helix inversion. Indeed, as mentioned above, helix inversions are very common in connection to these phases. The *schlieren* texture is a simple verification of the biaxial unit cell. Had the unit cell been uniaxial, as predicted by the undistorted clock model, the phases would simply look black since we are looking along the layer normal in this geometry, and this would have to correspond to the optic axis direction. The long pitch of the phases gives rise to easily detectable helix unwinding lines when the phase is viewed in a planar-aligned sample. Good examples of this can be seen in textures *c* and *d* of figure 1 in paper 4. In figure 5.5, the unwinding lines can be seen in the SmC_γ^* phase, and barely in SmC_β^* . This can have several reasons. First of all, the contrast of the lines is usually not very high when the sample is turned to a brightly transmitting orientation, as in this example. Second, the fairly thin cell gap should have a large influence on the helix formation, although the dielectric response as well as the low birefringence and absence of slow axis reorientation seen in the textures, indicate that the sample is not unwound. In principle, a possible explanation is that the SmC_β^* phase has a comparatively short pitch in 10F1M7. However, we can with certainty say that it is longer than $\sim 3 \mu\text{m}$, as a shorter pitch would have produced a selective reflection detected in the spectrophotometer studies on this compound, described in paper 3.

While the SmC_β^* and SmC_γ^* are difficult to distinguish by means of texture observations, they are easier to separate in the dielectric spectrum, provided that the sample

is thick enough (see chapter 6). The non-polar unit cell of SmC_β^* gives this phase a characteristic dielectric spectrum which is virtually “dead”, *i.e.* there are no strong absorptions, as seen in figure 5.4 where the dielectric loss data measured within the SmC_β^* phase of 10F1M7 are plotted in red. In contrast, the SmC_γ^* phase (light blue in figure 5.4) always exhibits some kind of low-frequency polar response, although it can vary in magnitude, mainly depending on experimental parameters. For instance, a too strong measuring field can induce switching of the sample in the SmC_γ^* phase, resulting in a very large increase of the absorption, in a manner similar to the SSFLC switching described in section 4.3.1. A common characteristic of the SmC_γ^* phase dielectric response is that it varies considerably with temperature within the phase, exhibiting an absorption maximum in the center of the phase. The susceptibility falls off rather smoothly on cooling as well as on heating, usually making it difficult to pinpoint the exact location of the phase transitions, as the phase is surrounded by non-polar phases giving essentially no response. This may be connected to the transitions being first-order, thus allowing considerable phase coexistence between the phases, as discussed in paper 3.

The polar response of the SmC_γ^* phase, together with complicated electrooptic switching curves detected in thin cells at temperatures where a bulk sample would be in the SmC_γ^* phase, has led many people to suggest that the phase is ferrielectric. If the distorted clock unit cell proposed for the phase (figure 5.2) is correct, the phase would at least have a ‘ferrielectric-like’ repeating unit, in the sense that its structure leads to an incomplete polarization cancellation, but ferrielectricity also implies the presence of a macroscopic polarization. It is in principle possible to imagine that the SmC_γ^* phase could be surface-stabilized to a state with a different number of layers having polarization up and layers with polarization down, which would then indeed result in a ferrielectric sample. However, it is now also a well-known fact that the sub-phases, in particular SmC_γ^* , can be completely squeezed out of the phase sequence by the action of surfaces (this is discussed in more detail in the following chapter), and it is thus questionable if a surface-stabilized SmC_γ^* structure can at all be obtained. If it can, this should at zero field show bistability and domains of polarization up and polarization down, each characterized by non-zero optical tilt of equal magnitude (smaller than the fully switched state) but to my knowledge this has not been reported in accounts of ‘ferrielectric’ electrooptic switching. On the other hand, Rudquist *et al.* [84] have shown that the most common type of electrooptic response that, for unclear reasons, is repeatedly attributed as ‘ferrielectric’, is perfectly described as the superposition of the response from coexisting SmC^* and SmC_a^* phases, a phenomenon which is often observed in very thin cells.

5.5 The SmC^* phase in AFLCs

– *is there a difference between SmC^* in FLCs and in AFLCs?*

There are several examples of reports where the SmC^* phase, present in an antiferroelectric liquid crystal compound, behaves quite differently from the SmC^* phase in ordinary FLCs [55, 85, 86]. As discussed in paper 3 and in the final chapter of this thesis, also the other AFLC phases can behave quite differently – in particular in the presence of surfaces – depending on whether or not the SmC^* phase is present in the phase

sequence. There are actually indications that the SmC^* phase is somewhat of an ‘alien’ phase in the phase sequence of AFLCs, as discussed extensively in paper 4, and when the SmC^* phase does appear in the AFLC phase diagram, we can therefore expect effects not present in ordinary ferroelectric liquid crystals. These may for instance be related to phase coexistence.

5.5.1 The issue of smectic and nematic order in AFLCs

Once the applicationally attractive electrooptic properties of the SmC_a^* phase had been realized, an intense materials development started in many groups around the world, focused on finding optimal AFLC mixtures. Since one of the first recognized major problems in employing AFLCs in display devices was the difficulty in obtaining a uniform alignment, a prime goal for this research was to find AFLC materials exhibiting a (chiral) nematic phase above the smectic phases. Such a phase aligns much easier than the SmA^* phase, and therefore this was first thought to be the simplest solution to the problem. But it turned out not to be so simple at all. Indeed, it seems that the combination $\text{N}^*\text{-SmC}_a^*$ is not only difficult to achieve, but perhaps even impossible. We will now motivate this by discussing the issue of translational order, ending up showing that the anticlinic layered structure of SmC_a^* and the non-layered but parallel-aligned molecule arrangement in the (chiral or achiral) nematic phase represent extreme examples on the smectic order-disorder scale in liquid crystals.

The lack of N^* in the phase sequence of AFLCs is a strong indication that the tendency to form layers in these materials is much stronger than in FLCs, in which there is often a chiral nematic phase above the SmA^* phase. We may therefore expect higher smectic order parameter values, *i.e.* sharper boundaries between layers with less molecular interdigitation, in antiferroelectric liquid crystals. It is well-known that materials with both N and SmC, or N^* and SmC^* , phases normally exhibit very diffuse layer boundaries, with a density modulation along the layer normal which approaches a sinusoidal function [87]. If a tilted phase develops under such circumstances, the tilt should be in the same direction in adjacent layers, *i.e.* synclinc order, since a low degree of translational order is more or less incompatible with an anticlinic, antiferroelectric, structure [9]. A large number of the molecules of the sample will then find themselves in the diffuse boundaries between two layers where, in the case of an overall anticlinic structure, the tilt direction would be undefined. Furthermore, X-ray experiments carried out by the Fukuda group in Tokyo also show that the smectic order parameter is indeed rather high in AFLC materials, suggesting a small degree of molecular interdigitation between layers [9].

In paper 4 we investigated the standard antiferroelectric liquid crystal compound MHPOBC, over an extended period in time, by means of X-ray, dielectric spectroscopy and texture studies. The sample was stored in the vicinity of 100°C in between measurements, and the measurements themselves were performed in the range 100°C - 140°C . The subphases of MHPOBC develop around 120°C and the material crystallizes between 60°C and 80°C , depending on supercooling, so such a high storage temperature is certainly not unusual in studies of this material. It turned out that the phase sequence of the compound was drastically altered after some days at high sample temperature. The main effect, as seen from the dielectric spectra (compare figures 1, 3 and 4 in paper 4) is that the synclinc SmC^* phase, not present in the fresh sample, develops. In connection to this, the SmC_β^* phase is suppressed and the paramorphic texture sequence, which was observed between SmC_α^* and SmC_a^* prior to the emergence

of SmC^* , is interrupted at the $\text{SmC}^* - \text{SmC}_\gamma^*$ transition. The X-ray experiments, carried out under similar circumstances, also showed distinct changes after a few days at the storage temperature. Our conclusion is that keeping MHPOBC at the high temperature where it develops its interesting phases, actually leads to a degrading of the sample. Probably, there is a decomposition of molecules, producing a mixture between different molecular species which might have very different lengths. The smectic structure developed by such a mixture must be expected to have a considerably lower smectic order than the pure compound, simply because there will be different optimal layer periodicities for the different components. We thus get close to the type of order in a nematic phase, and we believe that this is the reason that the SmC^* phase appears at the cost of the antiferroelectric liquid crystal phases.

5.6 Can we find a convergent picture of the AFLC phase sequence?

If we assume that the SmC^* phase does not belong to the ‘true’ AFLC phase sequence, we see that the sequence corresponds to a continuous increase in the unit cell size on heating towards SmA^* . The SmC_a^* phase, with a two-layer unit cell, is followed by the three-layer SmC_γ^* , which in turn is followed by the SmC_β^* phase with a four-layer unit cell. This was pointed out by Mach *et al.* [67] who in addition measured a five-layer periodicity, increasing in size on heating, in the SmC_α^* phase. However, the extension of the series to successfully include the SmC_α^* phase may be somewhat of a coincidence, as other experiments have indicated other periodicities in this phase. There also seems to be a fundamental difference between the SmC_α^* phase and the other chiral smectic C phases, as all other variants have commensurate unit cells, whereas SmC_α^* does not. Nevertheless, the experiments on MHPOBC, as well as those on the homologous series $n\text{F1M7}$ to be described in the following chapter, indicate that the AFLC phases follow very smoothly upon one another if the SmC^* phase is absent, indicating that they indeed have some basic features in common.

Let us end this chapter with an interesting observation. If we measure the pitch in terms of unit cells, it actually turns out that SmC^* , SmC_a^* , SmC_γ^* and SmC_β^* all have roughly the same pitch values:

<i>Phase</i>	<i>Typical pitch</i>	<i>Unit cell size</i>	<i>Number of unit cells in pitch</i>
SmC^*	$\sim 0.5\mu\text{m}$	$\sim 3\text{ nm}$	~ 200
SmC_β^*	$\sim 2.5\mu\text{m}$	$\sim 12\text{ nm}$	~ 200
SmC_γ^*	$\sim 1.6\mu\text{m}$	$\sim 9\text{ nm}$	~ 200
SmC_a^*	$\sim 0.5\mu\text{m}$	$\sim 6\text{ nm}$	~ 100

6 THE EFFECT OF CONFINEMENT ON POLAR LIQUID CRYSTALS

Remove child before folding
Warning label on a baby stroller

OVERVIEW

The last chapter of this thesis deals with the behavior of polar liquid crystals when they are confined between closely spaced surfaces. This is the sample geometry in which we normally study liquid crystals, and it is also the geometry of any display device, so an understanding of the effects of confinement is of large importance. I will pay particular attention to the case of AFLC materials, showing that they respond very differently to confinement depending on whether or not there is a synclitic SmC phase in the phase sequence. If this is the case, we can expect dramatic supercooling and phase coexistence effects induced by the surfaces even in samples which are often regarded as quite thick.*

6.1 How do surfaces affect the liquid crystal?

The presence of a surface has a profound effect on any liquid crystal, first of all because of the reduced symmetry imposed by the surface. As the molecules cannot penetrate into the surface, there will obviously be a local increase in the positional order at the surface. But also the orientational order tends to be increased. Furthermore, the sign invariance of the director is violated at the surface. In the case of a planar-aligned SmC phase in bookshelf geometry, for instance, only part of the smectic cone is available for the director orientation closest to the surface. If the planar anchoring is strong, effectively only two positions on the cone are available, and if the phase is chiral, these two positions will correspond to polarization pointing into or out of the surface, respectively. We have what is called *polar anchoring*. This means that the presence of the surface actually has the same effect as an electric field applied to the liquid crystal and in case of a chiral smectic phase we can thus expect one tilt direction being strongly favored at each surface. In a small volume close to the surface, this so-called *surface electroclinic effect* [88] induces a director tilt in the absence of electric fields even in the SmA* phase. Since the surface polarization points in the same direction with respect to the surface – usually out of the surface – at each cell boundary, the resulting director structure will tend to be twisted. The volume in which the surfaces can induce a polarization in the SmA* phase is, however, quite small, and the twist is therefore in general localized to a narrow region close to the substrates. Hence, there is often no visible effect of the director twist.

If we in addition have a strong unidirectional planar director anchoring at the surfaces, usually achieved by mechanically rubbing the alignment layer in one well-defined direction, we can impose a fairly large-scale uniform liquid crystal alignment. However, if the liquid crystal phase is a chiral smectic, *i.e.* a polar liquid crystal, the surface polarity will induce a director tilt with respect to the layer normal and, as the director is fixed by the direction of the mechanical rubbing, the result is that polar liquid crystals generally form layers not perpendicular to the rubbing direction, as one might first think, but at a certain angle, different from 0° and 90° , the exact value being set by the surface electroclinic effect, to this direction.

6.1.1 *The encounter of polar surfaces and (anti-) polar smectics*

In the chiral smectic C phases, which are intrinsically polar (at least on a local level), the interactions with the surfaces are even more important. In the case of AFLCs, it is also an intriguing question how the ‘new’ versions of the smectic C phase react to the surface influence. Experiments on ferroelectric SmC* liquid crystals are often performed on planar-aligned samples in which the compound is confined by coated glass substrates to a narrow cell gap t . As described in section 2.6, keeping t small is a necessity in order to render such a material ferroelectric, and a standard choice, in particular for electrooptic studies, has therefore often been to use test cells of $t \leq 5 \mu\text{m}$. When AFLCs were introduced, this procedure was often used also in the study of other phases of the smectic C* family, giving information about the behavior as influenced by bounding surfaces, while other techniques such as DSC and free-standing film experiments gave information about the bulk behavior. It soon turned out that the results obtained for thin cells could differ quite drastically from those obtained on bulk samples. The most obvious effects of cell gap reduction was the surface-induced coexistence between SmC* and SmC_a* over impressive temperature ranges, and that the temperature at which SmC_a* appeared was lowered [65, 89]. It was also soon understood that the effect on the subphases could be even more dramatic [90].

We investigated the effect of confinement on the AFLC phase sequence in detail (papers 3 and 6) and concluded that the sensitivity to surface influence can be very different between different compounds, the most important regulating parameter being whether or not the synclinal SmC* phase is part of the phase sequence. Before discussing the results of these studies we will extend the description of the phase-angle fluctuations of chiral smectic C liquid crystals given in section 2.1.2.2 to the case of thin samples.

6.2 Phase-angle fluctuations in thin cells

If in a dielectric spectroscopy experiment one wants to study a helix distortion mode in its ‘purest’ possible form, one should use very thick cells. In a cell of intermediate thickness, the helix is constantly in a distorted state, and this will of course influence the behavior: the susceptibility will decrease and the critical frequency increase. If the cell thickness is reduced down to the same order of magnitude as the pitch, the helix is suppressed and the helix distortion mode will be absent. An example illustrating this for the case of the SmC* phase is given in figure 6.1, in part from reference [91]. The empty symbols show the response as observed in a thin cell ($2.3 \mu\text{m}$). At decreasing temperature in the SmA* phase, the divergence-like rise of the susceptibility on

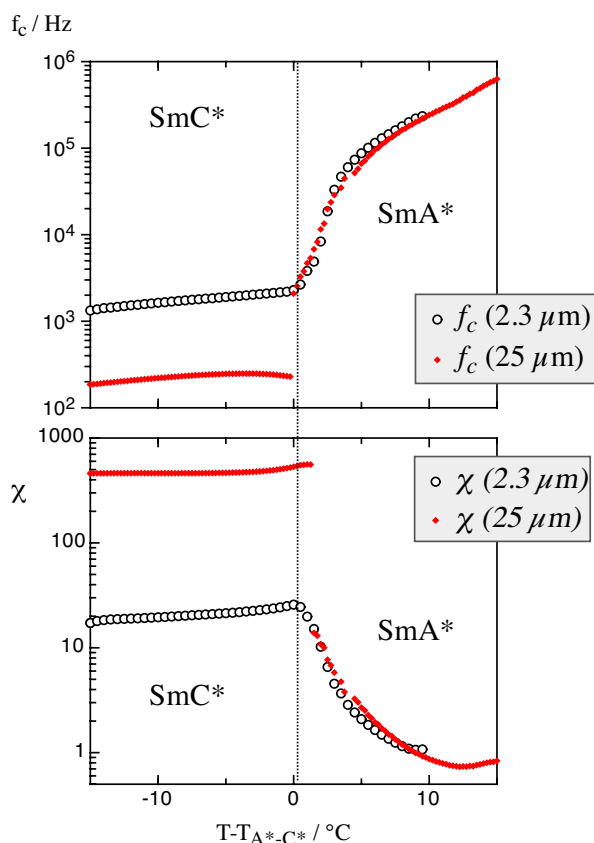


Figure 6.1 The critical frequencies and susceptibilities of the amplitudon and phason modes in the SmA^* and SmC^* phases of a mixture with a $SmA^*/C^*/C_a^*$ phase sequence [91]. In the thin cell the two modes of the SmC^* phase could not be resolved. This was possible in the $25\ \mu m$ cell, but for comparative reasons only the helix distortion mode (phason) has been plotted in the SmC^* phase, while the soft mode (amplitudon) is plotted in the SmA^* phase. Note the strong cell thickness dependence of the phason mode behavior.

approaching the lower-temperature phase, combined with the slowing-down in frequency, is the expected characteristic for a soft mode which is a precursor to a phase with strongly collective polar order. The onset of this polar order at the SmA^* - SmC^* transition is confirmed by the cusp after which the susceptibility falls down more slowly. In the SmC^* temperature region, the measured χ -value is about 20 to 25 and the critical frequency about 1 kHz. In a $25\ \mu m$ cell (filled symbols), on the other hand, the corresponding χ -value is about 500 and the frequency about ten times lower ($f_c \approx 100$ Hz). In both cases the response is due to phase-angle fluctuations, but while the response in the thick cell reflect distortions in the bulk SmC^* helix, the thin-cell response is a result of fluctuations in a permanently distorted structure, the characteristics of which are difficult to predict in a precise way. In contrast to the phason modes, the amplitudon (soft) mode, which is not connected to any large-scale structure, behaves very similarly in the two cells.

The surface-induced director twist structure, discussed above in relation to the surface electroclinic effect, is in the case of the intrinsically polar SmC^* phase much more important. The system will develop a twist-splay-bend in the 3D director configuration, corresponding to a two-dimensional splay-bend in \mathbf{P}_s within the smectic layer plane. For planar boundary conditions and neglecting chevrons (see below), this would correspond to a director twist of 2θ along the cell substrate normal when we go across the cell in the direction of the measuring field, as depicted in figure 6.2. Such an idealized cell will have no net macroscopic UP or DOWN polarization, but the local \mathbf{P}_s vector in the middle will couple to the applied field. If we have a chevron, we would in addition have a net UP or DOWN polarization [23]. The actual case may be more complex but in any case we will in general at least have a net polarization in the plane of the cell which will couple to our measuring field. Since no helix is present, the induced phase fluctuations will be observed as a new, different, dielectric mode. In fact, this

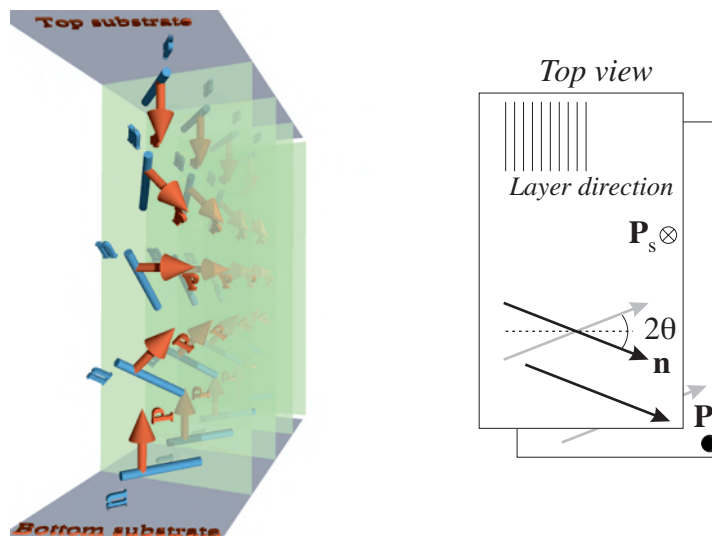


Figure 6.2 The sterically coupled \mathbf{n} and \mathbf{P} vector fields in a “splayed cell” in the idealized chevron-free planar configuration.

mode is actually present also in thick cells, where the helix can develop more or less unobstructed, but since the fluctuations related to the polarization splay will also result in a distortion of the helix, there is no way of distinguishing this mode from the normal helix distortion mode.

The experimental observation of this “splay mode” in different SmC* compounds is well described by Novotna *et al.* [92]. As could be expected, it turns out that the characteristics are strongly dependent on the cell thickness t ; the susceptibility is approximately proportional to the square of the cell thickness, $\chi_{splay} \sim t^2$, while the critical frequency decreases with increasing cell thickness according to $f_{splay} \sim 1/t^2$. One may note that the dependence on the cell thickness thus is the same as the dependence on the pitch of the helix distortion mode, *cf.* equations (2.1) and (2.2). In other words, the cell thickness replaces the pitch as characteristic length in unwound samples. This is of course what we would expect from a dimensional argument.

In case the cell is very thin ($\sim 1 \mu\text{m}$) or if the polar surface anchoring is not very strong, the director configuration at one of the two substrates may be reversed, and the non-twisted ferroelectric surface-stabilized state will result. As we saw in section 4.3.1, there will in general be in-layer phase-angle fluctuations related also to this structure, showing that \mathbf{P}_s is normally not directed along the substrate normal uniformly throughout the cell. The cell thickness dependence of the critical frequency is found to be the same as for the polarization splay state.

The thickness-dependent phason modes observed in thin cells have sometimes been called *thickness modes*, where the name refers to the fact that the cell thickness is the characteristic length parameter in the equations governing the behavior of the modes. This name is not particularly attractive, since it does not convey anything about the physical process involved. Rather than basing the name on a parameter, a better choice would be to give the modes names after the structures in which they occur. In the following, the mode of the splayed polarization configuration will therefore be referred to as the *splay mode*. That of the unsplayed SSFLC structure will not be discussed further, but it could for instance be called the *unsplayed mode*. As a general term, one could use surface-induced phason modes, rather than thickness modes.

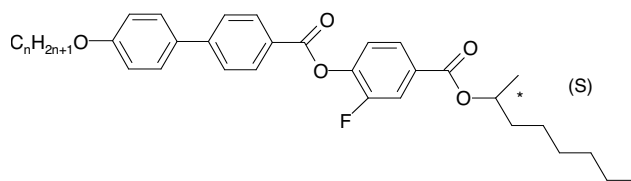


Figure 6.3 Generic chemical constitution of the antiferroelectric liquid crystal series (S)-nF1M7.

6.3 The cell-gap dependence of the AFLC phase sequence

Already in 1989, in the earliest experimental reports on MHPOBC shortly after that this substance was realized to be an antiferroelectric liquid crystal, it was pointed out that the SmC^* phase can co-exist with SmC_a^* over large temperature regions if the compound is filled into a thin cell [65]. Yet the matter was for a long time not thoroughly investigated and the awareness of it seems to have been rather poor, as exemplified by the story of ‘thresholdless antiferroelectrics’ [93, 94]. In an AFLC mixture exhibiting a $\text{SmA}^*\text{-SmC}^*\text{-SmC}_a^*$ phase sequence in bulk, a special type of SmC^* state was stabilized by the surfaces throughout the bulk temperature range of the SmC_a^* phase [91, 95], but this was first interpreted as a sign of a new type of antiferroelectric phase.

When we set out with the experimental work described in paper 3, one of the prime aims was to improve the general understanding of how the balance between SmC^* and SmC_a^* , and between these phases and the three AFLC subphases, could be affected by the influence of surfaces. Key questions were:

- up to which cell thickness can we expect modifications in the phase sequence due to surface influence?
- over which temperature ranges can surface-induced phase coexistence be seen?
- do the phenomena appear in the same way on cooling and on heating?
- can the subphases be completely quenched by surface action?
- how does the bulk phase sequence affect the behavior of the compound in thin cells? Can a SmC^* phase be induced in a thin cell even if it is not at all present in bulk?

For paper 6 this set was extended by considering not only the naturally formed structures but also those formed after addressing with electric fields, paying special attention to the question whether or not it is possible to *remove* surface-induced structures by ac-field addressing.

A very rewarding set of liquid crystals for investigating these questions was the homologous series (S)-nF1M7, where n ranged from 10 to 12. The general chemical constitution is shown in figure 6.3 and the phase sequences of the three homologues, as well as values of the spontaneous polarization and optical tilt, are listed in Table 6.1. The 12F1M7 homologues has been extensively studied over the last few years [96-100], but for our studies it is actually the two other homologues that are the most interesting. The $n = 10$ homologue stands out from the others by not exhibiting any SmC^*

Table 6.1 Phase sequences and saturation values of the spontaneous polarization and tilt for the three homologues of nF1M7 investigated in papers 3 and 6.

<i>n</i>	Phase sequence on heating (transition temperatures in °C)	Saturated P_s $n\text{Cm}^{-2}$	Saturated tilt degrees
1 0	$\text{SmC}_a^* - 76.5 - \text{SmC}_\gamma^* - 78.5 - \text{SmC}_\beta^* - 81.5 - \text{SmC}_\alpha^* - 84 - \text{SmA}^*$	95	25
1 1	$\text{SmC}_a^* - 70 - \text{SmC}_\gamma^* - 76 - \text{SmC}_\beta^* - 80.5 - \text{SmC}^* - 89 - \text{SmA}^*$	105	27
1 2	$\text{SmC}_a^* - 79.5 - \text{SmC}_\gamma^* - 83 - \text{SmC}_\beta^* - 85 - \text{SmC}^* - 92 - \text{SmA}^*$	100	27

phase, but instead the SmC_α^* phase, and 11F1M7 has unusually large temperature intervals in which the SmC_β^* and SmC_γ^* phases are stable. We will therefore only discuss these two homologues in the following.

6.3.1 Surface-enhanced supercooling and phase coexistence

Figures 6.5 and 6.4 show the dielectric absorption spectra from 11- and 10F1M7, respectively, measured at three different cell gaps using special wedge-shaped sample cells¹ (described in paper 3) on heating and on cooling. In the $\sim 35 \mu\text{m}$ cell gap measurements, all phases present in the bulk phase sequence are easily resolved. Furthermore, the phase transitions are rather sharp and coincide very well with results obtained on free-standing films of the compounds. We can thus conclude that this cell gap is large enough for the cell substrate influence to be neglected in both cases.

In the case of 11F1M7, the situation is very different already at $12 \mu\text{m}$ cell gap, a sample thickness which in many cases is regarded as fairly large. On heating, the phase sequence was not much affected, at least not concerning the transition temperatures, but on cooling, the SmC^* phase was heavily supercooled. First, the sample could be cooled some 3 K before any sign of a phase transition appeared, and thereafter the SmC^* response remained partially for another 12 - 13 K. This means that remains of the SmC^* phase existed throughout the subphase temperature range, making the detection of the subphases by dielectric spectroscopy impossible.

When the cell gap was reduced down to $1 \mu\text{m}$, the SmC^* phase (the absorption of which at this cell gap is most certainly a splay mode rather than a helix distortion mode) never disappeared: it appeared throughout the whole bulk temperature range of SmC_a^* . The SmC^* absorption was unaffected down to $\sim 60^\circ\text{C}$ and then started decreasing in intensity very slowly on further cooling. On re-heating, the absorption was constant at the level of the start of the heating measurement until 80°C , which is the temperature of the $\text{SmC}_\beta^* - \text{SmC}^*$ transition in bulk, where it increased very slightly in a step-like manner.

Surface-induced phases and supercooling effects could be seen also in 10F1M7, the compound without the SmC^* phase in the bulk phase sequence, but the bulk-like behavior here remained down to much smaller cell gap. Even at $1 \mu\text{m}$, traces of the SmC_γ^* phase could be easily recognized in the heating measurement, but on cooling, a fairly prominent surface-induced mode was supercooled down to a few degrees below the bulk $\text{SmC}_\gamma^* - \text{SmC}_a^*$ transition. The nature of this surface-induced mode is not

1. The cell gaps differ slightly from those given in paper 3 because the cell gap estimation method used at that time was less accurate.

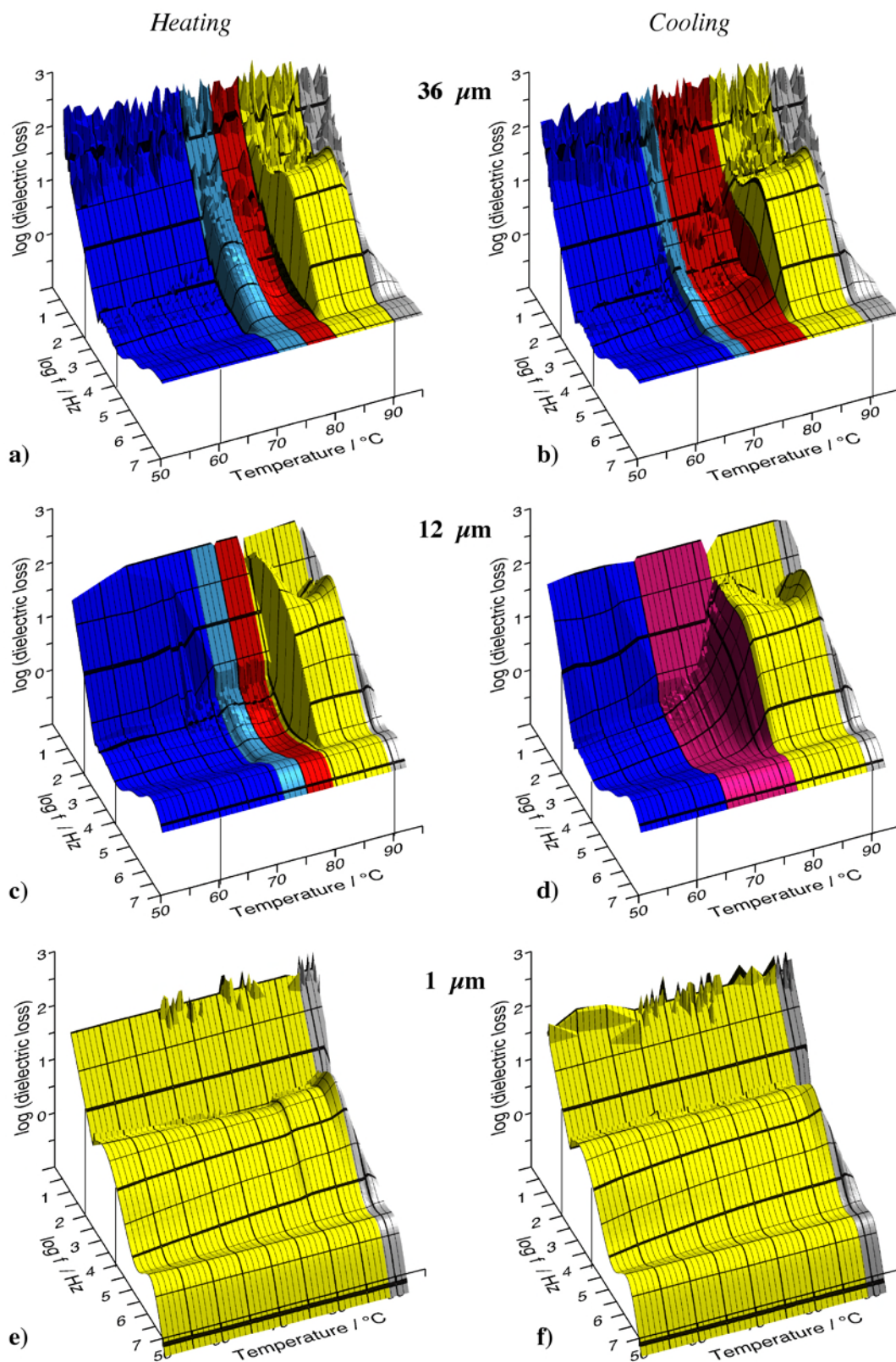


Figure 6.4 Dielectric absorption spectra on heating (left) and on cooling (right) from (S)-11F1M7 in a wedge-shaped sample, allowing measurements at different cell gaps. The color coding is: SmC_a^* – dark blue, SmC_γ^* – light blue, SmC_β^* – red, SmC^* – yellow, SmA^* – grey, coexisting phases – magenta

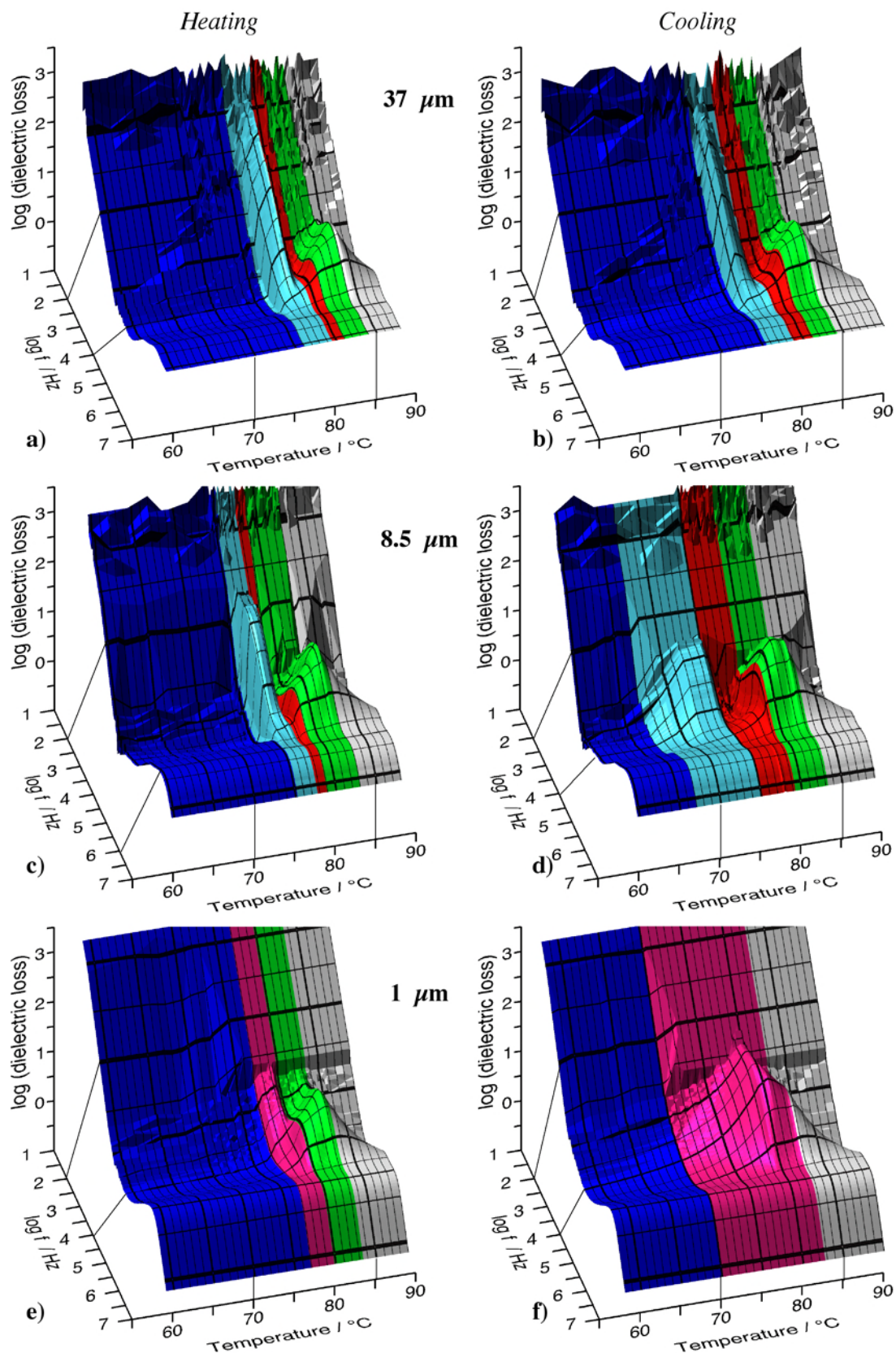


Figure 6.5 Dielectric absorption spectra on heating (left) and on cooling (right) from (S)-10F1M7 in a wedge-shaped sample, allowing measurements at different cell gaps. The color coding is: SmC_{α}^* – dark blue, SmC_{γ}^* – light blue, SmC_{β}^* – red, SmC_{α}^* – green, SmA^* – grey, coexisting phases – magenta.

clear, and it is difficult to say what phase actually is stable at $1\ \mu\text{m}$ cell gap on cooling from 83°C to 70°C . The response is still much weaker than from the ordinary SmC^* phase in 11F1M7 at the same cell gap. Possibly, the SmC^* phase is actually induced close to the surfaces while the bulk is still SmC_α^* . In any case, we can conclude that the sensitivity to surface influence is much lower in the case of 10F1M7, not exhibiting the synclinic, synpolar SmC^* phase, than for 11F1M7, where this phase is stable over a range of $\sim 10\ \text{K}$ in bulk. The same was observed for 12F1M7, also exhibiting a SmC^* phase in bulk. The results can most probably be generalized, suggesting that any AFLC exhibiting a SmC^* phase will show large deviations from the bulk phase sequence, mainly characterized by a drastic extension of the SmC^* temperature range towards lower temperatures, when the cell gap is reduced. Already at cell gaps in the order of $\sim 15\ \mu\text{m}$ we must expect to see this effect, suggesting that measurements performed on thinner cells in the case of SmC^* -producing AFLC materials do not reflect the bulk behavior.

6.3.2 Subphase quenching

The presence of the SmC^* phase in 11F1M7 had a suppressive effect on the formation of the subphases in thin samples. In the heating measurement at $12\ \mu\text{m}$ cell gap, both SmC_γ^* and SmC_β^* can be recognized, but the response of the former phase is almost completely quenched. On cooling, there is no way of recognizing either phase due to the supercooled remains of the SmC^* phase absorption. In the case of 10F1M7, the bulk-like subphase behavior remained quite long when the cell gap was reduced. Only at $8.5\ \mu\text{m}$ cell gap, *cf.* figure 6.5 *c* and *d*, was it possible to notice any clear difference from the measurement obtained in the thickest part of the sample. The absorption in the SmC_γ^* phase now had a slightly lower, but much more constant, susceptibility than in the bulk measurement. Comparing the $37\ \mu\text{m}$ and $8.5\ \mu\text{m}$ absorptions, it seems that the SmC_γ^* absorption is due to fluctuations in a structure which changes continuously with temperature in the bulk sample. When the sample boundaries get close enough, this structure is apparently stabilized in a single configuration compatible with the surfaces. The most plausible explanation is perhaps that the bulk mode is a SmC_γ^* helix distortion mode, and that the pitch diverges towards the center of the phase. In the thinner sample, the helix would then be unwound by the surfaces once the divergence starts, resulting in a splay mode rather than a helix distortion mode.

With respect to the question of whether the SmC_γ^* phase can develop a surface-stabilized ferroelectric structure (*cf.* section 5.4.2) it is worth pointing out that the texture observed at $8.5\ \mu\text{m}$ during the dielectric spectroscopy measurement showed no sign of ferroelectric domain structure whatsoever. The slow axis was essentially along the layer normal across the sample, and the texture exhibited a large amount of helix unwinding lines. If the stabilized dielectric response is indeed connected to an unwound helix, the state which has replaced the helical is thus not a ferroelectric one, but a twist-splay-bend state.

In the cooling run at this cell gap, both the SmC_β^* and the SmC_γ^* phases were supercooled, showing that it is not only synclinic phases which can be stabilized by surface influence. It rather seems that the surfaces stabilize any type of chiral smectic C structure once it has formed. We found support for this idea also in the study of electrically addressed 11F1M7 samples, described in paper 6. We cooled the 11F1M7 sample from the SmA^* phase down to 50°C , where the bulk liquid crystal is in the SmC_α^* phase, but where the thin sample is completely dominated by the supercooled SmC^*

state. We then addressed the sample with ac-fields of varying frequency (in the range 10 - 500 Hz) at an amplitude above the threshold for switching the sample to the saturated synclinic state. By shutting the field off abruptly, we could get the sample to relax to an almost antipolar SmC_a^* state rather than the supercooled polar SmC^* state, as can be seen in the dielectric spectra in figure 3 of paper 6. The interesting point is that when the sample was heated, the SmC_a^* state remained until 80°C , *i.e.* where the bulk compound enters the SmC^* phase. In other words, the subphases can be expelled from the phase sequence by making the samples thin enough, but the phase replacing them is not necessarily SmC^* . If the sample is in an SmC_a^* state before entering the sub-phase temperature range, it will stay in this state throughout this range. However, the SmC^* phase is never replaced by any other phase: the anticlinic state cannot be super-heated into the bulk SmC^* temperature range.

6.3.3 Metastable surface-induced structures

Comparing spectra c and d with a and b in figure 6.4, it is obvious that the SmC^* phase close to its low-temperature boundary is strongly influenced by the surface action. In addition to the normal HD-mode, there is clearly a low-frequency absorption, not present in the $36\ \mu\text{m}$ cell gap measurement, visible both on heating and on cooling. Such an additional SmC^* absorption has been reported several times in the case of AFLCs exhibiting this phase, and many different mechanisms have been proposed for its explanation [101-103]. With the aid of our combined dielectric spectroscopy – texture monitoring equipment, we could elucidate the nature of this additional mode.

Figure 6.6 shows the dielectric response of 11F1M7 at $3\ \mu\text{m}$ cell gap, after addressing in the SmC_a^* phase, in combination with textures at four different temperatures during the experiment. At this cell gap it was not possible to completely remove the supercooled polar SmC^* structure, as can be seen from the absorption at very low frequency throughout the SmC_a^* part of the spectrum and from the quite bright texture between crossed polarizers, one of which was parallel to the layer normal. However, the absorption was very weak, indicating that the sample was close to a true SmC_a^* state. On heating past the bulk SmC_a^* - SmC_γ^* transition temperature (70°C), no change could be seen in the dielectric spectrum nor in the texture. The SmC_γ^* was thus expelled at this cell gap and replaced by SmC_a^* . However, when the temperature reached 75°C , where the bulk sample enters the SmC_β^* phase, the remnant polar response which could not be removed in SmC_a^* disappeared and the texture (photograph *b* in the figure) also turned much darker. It thus seems that the SmC_β^* phase can actually develop also at this small cell gap, but only if one heats the sample from a non-polar SmC_a^* state into the temperature range of the subphase.

At 80°C the phase changed to SmC^* . The transition was accompanied by a quite surprising drastic change in the visual appearance of the sample, to the very bright texture shown in figure 6.6 *c*. As the sample is aligned with the layer normal \mathbf{k} along the polarizer, the bright texture clearly shows that the slow axis is not along \mathbf{k} . The helical pitch in the SmC^* phase of this compound is of the order of $p \sim 0.3\ \mu\text{m}$, so if the helix had developed, the effective slow axis would have been directed along \mathbf{k} . Hence, we can conclude that the spontaneously formed SmC^* state was not a helical one. While the bright texture was observed, the additional low-frequency dielectric absorption was also active. When the temperature had reached 86°C , *i.e.* still in the SmC^* phase, the

absorption quickly decreased in strength and at the same time, the texture changed to the dark one shown in figure 6.6 *d*, suggesting that the helix now did form.

The yellowish white color of the bright SmC^* state reflects a birefringence which is far below that of the fully switched SmC^* state at this cell gap, and we can thus conclude that the structure giving rise to the additional dielectric absorption and the bright texture is not a uniform one. Considering that the state is apparently stabilized by the influence of surfaces, and that the slow axis is turned away from the layer normal but the birefringence is so low, it seems very likely that the state is a twist-splay-bend SmC^* state. The question which now arises is of course why this metastable non-helical SmC^* state forms spontaneously. Considering that the cell gap is roughly ten times longer than the helical pitch, we do not expect surface stabilization. In fact, the non-helical state formed also at cell gaps as thick as $12\ \mu\text{m}$, as can be seen from its absorption in the figure 6.4 *c* spectrum (more details are given in paper 6). We believe that the key issue is that we enter the SmC^* phase on heating from the SmC_β^* phase. This phase has such a long helix that it can be expected to be more or less surface-stabilized in quite thick samples. As is clear from the helix unwinding experiments performed on this compound, described in section 4.2.1, the SmC^* helix has large difficulties to form once it has been unwound. When heating from the SmC_β^* state the transition to the SmC^* phase takes place regardless of whether the sample is helical. Since the SmC_β^*

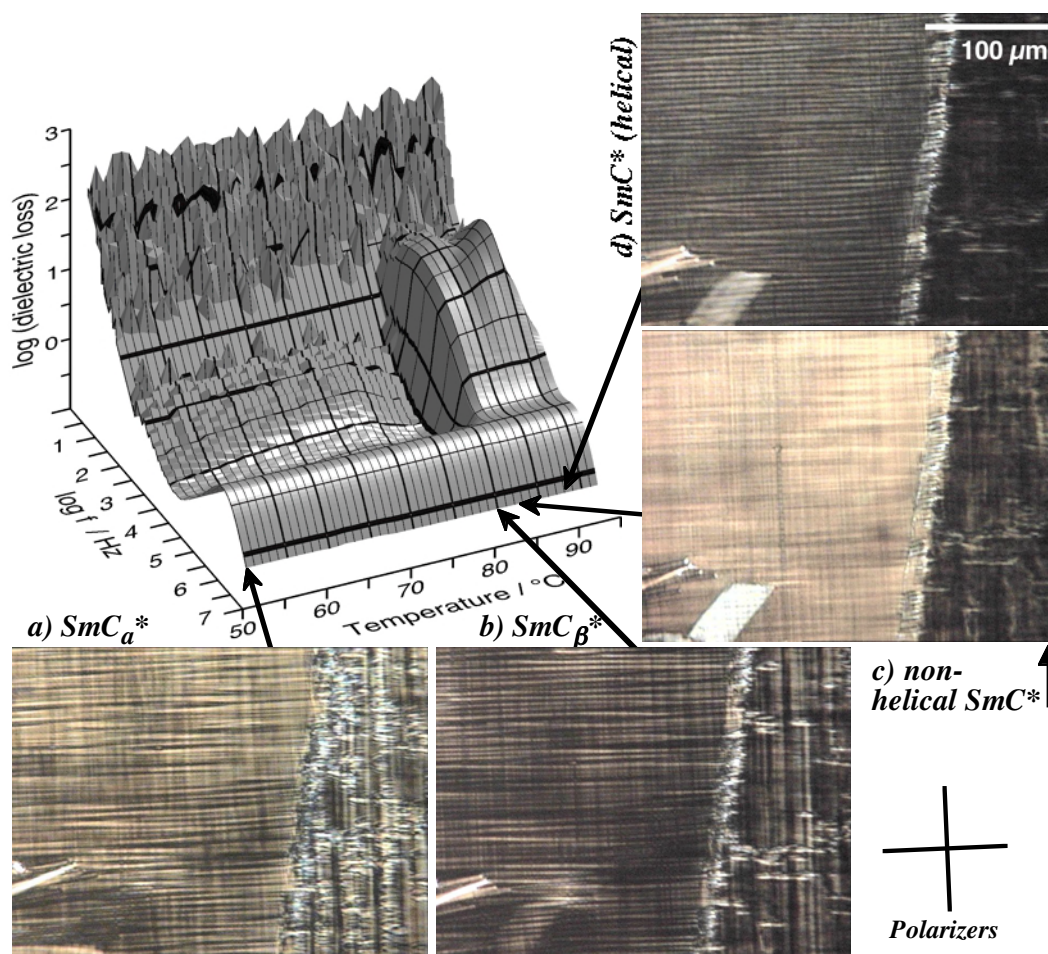


Figure 6.6 Dielectric absorption spectrum and textures from a $3\ \mu\text{m}$ sample of 11F1M7 which has been addressed at 50°C prior to the heating measurement. For explanations, see main text.

state in this case is surface-stabilized, *i.e.* non-helical, the initial SmC* is also non-helical.

6.4 Chevron and parabolic focal conic defects in antiferroelectric liquid crystals

As mentioned in chapter 3, the large interest in polar liquid crystals without layer shrinkage is mainly due to the fact that they do not develop the zigzag defects which are so detrimental to electrooptic device performance. On the other hand, if the prime aim is not to manufacture a device but to improve the general understanding of liquid crystals, smectics which *do* show layer shrinkage are just as interesting as those that do not. We will therefore briefly go back to the issue of layer shrinkage, but now focusing on the defects which it gives rise to. We will not discuss the layer shrinkage-related defect structures (vertical and horizontal chevron, parabolic focal conic) as such – the reader not acquainted with chevron defects is referred to previous work, *e.g.* references [23, 48, 104-107] – but we will direct our attention to how these defects affect the planar textures, with particular reference to the different phases of antiferroelectric liquid crystals.

6.4.1 The formation of horizontal chevron defects at the onset of tilt

Figure 6.7 shows textures of planar-aligned samples of 10- and 11F1M7 on cooling from the SmA* phase down to SmC_a*. The cell gaps are 8.5 μm and 12 μm, respectively, so the corresponding dielectric spectra are those shown in figure 6.5 *d* and figure 6.4 *d*, respectively. In both texture series, the sample is oriented for maximum extinction in the SmA* phase, *i.e.* the average layer normal direction is along one of the crossed polarizers. In the 10F1M7 series, this direction is almost vertical while it in the 11F1M7 photographs is directed along the one o'clock - seven o'clock direction. The initial SmA* texture is thus mainly black, but at the transition to the tilted phase, whether it is SmC* (11F1M7) or SmC_α* (10F1M7) this changes due to the creation of a large amount of defects. The textural signature of these defects is a set of bright ribbons directed perpendicular to the layers. At first the ribbons are quite featureless, but on further cooling a fishskin-like pattern develops. Each ribbon generally consists of two halves, the pattern in one being the mirror image of that of the other. However, the bright ribbons do not cover the whole texture, but there are also another type of ribbon present, in which the texture looks similar to that of the SmA* phase. The good extinction in these ribbons suggest that the layer structure here was essentially unaffected by the phase transition (at least in the plane of the cell), whereas the bright colors of the fishskin ribbons indicate that the geometry of the layers has changed on entering the tilted phase.

On cooling into the SmC* phase of 11F1M7, it becomes obvious how the layers are running within the two sets of ribbon. In figure 6.7 *h*, the texture is covered with very coarse helix unwinding lines. These lines always run along the layers, so they even though we of course cannot resolve the smectic layer structure with visible light, these lines show us the general orientation of the layers. In the dark ribbons the lines are slightly wavy, but in principle they run uniformly perpendicular to the length of the ribbon. In contrast, the lines in the fishskin-like ribbons are clearly kinked. The layers

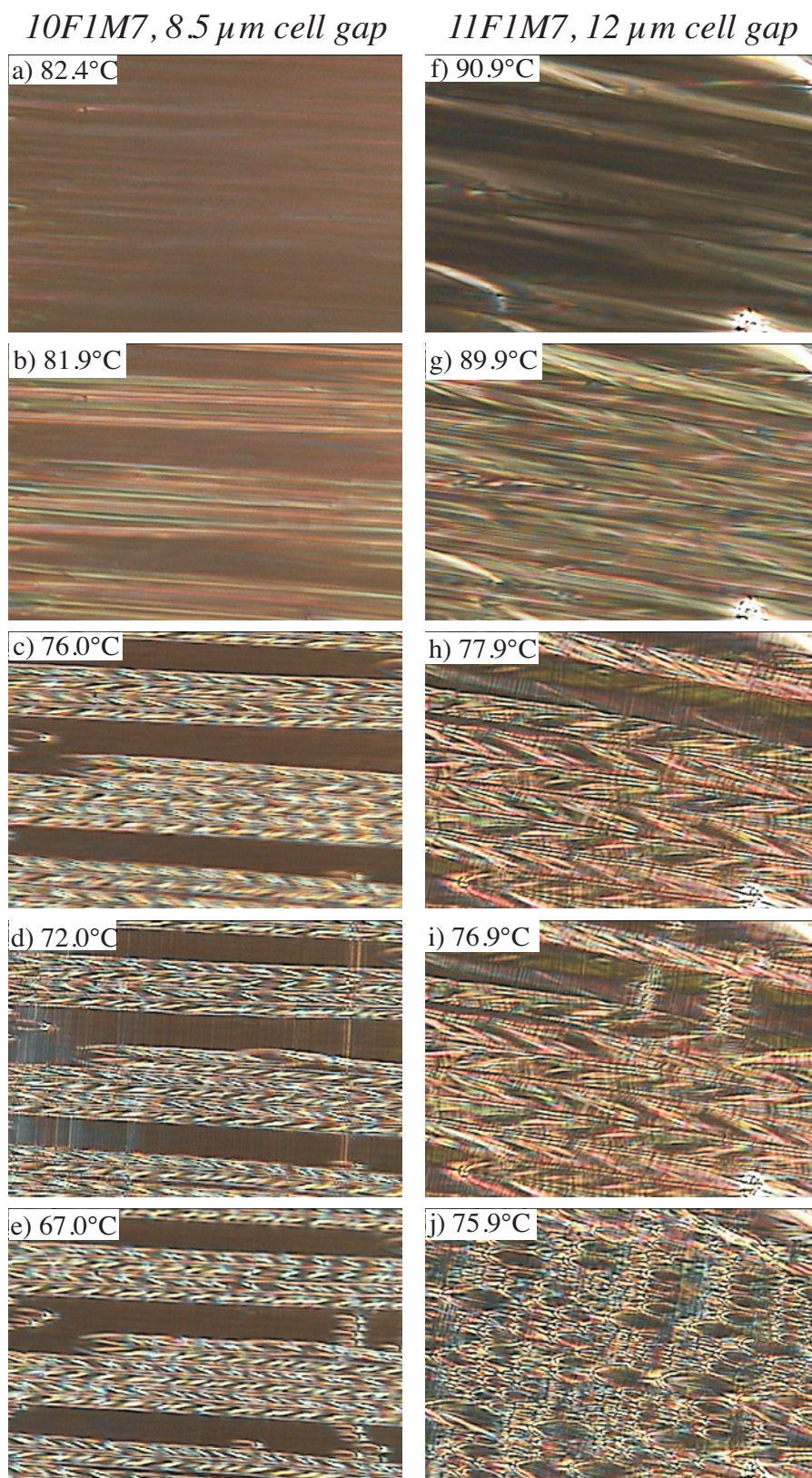


Figure 6.7 Textures of 10F1M7 (left) and 11F1M7 (right) in planar-aligned samples on cooling from the SmA^* phase down to SmC_a^* . The corresponding dielectric spectra are displayed in figure 6.5 d and figure 6.4 d, respectively. The 10F1M7 photographs show: (a) SmA^* , (b) SmC_α^* , (c) SmC_β^* , (d) SmC_γ^* and (e) SmC_a^* . The 11F1M7 series shows: (f) SmA^* , (g) high-temperature SmC^* , (h) supercooled SmC^* , (i) supercooled SmC^* with the SmC_γ^* phase just entering, and (j) SmC_γ^* with some remains of supercooled SmC^* .

run with an angle, roughly corresponding to the optical tilt angle, to the orientation they had in the SmA^* phase, with the two ribbon halves having opposite sign of the inclination.

Regarding the dark ribbons, it is difficult to say anything affirmative about their structure from the textures alone. It is clear that the layers are not kinked in the plane of the cell, *i.e.* there are no horizontal chevrons, but we can not rule out that the ribbons exhibit vertical chevrons, *i.e.* a kink in the layers in the direction along the substrate normal. However, the zig-zag defects generally connected to the meeting of two different types of vertical chevron cannot be seen, so if this is the case, it must be a rather uniform chevron structure. The division into two sets of ribbon does not occur at very small cell gaps. In the case of 10F1M7, the minimum cell gap for this to happen was $\sim 5 - 8 \mu\text{m}$ and in the case of 11F1M7 it was slightly smaller, $\sim 4 - 5 \mu\text{m}$.

The coarseness of the helix unwinding lines in the SmC^* phase of 11F1M7 is interesting in itself, as the helical pitch of this phase is roughly $p \sim 0.3 \mu\text{m}$, as determined by selective reflection studies on quasi-homeotropically aligned samples. The cell gap at which the textures are photographed is $12 \mu\text{m}$, where one normally would not expect to see any trace of the short helix. The average distance between two unwinding lines in figure 6.7 *h* is approximately $2 \mu\text{m}$. This does not correlate well with the SmC^* pitch, but much better with the SmC_β^* pitch. The photograph is taken at $\sim 78^\circ\text{C}$, where the SmC_β^* phase is stable in a bulk sample, but the surfaces apparently stabilize the SmC^* phase. The SmC_β^* -like helix unwinding lines suggests that there is some kind of coexistence between the two phase structures, which would not be surprising in the supercooled SmC^* region. However, the coarse helix unwinding lines are actually observed also at higher temperatures within the SmC^* phase, also where the phase is stable in bulk samples. The behavior is in principle the same as that of the SmC^* phase of the degraded MHPOBC, discussed in the preceding chapter and in paper 4, and it supports the idea that the SmC^* phase is not quite natural to AFLCs but, when it exists, it displays a complicated coexistence with SmC_β^* .

6.4.2 Horizontal chevrons in anticlinic structures

At the transition to the SmC_γ^* phase of 11F1M7, the texture undergoes a rather violent texture change. The transition is first announced by the appearance of a number of small parabolic focal conic defects in the dark ribbons, and we also notice that the ribbon structure starts breaking up (compare right-hand end of the dark ribbon in figure 6.7 *h* and *i*, or – even clearer – the textures of the corresponding phase transition in MHPOBC, depicted in figure 3 *d* and *e* in paper 4). At 1 K lower temperature, when the SmC_γ^* phase has really developed, the texture of the high-temperature phases is not to be recognized. The ribbon structure is essentially gone and the whole sample area is instead covered with parabolic focal conic defects of varying sizes. On cooling into the SmC_a^* phase this texture remains more or less unchanged.

The larger degree of paramorphosis in the cooling sequence of the 10F1M7 sample indicates that the formation of the SmC^* phase has a large influence on the interaction between the liquid crystal and the surfaces. When the phase between SmC_β^* and SmA^* is SmC_α^* rather than SmC^* , the fishskin-ribbon system remains undisturbed all the way through the SmC_a^* phase. Why this is the case is not yet clear, but we may notice that the horizontal chevron structure is actually not advantageous for anticlinic phases. In figure 6.8, the formation of the horizontal chevron structure at the SmA^* -

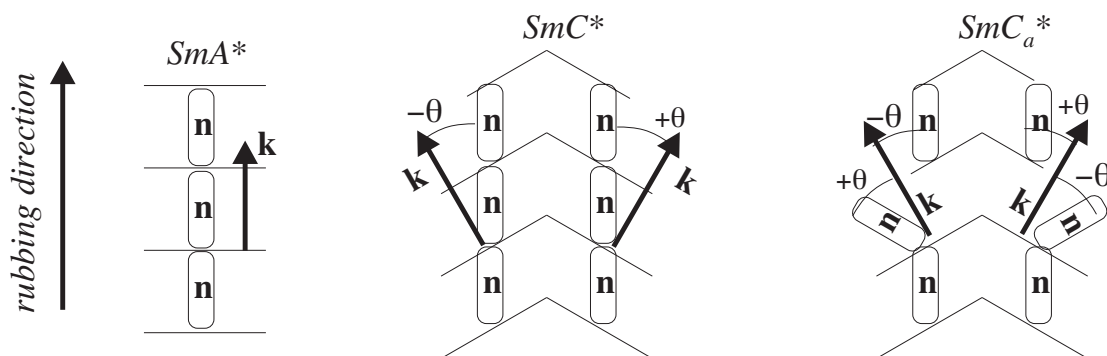


Figure 6.8 Schematic illustration of the geometrical conflict which appears at the transition from a SmC^* phase with horizontal chevrons to the anticlinic SmC_a^* phase.

SmC^* transition is schematically illustrated. At the isotropic - SmA^* or cholesteric - SmA^* transition the director aligns parallel to the rubbing direction and the layers are formed with a thickness corresponding to the orthogonal director configuration. At the onset of tilt in the SmC^* phase, the effective layer thickness is normally reduced. As the layer spacing at the surface is fixed at the value set in the SmA^* phase, the smectic layers must fold either in the plane perpendicular to the cell (vertical chevrons) or in the plane of the cell. The latter, horizontal chevron, case is depicted in the figure (case *b*). The chevron interface mediates changes between the two possible layer directions, corresponding to the director being on opposite sides of the smectic cone.

If the sample is now cooled into a SmC_a^* phase, the horizontal chevron structure would correspond to the case depicted in figure 6.8 *c*, assuming that also the liquid crystal closest to the surfaces changes to the anticlinic state. Obviously, this is not a very convenient state: every second layer will be as happy with the surface alignment as it was in the SmC^* phase, but every other layer now exhibits a director configuration which is in severe conflict with the rubbing direction. We can thus expect that if a stable horizontal chevron structure has been formed, for instance on cooling from SmA^* to a SmC^* phase, a transition to an anticlinic phase will disrupt the anchoring at the surface, producing a major change in texture. In case the cell can be regarded as thick, as in the two cases illustrated in figure 6.7, an alternative way to compensate for the too thin layers may be to form parabolic focal conic defect structures. This is supported by textures observed on re-heating into the long-pitch subphases from the SmC_a^* phase: the unwinding lines then show that the layers are less kinked in the plane of the cell. The important remaining questions are of course why the change from horizontal chevron to parabolic focal conic defects occurs only if the SmC^* phase has been formed, and why the horizontal chevrons are stable throughout the phase sequence of 10F1M7, including the SmC_a^* phase.

7 CONCLUSIONS AND OUTLOOK

- *Where was I?*
- *Oh, I think you were finished.*
Monty Python's 'Life of Brian'

Ferro- and antiferroelectricity in liquid crystals occur in chiral tilted smectics, in the SmC^* and SmC_a^* phases, respectively. The balance between these phases, and the intermediate subphases, SmC_α^* , SmC_β^* and SmC_γ^* , is sensitive and can easily be shifted by various parameters. The 'true' antiferroelectric liquid crystal phase sequence develops best in samples of very high purity in bulk samples. Reducing the purity, chemical or optical, will promote the formation of the SmC^* phase, first of all at the cost of the subphases, but also the SmC_a^* phase can be fully or partially suppressed. In an AFLC where the SmC^* phase develops, the influence from surfaces strongly stabilizes this phase, leading to dramatic supercooling and phase coexistence effects in samples as thick as $\sim 15 \mu\text{m}$. At typical display cell gaps, $\sim 2 \mu\text{m}$, the SmC^* phase generally dominates the whole mesophase sequence, when the liquid crystal is cooled from SmA^* . The surface-induced SmC^* structure can, however, be successfully removed by addressing the sample with ac electric fields.

The combination of dielectric spectroscopy and a continuous monitoring of the sample texture is very powerful in the study of polar liquid crystals. We have successfully employed this technique to elucidate the origin of anomalous dielectric absorptions in the SmC^* phase which have previously been mistaken for signs of new phases. It turned out that the absorptions were due to non-equilibrium surface-induced twist-splay-bend structures developing at unexpectedly large cell gaps. Despite the short pitch of the SmC^* phase, the helix can be metastably unwound by the surfaces at cell gaps up to $\sim 15 \mu\text{m}$. It is likely that this is related to partial coexistence with the long-pitch SmC_β^* subphase. Studies of textural defects during dielectric spectroscopy measurements showed that the SmC_β^* and SmC^* phases can transfer into each other without any major visible changes, while the transition to the SmC_γ^* phase on cooling induced a complete rearrangement of the liquid crystal surface alignment.

The technique can also be used to study the switching dynamics of polar liquid crystals. Of particular interest is the investigation of the unwinding of the helix of bulk SmC_a^* samples and the Frederiks transition in surface-stabilized SmC_a^* samples. In both cases the application of an electric field induces a transition towards a vertical tilt plane prior to switching to the synclinic state.

By means of X-ray and optical investigations, we have furthermore studied two polar liquid crystals, one ferroelectric and one antiferroelectric, which display a constant layer thickness throughout the temperature range of the tilted phases. The origin of this attractive property is the high degree of orientational disorder in all smectic phases, and that the macroscopic tilt is created through a biasing of tilt direction fluctu-

ations rather than an effective increase of the molecular tilt. The semi-fluorinated compounds also exhibit unusually weak tilt direction correlations across the smectic layer boundaries, which is most likely related to an anti-parallel packing.

The investigations of impurity effects on antiferroelectric liquid crystals clearly showed that in standard compounds we may encounter a chemical degradation simply from performing experiments on them. The nature of the degradation is not yet clear and is an obvious topic of future research, preferably incorporating proper chemical analytical techniques. The issue of orientational disorder seems to be of general importance, not only for developing polar liquid crystals attractive for application in electrooptic devices, but also for understanding the antiferroelectric liquid crystal phase sequence.

A blind spot in the field of polar effects in soft matter is ferro- and antiferroelectricity in lyotropics. Smectic A and C structures are common also in these media, and by choosing a chiral solvent we may expect the development of a spontaneous polarization also here. The additional degree of freedom given by the concentration as state variable makes the systems more complex than thermotropics, but it might also make optimization easier. In any case, it is an area which certainly should be investigated.

APPENDIX A THE QUESTION OF MOLECULAR SHAPE

Många är stora som hus eller så, men dom flesta är små, mycket små, mycket små.
Olle Adolphsson, Okända djur

Very often in the discussion of calamitic liquid crystals, the molecules making up the phase are treated as ‘rigid rods’. In graphical representations of mesophases, one frequently encounters cigar-shaped molecules, but in some cases, in particular when the biaxiality of the molecules should be stressed, bricks are preferred. In the field of polar liquid crystals, a whole sub-field of ‘banana-shaped’ molecules has developed. The approximative approach to the molecular shape is indeed very useful in most situations, and often absolutely necessary, but one should still be aware of how the molecules look in reality, and in which cases it is necessary to consider the deviation from cigar (brick, banana...) shape. The chemical constitution of the molecules has important consequences for how they pack and organize in different directions, as well as for their dynamics, internal and external. Last but not least, the macroscopic physical properties of the mesophase, such as polarization, viscosity and optical anisotropy, will always have their origin in the structure of the molecule. As this thesis treats only calamitic thermotropic liquid crystals we will leave all other types out in the following brief survey of liquid crystal chemistry, to a large extent based on chapter 3.2 in the textbook by Collings and Hird [108].

A.1 Hard core, chains and other essential ingredients

The ‘rod’ in calamitic liquid crystals is normally not a very homogeneous entity. If it is truly rigid from one end to the other, liquid crystalline phases generally do not form. Instead the molecules usually have flexible tails on at least one side – often both – of a rigid core. The physical origin of the stratification occurring in smectics is not fully understood, but de Gennes suggested that a segregation effect, in the sense that the rigid cores of the molecules want to stick together, as do the flexible tails, plays an important role [2]. Molecules which are symmetric along the long axis, *i.e.* where the core units are similar and the tails are of approximately the same length, promote the lateral inter-molecular interactions giving rise to this effect, and are thus suitable for the generation of smectic phases. Since there are as many molecules directed with a certain tail R pointing upwards as there are with R pointing downwards, the core-core and tail-tail interactions will be suppressed by making one end group much longer than the other. This is instead a good choice if a nematic phase is desired. It also turns out that a broad core or one which is long compared to the flexible tails, favors the formation of the nematic phase at the cost of smectic order. Long end chains tend to entangle

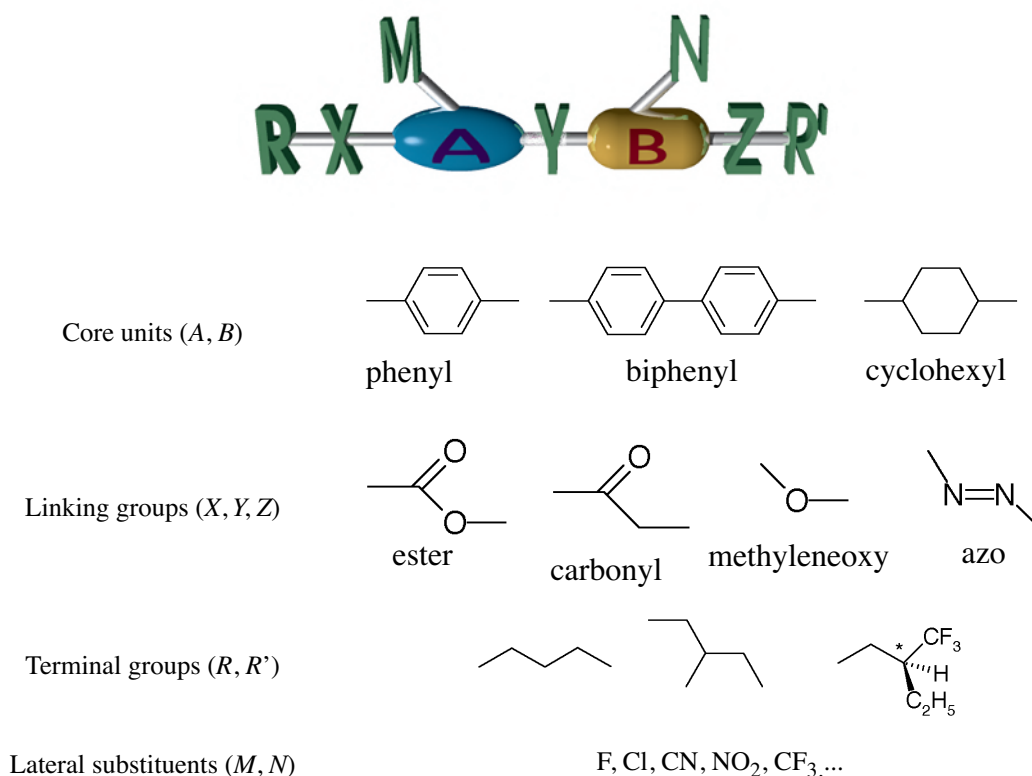


Figure A.1 A generic ‘template’ for the constitution of liquid crystal molecules (mesogens), redrawn from [108], and typical choices for each group. The different components are normally referred to as the *core units*, *linking groups*, *terminal groups* and *lateral substituents*. Between X and Z the molecule can be regarded as rigid, while the terminal groups are often hydrocarbon chains with a large degree of flexibility.

from molecule to molecule, which promotes a stratified structure.

A generic template of a calamitic mesogen is pictured in figure A.1, together with a few examples of common building blocks. The rigidity of the molecule is due to the *mesogenic core* which consists of linked ring systems (symbolized by A and B in the figure) such as phenyls or cyclohexyls. Two rings can be regarded as a practical minimum for mesophase formation. There are examples of mesogens with only one ring system, but these are very rare, while liquid crystals with more than two rings are common. Antiferroelectric liquid crystals, for instance, almost all have three rings in the core. In general, the increased length to breadth ratio resulting from the addition of a ring to the core stabilizes liquid crystal phases, in particular smectics. The rings can be directly connected, as in a biphenyl, or they can be linked via a *linking group* (Y in figure A.1). If a linking group is used, this should generally maintain the linearity of the core, though a slight bend can help to promote tilting in smectic phases. This is also promoted by the presence of strong lateral dipoles, and it is therefore common in particular in polar smectics to place an ester linking group at position Y in a molecule with two long terminal alkoxy chains.

The optical and dielectric properties of the liquid crystal are mainly dictated by the core structure, even though long end chains can ‘dilute’ the optical properties of the core, resulting *e.g.* in decreased birefringence. As the core is far from cylindrically symmetric, the mesogenic molecules are always inherently biaxial, *i.e.* the core is more ‘brick-like’ than ‘cigar-like’. In general, most or all of the biaxiality is averaged

out through fluctuations, leading to the macroscopic phase being uniaxial (nematic or SmA) or only weakly biaxial (SmC).

The required flexibility is provided by the terminal groups of the molecule (R and R'), which most often are some type of alkyl chain, sometimes branched at the end. They are, however, far from completely flexible as illustrated for instance by the so-called *odd-even* effect – referring to a certain physical property changing back and fourth as the alkyl chain is extended one carbon at a time – important both in the fields of nematics and polar liquid crystals. The terminal groups can be connected directly to the core, or via linking groups (X and Z). With for instance a carbonyl as linking group, one can introduce a strong dipole into the structure, generally enhancing smectic organization, in particular the tilted ones. On the other hand, the linking groups tend to increase the lateral size of the molecule which disrupts lamellar packing, thus favoring nematic organization at the cost of smectic. A danger in incorporating linking groups is that they are often sources of chemical instability. A famous example is the first ferroelectric liquid crystal DOBAMBC, which due to an imine linking group has a notorious tendency to decompose when illuminated by visible light.

Table A.1 Summary of general rules of thumb for the connection between the molecular structure and the mesophases generated.

<i>Part of the molecule</i>	<i>Characteristics promoting the nematic phase</i>	<i>Characteristics promoting smectic phases</i>	<i>Requirements for FLCs / AFLCs</i>
Core group (A and B)	<ul style="list-style-type: none"> • Short and bulky • Dissimilar constituents 	<ul style="list-style-type: none"> • Long and slim • Similar constituents (symmetric) 	<ul style="list-style-type: none"> • Three rings for AFLCs
Terminal groups (R and R')	<ul style="list-style-type: none"> • Short • R and R' dissimilar 	<ul style="list-style-type: none"> • Long • R and R' of similar length 	<ul style="list-style-type: none"> • One terminal group chirally branched • Should induce strong steric hindrance of rotation about the long axis • Achiral end chain not too long
Lateral substituents (M and N)	<ul style="list-style-type: none"> • Large (reasonably...) • Non-polar 	<ul style="list-style-type: none"> • Small • Polar 	<ul style="list-style-type: none"> • Polar
Linking groups (X , Y and Z)	<ul style="list-style-type: none"> • Broadening 	<ul style="list-style-type: none"> • Not broadening • Polar 	<ul style="list-style-type: none"> • Strong lateral dipoles (<i>i.e.</i> ester linkage) •

Lateral substituents (M and N), *i.e.* atoms or groups of atoms attached off the linear axis of the molecule, most often to the core units, in general have a tendency to counteract mesophase formation. They are particularly detrimental to the stability of smectic phases. In principle lateral substitution is thus avoided, but it can be useful for tailoring certain physical properties such that a compound can be used in applications. The most common choice is the fluoro substituent because of its combination of small size and high electronegativity

A.2 The molecules of polar liquid crystals

As explained in section 2.1, the presence of chiral molecules is (usually¹) a necessary condition for achieving a polar liquid crystal phase. The chiral center can be placed in various places of the molecule, but most often it is located in one of the terminal chains, a choice which by necessity means that the chain is branched. The steric effects of branching the terminal chain in principle disrupt the liquid crystal phase stability, and therefore the branch is often located to the end of the chain, where the flexibility of the chain somewhat dilutes the negative effects of the branch. However, this solution facilitates rotation of the chiral center around the long axis of the molecule, thus decreasing the resulting spontaneous polarization. This effect can in turn be reduced somewhat by making one of the chiral center branches extended in length, but with the risk of reducing the general mesophase stability. A positive effect of the branching is that it can actually facilitate the required molecular tilting. An interesting special case of this are the achiral swallow-tailed mesogens which produce an anticlinic tilted SmC_a phase [109].

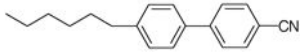
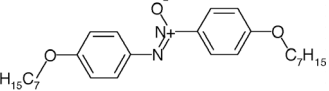
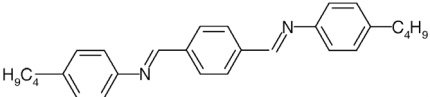
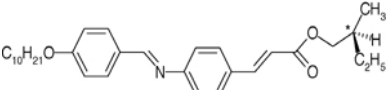
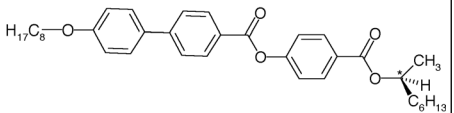
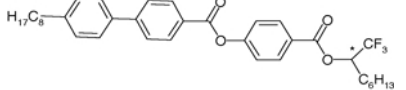
Apart from chirality, we also require a strong lateral dipole, often provided by ester or ether linking groups. The dipole is obviously needed for generating the desired mesoscopic polarization, but it also tends to stabilize the formation of the tilted SmC^* phase as opposed to SmA^* . It is important to limit the freedom of rotation of the dipole around the molecular long axis, since this will lead to an effective cancellation of the polarization. This is often achieved by locating the dipolar group close to either the chiral center or to the rigid core, since these groups are sterically hindered in their long axis rotation. It can be particularly efficient to include a polar group at the chiral center since only the chiral branching can produce an asymmetric biasing in rotations (the rotation of the core group is of course also biased, but there are always two values of the long axis rotation angle, ψ in figure 1.1, separated by 180° , which are equivalent). This is not uncommon, but it has the disadvantage of making the molecule more susceptible to racemization. This is not only detrimental to the magnitude of the spontaneous polarization but it can have drastic effects on the general phase sequence of the material.

The standard approach to producing a ferroelectric liquid crystal for use in applications is not to synthesize a chiral SmC^* -producing molecule with high polarization, but rather to prepare an achiral SmC host and dope it with a small quantity of chiral and polar dopant. This way one can combine different desirable properties which are often conflicting in a single compound, such as low viscosity together with high polarization. The dopant molecules actually need not be mesogenic on their own, but they should at least have a 'mesogenic-like' structure. We used such a dopant molecule as the 'ferroelectric-like' dopant in a study of chiral doping of syn- and anticlinic racemic $\text{SmC} / \text{SmC}_a$ hosts [110, 111].

Materials which exhibit the antiferroelectric SmC_a^* phase are rather similar in their structure. The core is almost always a three-ring system with two ester groups pointing in the same direction, towards the chiral branched terminal chain. Compared to typical FLC molecules, the compounds exhibiting antiferroelectric phases generally have large molecular dipoles and a large difference in size between the branches of the chiral end chain, a structure which probably facilitates the anticlinic organization. A

1. We here choose not to go into the special case of bent- (banana-) shaped molecules, where polarity may arise despite the lack of molecular chirality. In this case the *phase* is, however, still chiral.

Table A.2 Some examples of well-known calamitic liquid crystal molecules and their phase sequences. In case of the molecules exhibiting polar phases, the asterisk indicates the chiral center. Highly bent-shaped ('banana-shaped') mesogens are deliberately left out, since these can exhibit quite special properties which are outside the scope of this thesis.

Compound	Phase sequence
 <p>5CB</p>	Crystal - 24.0 - N - 35.0 - Isotropic (from [108])
 <p>HOAB</p>	Crystal - 74.4 - SmC - 95.4 - N - 124.2 - Isotropic (from [112])
 <p>TBBA</p>	Crystal - 113.0 (S - 74.0 - H - 89.2) - G - 144.5 - SmC - 172.0 - SmA - 199.0 - N - 235.0 - Isotropic (from [112]. The 'S' phase is probably an unidentified soft crystal phase.)
 <p>(S)-DOBAMBC</p>	Crystal - 76.0 (SmI* - 63.0) - SmC* - 95.0 - SmA* - 117.0 - Isotropic Ps = 4 nCcm ⁻² (from [108])
 <p>(S)-MHPOBC</p>	$\text{Crystal} \leftarrow \begin{matrix} (SmI_a^*) & 84 & 119.5 & 120.5 \\ 59 & \rightleftharpoons SmC_a^* & \rightleftharpoons SmC_\gamma^* & \rightleftharpoons SmC_\beta^* \\ & 67 & 118.5 & 119.7 \end{matrix}$ $\begin{matrix} 121.9 & 123.0 & 150.2 \\ \rightleftharpoons SmC_\alpha^* & \rightleftharpoons SmA^* & \rightleftharpoons Isotropic \\ 121.2 & 122.5 & 149.5 \end{matrix}$ <p>From paper 4.</p>
 <p>TFMHPBC</p>	SmC _a * - 74.3 - SmC _α * - 75.0 - SmA* (From [113].)

typical combination of branches is a hydrogen atom (short), a CH₃ group (medium length) and a C₆H₁₃ group (long). The CH₃ group is often replaced by a fluorinated equivalent, CF₃.

A.3 Molecular packing and freedom of movement in liquid crystal phases

The nature of molecular fluctuations is very important for the understanding of smectics in general and the appearance of mesoscopic polarization in particular. Here we will briefly look into what type of fluctuation we can expect in liquid crystals in general, and when the rigid rod approximation is appropriate, to the molecule as a whole or to certain parts of it.

The relatively high flexibility of the terminal groups of the mesogens is sometimes expressed by saying that the terminal chains are ‘melted’ while the cores are still solid [114], at least in the smectic phases. Graphically, this idea is sometimes expressed as in the right picture of figure A.2. While the completely rigid system on the left is obviously far too ordered to describe a mesophase structure, the right-hand model leads to a very bad packing efficiency. As free space always costs much energy, such a picture is therefore not a very realistic one. Something in between these two extremes is probably closer to the real situation. This can also be inferred from a study of the molecular rotation around the long axes, \mathbf{m} , which is often thought to be more or less unhindered in the nematic and smectic A phases due to their cylindrical symmetry. It turns out, however, that, while this is true macroscopically, it is far from true on a local scale. Chistyakov [6] and Leadbetter [115] have both pointed out that the average lateral molecular spacing measured through wide-angle X-ray scattering falls right between the dimensions of the molecule along and across the ring systems of the core. The spacing is typically found to be $\sim 5\text{\AA}$, whereas the maximum lateral molecule dimension is $\sim 6.5\text{\AA}$ and the minimum $\sim 3.5\text{\AA}$ [115]. If there were no correlations in orientation about the long axes, such that each molecule could rotate freely about \mathbf{m} , the average spacing must be at least in the order of the maximum lateral dimension. It is thus clear that rotations about the long molecule axis must be strongly cooperative in nature and that the assumption of average cylindrical symmetry cannot be valid for nearest neighbor interactions. Indeed, Leadbetter points out that this holds even for the isotropic phase!

Quite often, fluctuations are divided into collective and non-collective fluctuations. In the latter term, molecular fluctuations about the long and about the short axes are included. Calling them non-collective is apparently slightly misleading, since the close packing that prevails in all liquid crystalline systems makes all fluctuations cooperative

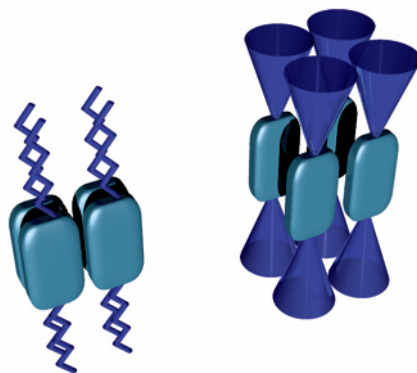


Figure A.2 Two extreme views on the order of the terminal groups. The real situation is probably somewhere in between the too rigid and ordered left-hand picture and the right-hand picture with ‘melted’ terminal chains. The latter situation obviously decreases the packing efficiency seriously and is therefore unlikely to occur, at least on the single-molecule scale.

to some extent. Leadbetter introduced the 'coherence volume', typically consisting of ~10 molecules, within which the molecular orientation is non-random [31, 116]. The 'non-collective' fluctuations of the molecules is perhaps better interpreted as fluctuations of the coherence volume. Fluctuations of a single molecule in its local liquid crystal environment has been compared to the task of moving from one end of a full-packed restaurant car of an express train to the other [117]. Collective fluctuations, in contrast, are movements where a very large number of molecules, for instance a whole smectic layer, move towards a common goal. Such fluctuations can only be induced by a strong external force field acting on the molecules, and can perhaps be compared to a well-coordinated aerobics group, where the leader plays the role of the external field.

REFERENCES

- [1] J. W. Goodby and G. Gray in *Handbook of Liquid Crystals*, Vol. 1 (Eds, Demus, D., Goodby, J. W., Gray, G., Spiess, H.-W. and Vill, V.), Wiley-VCH, pp. 17-23 (1998)
- [2] P. G. de Gennes and J. Prost, *The Physics of Liquid Crystals*, Clarendon Press, Oxford (1993)
- [3] S. Chandrasekhar, *Liquid Crystals*, Cambridge University press, Cambridge (1992)
- [4] I. Hargittai and M. Hargittai, *Symmetry through the Eyes of a Chemist*, VCH, New York (1987)
- [5] J. Als-Nielsen, J. K. Litster, R. J. Birgeneau, M. Kaplan, C. R. Safinya, A. Lindegaard-Andersen and S. Mathiesen *Phys. Rev. B*, **22**, 1, pp. 312-20 (1980)
- [6] I. Chistyakov in *Advances in Liquid Crystals*, Vol. 1 (Ed, Brown, G.), Academic Press, pp. 143-168 (1975)
- [7] G. Vertogen and W. H. de Jeu, *Thermotropic Liquid Crystals, Fundamentals*, Springer-Verlag, Berlin
- [8] J. Seddon in *Handbook of Liquid Crystals, Vol. 1*(Eds, Demus, D., Goodby, J. W., Gray, G., Spiess, H.-W. and Vill, V.), Wiley-VCH, pp. 635-679 (1998)
- [9] Y. Takanishi, A. Ikeda, H. Takezoe and A. Fukuda *Phys. Rev. E*, **51**, 1, pp. 400-406 (1995)
- [10] A. de Vries *Mol. Cryst. Liq. Cryst.*, **10**, 1-2, pp. 31-7 (1970)
- [11] J. W. Goodby in *Handbook of Liquid Crystals*, Vol. 2A (Eds, Demus, D., Goodby, J. W., Gray, G., Spiess, H.-W. and Vill, V.), Wiley-VCH, pp. 3-21 (1998)
- [12] S. T. Lagerwall, A. Dahlgren, P. Jägelmalm, P. Rudquist, K. D'havé, H. Pauwels, R. Dabrowski and W. Drzewinski *Adv. Funct. Mater.*, **11**, 2, pp. 87 - 94 (2001)
- [13] F. Gießelmann, A. Langhoff and P. Zugenmaier *Liq. Cryst.*, **23**, 6, pp. 927-931 (1997)
- [14] T. Hegmann, J. Kain, S. Diele, G. Pelzl and C. Tschierske *Angew. Chem.-Int. Edit.*, **40**, 5, pp. 887-890 (2001)
- [15] R. B. Meyer, L. Liebert, L. Strzelecki and P. Keller *J. Phys. Lett.*, **36**, 3, pp. L69-71 (1975)
- [16] J. P. F. Lagerwall *Phase Characterization of Polar Liquid Crystals Using Dielectric Spectroscopy*, Licentiate thesis, Chalmers, Göteborg (2000)
- [17] A. Levstik, T. Carlsson, C. Filipic, I. Levstik and B. Zeks *Phys. Rev. A*, **35**, 8, pp. 3527-34 (1987)
- [18] F. Gouda *Dielectric Relaxation Spectroscopy of Chiral Smectic Liquid Crystals*, Ph.D. thesis, Chalmers University of Technology, Göteborg (1992)
- [19] L. A. Beresnev, L. M. Blinov, M. A. Osipov and S. Pikin *Mol. Cryst. Liq. Cryst.*,

158A, pp. 1-150 (1988)

[20] K. Hiraoka, H. Takezoe and A. Fukuda, *Proceedings from FLC'93, Tokyo, Japan* (September 28 - October 1, 1993). *Ferroelectrics*, **147**, pp. 13-25 (1993)

[21] M. Buivydas, F. Gouda, G. Andersson, S. T. Lagerwall and B. Stebler *Liq. Cryst.*, **23**, 5, pp. 723-739 (1997)

[22] M. Buivydas, F. Gouda, S. T. Lagerwall and B. Stebler *Liq. Cryst.*, **18**, 6, pp. 879-886 (1995)

[23] S. T. Lagerwall, *Ferroelectric and Antiferroelectric Liquid Crystals*, Wiley-VCH (1999)

[24] N. A. Clark and S. T. Lagerwall *Appl. Phys. Lett.*, **36**, 11, pp. 899-901 (1980)

[25] A. de Vries *J. Chem. Phys.*, **70**, 6, pp. 2705-9 (1978)

[26] S. Diele, P. Brand and H. Sackmann *Mol. Cryst. Liq. Cryst.*, **16**, 1-2, pp. 105-16 (1972)

[27] A. de Vries *J. Chem. Phys.*, **71**, 1, pp. 25-31 (1979)

[28] A. de Vries *Journal de Physique Lettres*, **35**, 9, pp. L139-40 (1974)

[29] A. De Vries *Mol. Cryst. Liq. Cryst. Lett.*, **41**, 2, pp. 27-31 (1977)

[30] A. J. Leadbetter and R. M. Richardson *Mol. Phys.*, **35**, 4, pp. 1191-200 (1978)

[31] A. J. Leadbetter and E. K. Norris *Mol. Phys.*, **38**, 3, pp. 669-86 (1979)

[32] A. de Vries, A. Ekachai and N. Spielberg *Mol. Cryst. Liq. Cryst. Lett.*, **49**, 5, pp. 143-152 (1979)

[33] A. de Vries *Mol. Cryst. Liq. Cryst. Lett.*, **49**, 6, pp. 179-85 (1979)

[34] J. V. Selinger, P. J. Collings and R. Shashidhar *Phys. Rev. E*, **64**, 6, pp. 061705/1-9 (2001)

[35] A. de Vries *Mol. Cryst. Liq. Cryst.*, **11**, 4, pp. 361-83 (1970)

[36] Y. Takanishi, Y. Ouchi, H. Takezoe, A. Fukuda, A. Mochizuki and M. Nakatsuka *Jpn. J. Appl. Phys. Lett.*, **29**, 6, pp. L984-L986 (1990)

[37] Y. Takanishi, Y. Ouchi, H. Takezoe, A. Fukuda, A. Mochizuki and M. Nakatsuka *Mol. Cryst. Liq. Cryst.*, **199**, pp. 111-18 (1991)

[38] T. R. Taylor, S. L. Arora and J. L. Ferguson *Phys. Rev. Lett.*, **25**, 11, pp. 722-6 (1970)

[39] A. de Vries in *Advances in Liquid Crystal Research and Applications*(Ed, Bata, L.), Pergamon Press, Oxford, Budapest, pp. 71-80 (1980)

[40] A. Wulf *Mol. Cryst. Liq. Cryst.*, **47**, 3-4, pp. 225-36 (1978)

[41] N. A. Clark and S. T. Lagerwall in *Ferroelectric Liquid Crystals*(Ed, Goodby, J. W.), Gordon & Breach, (1991)

[42] J. S. Patel, L. Sin Doo and J. W. Goodby *Phys. Rev. A*, **40**, 5, pp. 2854-6 (1989)

[43] Y. Takanishi, K. Hiraoka, V. K. Agrawal, H. Takezoe, A. Fukuda and M. Matsushita *Jpn. J. Appl. Phys.*, **30**, 9A, pp. 2023-7 (1991)

[44] R. Bartolino, J. Doucet and G. Durand *Ann. Phys.*, **3**, 2-4, pp. 389-95 (1978)

[45] M. Buivydas, S. T. Lagerwall, I. Dierking, F. Gouda and A. Mochizuki, *Proceedings from FLC'97, Brest, France* (1997). *Ferroelectrics*, **212**, pp. 67-78 (1998)

[46] Y. P. Panarin, V. Panov, O. Kalinovskaya and J. K. Vij *J. Mater. Chem.*, **9**, 12, pp. 2967-2969 (1999)

- [47] N. A. Clark, T. Bellini, R. Shao, D. Coleman, S. Bardon, D. R. Link, J. E. Maclennan, X. H. Chen, M. D. Wand, D. M. Walba, P. Rudquist and S. T. Lagerwall *Liq. Cryst.*, (2001)
- [48] T. P. Rieker, N. A. Clark, G. S. Smith, D. S. Parmar, E. B. Sirota and C. R. Safinya *Phys. Rev. Lett.*, **59**, 23, pp. 2658-61 (1987)
- [49] F. Giebelmann, P. Zugenmaier, I. Dierking, S. T. Lagerwall, B. Stebler, M. Kaspar, V. Hamplova and M. Glogarova *Phys. Rev. E*, **60**, 1, pp. 598-602 (1999)
- [50] M. D. Radcliffe, M. L. Brostrom, K. A. Epstein, A. G. Rappaport, B. N. Thomas, R. F. Shao and N. A. Clark *Liq. Cryst.*, **26**, 6, pp. 789-794 (1999)
- [51] T. P. Rieker and E. P. Janulis *Liq. Cryst.*, **17**, 5, pp. 681-7 (1994)
- [52] T. P. Rieker and E. P. Janulis *Phys. Rev. E*, **52**, 3, pp. 2688-91 (1995)
- [53] M. Radcliffe (2002).
- [54] P. Davidson, D. Petermann and A. M. Levelut *J. Phys. II*, **5**, 1, pp. 113-31 (1995)
- [55] M. Skarabot, K. Kocevar, R. Blinc, G. Heppke and I. Musevic *Phys. Rev. E*, **59**, 2, pp. R1323-6 (1999)
- [56] T. E. Lockhart, E. Gelerinter and M. E. Neuber *Phys. Rev. A*, **25**, 4, pp. 2262-71 (1982)
- [57] T. E. Lockhart, D. W. Allender, E. Gelerinter and D. L. Johnson *Phys. Rev. A*, **20**, 4, pp. 1655-60 (1979)
- [58] A. Mochizuki and S. Kobayashi *Mol. Cryst. Liq. Cryst.*, **243**, pp. 77-90 (1994)
- [59] A. Wulf *Phys. Rev. A*, **17**, 6, pp. 2077-82 (1978)
- [60] J. Fünfschilling and M. Schadt *Jpn. J. Appl. Phys.*, **35**, 11, pp. 5765-5771 (1996)
- [61] Z. Shiyong, W. Bing, S. S. Keast, M. E. Neubert, P. L. Taylor and C. Rosenblatt *Phys. Rev. Lett.*, **84**, 18, pp. 4140-3 (2000)
- [62] B. Wen, Z. Shiyong, S. S. Keast, M. E. Neubert, P. L. Taylor and C. Rosenblatt *Phys. Rev. E*, **62**, 6, pp. 8152-8 (2000)
- [63] H. Takezoe, A. D. L. Chandani, E. Gorecka, Y. Ouchi, A. Fukuda, K. Terashima, K. Furukawa and A. Kishi, *Oral O 26 at FLC'89, Göteborg, Sweden* (July 27 - 30, 1989).
- [64] M. Fukui, H. Orihara, Y. Yamada, N. Yamamoto and Y. Ishibashi *Jpn. J. Appl. Phys. Lett.*, **28**, 5, pp. L849-850 (1989)
- [65] A. D. L. Chandani, Y. Ochi, H. Takezoe and A. Fukuda *Jpn. J. Appl. Phys. Lett.*, **28**, 7, pp. L1261-4 (1989)
- [66] P. Mach, R. Pindak, A. M. Levelut, P. Barois, H. T. Nguyen, C. C. Huang and L. Furenliid *Phys. Rev. Lett.*, **81**, 5, pp. 1015-18 (1998)
- [67] P. Mach, R. Pindak, A. M. Levelut, P. Barois, H. T. Nguyen, H. Baltes, M. Hird, K. Toyne, A. Seed, J. W. Goodby, C. C. Huang and L. Furenliid *Phys. Rev. E*, **60**, 6, pt.A-B, pp. 6793-6802 (1999)
- [68] P. M. Johnson, D. A. Olson, S. Pankratz, H. T. Nguyen, J. W. Goodby, M. Hird and C. C. Huang *Phys. Rev. Lett.*, **84**, 21, pp. 4870-4873 (2000)
- [69] A. Cady, J. A. Pitney, R. Pindak, L. S. Matkin, S. J. Watson, H. F. Gleeson, P. Cluzeau, P. Barois, A. M. Levelut, W. Caliebe, J. Goodby, M. Hird and C. C. Huang *Phys. Rev. E*, **64**, pp. 050702/1-4 (2001)
- [70] M. Cepic, B. Rovsek and B. Zeks, *Proceedings from ECLC'99, Hersonissos, Crete, Grece* (April 25 - 30, 1999). *Mol. Cryst. Liq. Cryst.*, (1999 (?))

- [71] B. Zeks and M. Cepic, *Proceedings from SPIE'98, Proceedings of the SPIE - The International Society for Optical Engineering*, **3318**, pp. 68-77 (1998)
- [72] A. Fukuda, Y. Takanishi, T. Isozaki, K. Ishikawa and H. Takezoe *J. Mater. Chem.*, **4**, 7, pp. 997-1016 (1994)
- [73] M. Linehan, *Personal communication* (2001)
- [74] E. Gorecka, *Personal communication* (2001)
- [75] P. Gisse, V. L. Lorman, J. Pavel and H. T. Nguyen, *Proceedings from FLC'95, Cambridge, UK* (July 23 - 27, 1995). *Ferroelectrics*, **178**, pp. 297-309 (1996)
- [76] P. Gisse, M. Sidir, V. L. Lorman, R. Farhi, J. Pavel and H. T. Nguyen *J. Phys. II France*, **7**, pp. 1817-1828 (1997)
- [77] K. Hiraoka, A. Taguchi, Y. Ouchi, H. Takezoe and A. Fukuda *Jpn. J. Appl. Phys. Lett.*, **29**, 1, pp. L103-L106 (1990)
- [78] J.-F. Li, E. A. Shack, Y.-K. Yu, X.-Y. Wang, C. Rosenblatt, M. E. Neubert, S. S. Keast and H. Gleeson *Jpn. J. Appl. Phys. Lett.*, **35**, 12A, pp. L1608-10 (1996)
- [79] T. Sako, Y. Kimura, R. Hayakawa, N. Okabe and Y. Suzuki *Jpn. J. Appl. Phys. Lett.*, **35**, 1B, pp. L114-16 (1996)
- [80] A. Jakli *J. Appl. Phys.*, **85**, 2, pp. 1101-4 (1999)
- [81] S. Tatemori, H. Uehara, J. Hatano, S. Saito, H. Saito and E. Okabe, *Proceedings from FLC'99, Darmstadt, Germany* (August 29 - September 3, 1999). *Ferroelectrics*, (1999)
- [82] F. Gouda, K. Skarp and S. T. Lagerwall *Ferroelectrics*, **113**, 1-4, pp. 165-206 (1991)
- [83] M. Cepic, G. Heppke, J.-M. Hollidt, D. Löttsch, D. Moro and B. Zeks, *Proceedings from ILCC'94, Budapest, Hungary* (July 3 - 8, 1994). *Mol. Cryst. Liq. Cryst.*, **263**, pp. 207-216 (1995)
- [84] P. Rudquist, D. Krueker, S. T. Lagerwall, J. E. MacLennan, N. A. Clark and D. M. Walba *Ferroelectrics*, **246**, 1-4, pp. 927-39 (2000)
- [85] J. Pavel, P. Gisse, H. T. Nguyen and P. Martinot-Lagarde *J. Phys. II*, **5**, pp. 355 - 368 (1995)
- [86] V. Bourny, J. Pavel, V. Lorman and H. T. Nguyen *Liq. Cryst.*, **27**, 5, pp. 559-66 (2000)
- [87] J. Als-Nielsen, R. J. Birgeneau, M. Kaplan, J. D. Litster and C. R. Safinya *Phys. Rev. Lett.*, **39**, 6, pp. 352-5 (1977)
- [88] J. Xue and N. A. Clark *Phys. Rev. Lett.*, **64**, 3, pp. 307-10 (1990)
- [89] H. Moritake, N. Shigeno, M. Ozaki and K. Yoshino, *Proceedings from ILCC'92, Pisa, Italy* (June 21-26, 1992). *Liq. Cryst.*, **14**, pp. 1283-1293 (1993)
- [90] M. Cepic, G. Heppke, J. M. Hollidt, D. Löttsch and B. Zeks, *Proceedings from FLC'93, Tokyo, Japan* (September 28 - October 1, 1993). *Ferroelectrics*, **147**, pp. 159-170 (1993)
- [91] P. Rudquist, J. P. F. Lagerwall, M. Buivydas, F. Gouda, S. T. Lagerwall, N. A. Clark, J. E. MacLennan, R. F. Shao, D. Coleman, S. Bardou, T. Bellini, D. R. Link, G. Natale, M. A. Glaser, D. M. Walba, M. D. Wand and X. H. Chen *J. Mater. Chem.*, **9**, 6, pp. 1257-1261 (1999)
- [92] V. Novotna, M. Glogarova, A. Bubnov and H. Sverenyak *Liq. Cryst.*, **23**, 4, pp. 511-518 (1997)

- [93] A. Fukuda, S. S. Seomun, T. Takahashi, Y. Takanishi and K. Ishikawa, *Proceedings from ILCC'96, Kent, Ohio, USA* (June 24 - 28, 1996). *Mol. Cryst. Liq. Cryst.*, **303**, pp. 379-390 (1997)
- [94] S. Inui, N. Iimura, T. Suzuki, H. Iwane, K. Miyachi, Y. Takanishi and A. Fukuda *J. Mater. Chem.*, **6**, 4, pp. 671-673 (1996)
- [95] P. Rudquist, J. P. F. Lagerwall, M. Buivydas, F. Gouda, S. T. Lagerwall, R. F. Shao, D. Coleman, S. Bardon, D. R. Link, T. Bellini, J. E. MacLennan, D. M. Walba, N. A. Clark and X. H. Chen, *Proceedings from SID'99, San José SID Digest*, pp. 409 (1999)
- [96] L. J. Baylis, H. F. Gleeson, A. J. Seed, P. J. Styring, M. Hird and J. W. Goodby *Mol. Cryst. Liq. Cryst.*, **328**, pp. 13-20 (1999)
- [97] D. Kilian, S. Hiller, J. W. Goodby, I. Nishiyama, S. A. Pikin and W. Haase, *Poster at ILCC'94, Budapest, Hungary* (1994).
- [98] J. W. O'Sullivan, Y. P. Panarin, J. K. Vij, A. J. Seed, M. Hird and J. W. Goodby *J. Phys: Condens. Matter*, **8**, pp. L551-L556 (1996)
- [99] N. M. Shtykov, J. K. Vij, R. A. Lewis, M. Hird and J. Goodby *Phys. Rev. E*, **62**, 2, pp. 2279-87 (2000)
- [100] P. Panarin Yu, H. Xu, S. T. MacLughadha, J. K. Vij, A. J. Seed, M. Hird and J. W. Goodby *J. Phys: Condens. Matter*, **7**, 27, pp. L351-60 (1995)
- [101] Y. P. Panarin, O. Kalinovskaya, J. K. Vij and J. W. Goodby *Phys. Rev. E*, **55**, 4, pp. 4345-4353 (1997)
- [102] V. Bourny, J. Pavel, P. Gisse and H. T. Nguyen *Ferroelectrics*, **241**, pp. 247 - 254 (2000)
- [103] S. Sarmiento, P. S. Carvalho, M. R. Chaves, F. Pinto and H. T. Nguyen *Liq. Cryst.*, **28**, 12, pp. 1839-45 (2001)
- [104] N. A. Clark and T. P. Rieker *Phys. Rev. A*, **37**, 3, pp. 1053-6 (1988)
- [105] I. Dierking, L. Komitov and S. T. Lagerwall *Liq. Cryst.*, **24**, 5, pp. 769-774 (1998)
- [106] N. A. Clark, T. P. Rieker and J. E. MacLennan, *Proceedings from FLC'87, Bordeaux-Arcachon, France* (September 1987). *Ferroelectrics*, **85**, pp. 467-85 (1988)
- [107] Y. Ouchi, Y. Takanishi, H. Takezoe and A. Fukuda *Japanese Journal of Applied Physics, Part 1 (Regular Papers & Short Notes)*, **28**, 12, pp. 2547-51 (1989)
- [108] P. J. Collings and M. Hird, *Introduction to Liquid Crystals*, Taylor & Francis, London (1997)
- [109] D. D. Parghi, S. M. Kelly and J. W. Goodby, *Proceedings from Freiburg'98, Freiburg, Germany* (1998). *Freiburger Arbeitstagung conference book*, (1998)
- [110] D. D. Parghi, J. P. F. Lagerwall and G. Heppke, *Proceedings from ECLC'99, Hersonissos, Crete, Grece* (April 25 - 30, 1999). *Mol. Cryst. Liq. Cryst.*, **351**, pp. 360-370 (1999)
- [111] J. P. F. Lagerwall, D. D. Parghi and G. Heppke, *Proceedings from FLC'99, Darmstadt, Germany* (August 29 - September 3, 1999). *Ferroelectrics*, **244**, pp. 511 - 521 (2000)
- [112] V. Vill, *LiqCryst Database*, Version 3.3
- [113] T. Isozaki, K. Ishikawa, H. Takezoe and A. Fukuda, *Proceedings from FLC'93, Tokyo, Japan* (September 28 - October 1, 1993). *Ferroelectrics*, **147**, pp. 121-134

Chapter

(1993)

[114] D. Guillon and A. Skoulios *J. Phys.*, **37**, 6, pp. 797-800 (June 1976)

[115] A. J. Leadbetter in *The Molecular Physics of Liquid Crystals*(Eds, Luckhurst, G. and Gray, G.), Academic Press, London, pp. 285-316 (1979)

[116] A. J. Leadbetter and P. G. Wrighton, *Proceedings from ILCC'78, Bordeaux, France* (1-5 July 1978). *Journal de Physique Colloque*, **40**, pp. 234-42 (1979)

[117] F. Gießelmann, *Personal communication* (2001)

ACKNOWLEDGEMENTS

– I'm Brian, and so is my wife!
Monty Python's 'Life of Brian'

This work was carried out within the framework of the Chalmers Graduate School of Materials Science in the group of Liquid Crystal Physics. I would first of all like to thank the directors of the school, Per Jacobson and, later on, Igor Zoric, for not only financing my doctoral studies but even extending the support to the participation in conferences. The activities organized within the graduate school have always been pleasant and inspiring, transmitting a very broad view of materials science.

My supervisors, Bengt Stebler and Per Rudquist, deserve special acknowledgement. Bengt has an almost superhuman ability to keep positive, creating smiles on people's faces in one way or another, even in situations where one would rather have expected the opposite behavior. Per also has a wonderful sense of humor and an attitude towards science which is very constructive, making discussions as well as lab work very exciting. The generous and positive attitude is also very much a characteristic of Marek and Tomasz Matuszczyk who have helped me so much in the lab. Two persons who have not been directly involved in my scientific work, but have nevertheless contributed greatly to a better atmosphere, are David Hermann and Tomas Carlsson. My thanks go to them for several very nice dinners and other joyful events as well as for discussions of general scientific interest. I have greatly enjoyed the company of my fellow students (although by now they are all doctors) Pontus Jägemalm, Koen D'havé, Johann Meier and Giusy Scalia. Through Giusy I also got to know the 'Italian gang' at Chalmers with whom I've shared many joyful moments. Grazie a tutti!

I have had the pleasure to get to know several guests of the group, as well as being one in other groups. During my first year as a graduate student, Ingo Dierking was in Göteborg as a Humboldt post-doc. He taught me a lot on the basics of liquid crystals, in particular in connection to the construction of the group web site, to which he contributed very much. Ingo came from the liquid crystal group in Clausthal-Zellerfeld and so does Frank Gießelmann, who visited the group during the summer 2000. This visit was the start of our collaboration which got very intense during the fall of 2001 when I had the great pleasure to visit the groups of his and Peter Zugenmaier's. Not only were these three months extremely productive scientifically but they were also lots of fun, much due to all the nice people in the group (special mention to Alexander Saipa and Arne Langhoff) and of course Sabine and Niels Gießelmann.

The stay in Clausthal was not my only long-term stay in Germany during my studies. In 1998 I had the pleasure to work as a guest in the group of Gerd Heppke, at the TU-Berlin. During this stay, my interest in the antiferroelectric liquid crystal sub-phases started and I also developed my technical skills in several areas. I felt very welcome also in this group and several long-lasting friendships started during those three

months. In particular I would like to mention Daniel Krüerke and Deven Parghi with whom I still have very lively contacts.

All these people not only transmit a great joy in doing research, through a positive, open and generous attitude, but they also help out when collective practical efforts are needed, rather than staying away waiting for others to solve the problem. Had the Göteborg group had only members like them, the atmosphere would have been fantastic.

As a physicist doing experimental materials science research in a physics group, I have of course been completely dependent on the generosity of the synthetic chemists around the world, providing the liquid crystal compounds without which this thesis would have been impossible. Again the group of professor Heppke has been very supportive in this sense, but I also wish to express my gratitude to the Dabrowski group in Warsaw, Displaytech in Boulder, Colorado, and the liquid crystal research group at 3M, headed by Dr. Marc Radcliffe.

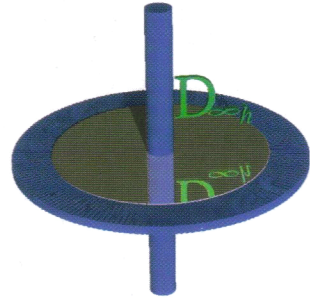
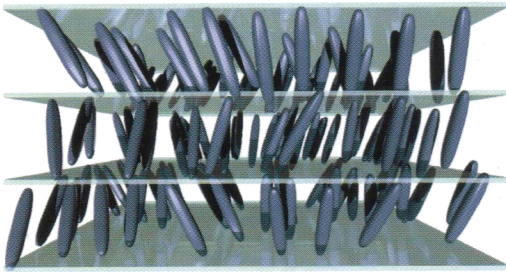
A group cannot run without people caring also about non-scientific matters. In the case of the Göteborg group, the heroes in this area are our secretary Ingela Malmgren, always so reliable and helpful, and our technician Johan Persson. I have known Johan since long before I started in the group and I owe him very, very much. He has solved problems with cars, stereos and computers, just to mention a few cases where he has saved me, and he is simply a very good friend.

When I started my doctoral studies in 1997 I was convinced that the professor I would acknowledge when writing these words would not be my father, Sven Lagerwall. Unfortunately, the group is still waiting for its new leader, so my thanks for the scientific leadership still have to go to Sven alone. So now that I have come to my family, I would also like to thank my mother for all she has done, for me and for others, and my sisters for being who they are.

Financial support from the Deutsche Akademischer Austauschdienst, Kungliga fysikografiska sällskapet, the European Union network ORCHIS, and the Chalmers Graduate School of Materials Science is gratefully acknowledged.

Göteborg, 9 April 2002

Smectic A



Smectic C

